BEDLOAD TRANSPORT: THE EFFECTS OF PARTICLE SHAPE AND AN INVESTIGATION OF A WIDE RANGE OF TRANSPORT RATES

by

Matthew C. Moore

Thesis submitted to the Faculty of the

Virginia Polytechnic Institute and State University

in partial fulfillment of the requirements for the degree of

Master of Science

in

Civil Engineering

APPROVED:

P. Diplas, Chairman

W.E. Cox

T. Younos

JUNE, 1994

Blacksburg, Virginia

BEDLOAD TRANSPORT: THE EFFECTS OF PARTICLE SHAPE AND AN INVESTIGATION OF A WIDE RANGE OF TRANSPORT RATES

by

Matthew C. Moore

Committee Chairman: Panayiotis Diplas
Civil Engineering

(ABSTRACT)

The effects of particle shape on bedload transport and a wide range of bedload transport rates using both bed subsurface and surface layer based approaches are investigated using fractional transport analysis with a similarity approach. Bedload transport data from a stream containing flat, low density shale particles indicates that the reference transport critical shear stress for the median surface grain size is approximately 2 to 3 times higher than those for more spherical particles. This conclusion indicates a lower susceptibility of disc-like particles to initial entrainment and lower transport rates for given flow conditions than more rounded particles. Analysis of a wide range of transport rates verifies that the slope of the log-log bedload transport rate - bed shear stress relation decreases with increasing transport rate and becomes constant at very high transport rates. This result implies that the dependence of the transport rate on grain size decreases with increasing transport rate. Comparison of bed subsurface and surface layer based bedload transport approaches indicates that the two approaches produce similar transport - shear relations and reference shear stress values.

Acknowledgments

I have many to thank for their help and guidance during the course of this study.

I would like to thank my advisor, Dr. Panayiotis Diplas, for the opportunity to work with him, and for his assistance over the course of this study.

I thank the members of my committee, Dr. W.E. Cox, and Dr. T. Younos, for their assistance during my graduate studies and in the preparation and refinement of this thesis.

I would like to thank the Via family and the faculty and staff of the Charles E. Via, Jr. Department of Civil Engineering for their generous support during my undergraduate and graduate studies.

I thank my parents for their encouragement and support over the years.

I thank for her support and understanding.

I thank for his advice and for listening.

The support of this work by the National Science Foundation (Grant # CTS-9257335) is gratefully acknowledged.

Table of Contents

List of Tables

List of Figures

Symbols

a = longest grain axis, [L]

A_p = projected area of grain normal to the flow direction, [L^2]

b = intermediate grain axis, [L], and exponent

c = shortest grain axis, [L]

D = characteristic grain size, [L]

D_g = subsurface geometric mean grain size, [L]

$\bar{D}_i$ = characteristic grain size of *i*th grain size range, [L]

D_{lg} = geometric mean size of bedload, [L]

D_{l50} = median size of bedload, [L]

D_m = characteristic mixture diameter, [L]

D_N = nominal grain diameter, [L]

D_{sg} = surface geometric mean grain size, [L]

D_{50s} = surface median grain size, [L]

D_{50} = subsurface median grain size, [L]

D_* = dimensionless grain size

e = empirical coefficient in pivot angle equation accounting for grain shape

f = empirical coefficient in pivot angle equation accounting for bed material nonuniformity

f_i = fraction of subsurface bed material in *i*th grain size range

F_i = fraction of surface bed material in *i*th grain size range

g = acceleration of gravity, $[L/T^2]$

g_o = surface-based reduced hiding function

g_r = hiding function appropriate for Paintal's transport relation

h = hiding function

H = flow depth, [L]

i, j = indices used for grain size and density respectively

k = proportionality constant in pivot angle analysis

K_b = base grain size in pivot angle equation, [L]

k_s = bed roughness length, [L]

p_i = fraction of bedload in *i*th grain size range

p/D = relative protrusion ($p/D = 0$ for coplanar or flat bed)

q_B = total volumetric bedload transport rate per unit width, $[L^2/T]$

q_{Bi} = volumetric bedload transport rate per unit width for the *i*th grain size range, $[L^2/T]$

q_{Bsi} = volumetric bedload transport rate per unit width for the *i*th grain size range for a surface based relation, $[L^2/T]$

q_w = bedload transport rate as immersed weight per unit width per unit time, $[M/T^3]$

R = submerged specific gravity = ρ_s/ρ - 1

R_h = hydraulic radius, [L]

R_* = grain Reynolds number = u_*D/ν

S = slope

u = fluid flow velocity, [L/T]

u_S = grain settling velocity, [L/T]

u_S^* = dimensionless grain settling velocity

u_* = shear velocity = $(\tau/\rho)^{1/2}$, [L/T]

u_{*_t} = transitional shear velocity used in the analysis of the surface layer, [L/T]

V_p = volume of grain, [L^3]

W^* = total dimensionless bedload transport rate

W_i^* = dimensionless bedload transport rate for *i*th grain size range

W_{si}^* = dimensionless bedload transport rate for *i*th grain size range for a surface based relation

W_r^* = dimensionless reference transport rate

y = distance up from a zero velocity datum, [L]

γ, γ_s = fluid and grain specific weight respectively, [M/L^2T^2]

ρ' = ρ_s - ρ, [M/L^3]

μ_s = coefficient of static friction

ν = kinematic viscosity, [L^2/T]

ρ, ρ_s = fluid and grain density respectively, [M/L^3]

σ = subsurface grain size distribution standard deviation

σ_g = subsurface grain size distribution geometric standard deviation

σ_{lg} = bedload grain size distribution geometric standard deviation

σ_{sg} = surface layer grain size distribution geometric standard deviation

σ_ϕ = grain size distribution using the ϕ scale representation of grain size, $\sigma_g = 2^{\sigma\phi}$

τ = bed shear stress = $\gamma R_h S = \gamma HS$ (for wide channels), [M/LT^2]

τ_c = critical bed shear stress, [M/LT^2]

τ_{ci} = critical bed shear stress for *i*th grain size range, [M/LT^2]

τ_{ci}^* = dimensionless critical bed shear stress for *i*th grain size range

τ_c^* = dimensionless critical bed shear stress

τ_{ri}^* = dimensionless reference bed shear stress for the *i*th grain size range corresponding to W_r^*

τ_{r50}^* = dimensionless reference bed shear stress for the median grain size

τ_{r50s}^* = dimensionless reference bed shear stress for the surface layer median grain size

τ_{si}^* = dimensionless bed shear stress for the *i*th grain size range (surface based relation)

τ_{sg}^* = dimensionless bed shear stress for corresponding to D_{sg}

τ^* = dimensionless bed shear stress = $\tau/(\gamma_s-\gamma)D$

τ_{50}^* = dimensionless bed shear stress for the subsurface median grain size

τ_{50s}^* = dimensionless bed shear stress for the surface median grain size

ϕ = phi scale representation of grain size

ϕ_i = normalized bed shear stress for *i*th grain size range = τ_i^*/τ_{ri}^*

ϕ_{sgo} = normalized bed shear stress (surface based relation)

Φ = pivot angle

Chapter 1. Introduction

1.1 Sediment Transport Classification

Knowledge of sediment transport in streams is necessary for determining processes such as sediment yield, water quality, sediment influx into impoundments, bed degradation downstream of dams, design and maintenance of channels, and flood characteristics. These items are interrelated and often depend on the type of sediment transport, i.e., suspended load or bedload, and the size of particles in motion. The term "sediment load" refers to the material transported by a stream. Commonly, the suspended load consists of particles in the sand and finer size ranges (less than 2 mm), while the bedload contains particles in the sand and coarser size ranges. Thus, sand grains can move either as bedload or suspended load depending on the flow conditions.

The relative importance of each type of load depends on the stream and given flow conditions. Generally, low slope sand-bed streams in the lower reaches of a stream transport material predominately by suspension, while in the steeper gravel bed headwaters the bedload contribution increases. Although fine material may move as washload almost continually, the most significant sediment transport occurs infrequently during floods when the flow strength exceeds the critical value for initiating transport. This critical flow strength value is dependent on many

factors including the type of stream, sediment size and shape, and bed sediment size distribution.

1.2 Overview of Bedload Transport and Gravel-Bed Streams

This study focuses on bedload transport in gravel-bed streams. The bedload transport rate may be quantified by defining the bedload discharge or the amount of material passing a given point in the stream per unit time. The bedload discharge or transport rate can be measured in the field and laboratory using a variety of techniques such as the Helley-Smith bedload sampler, a vortex trough, or by simple collection at the downstream end of the experimental flume.

In addition to the sediment discharge, the bedload size distribution and hydraulic conditions at the time of bedload measurement are necessary for meaningful data analysis and for relating the bedload discharge to the size distribution of the parent bed material and the hydraulic conditions. The relation between bedload and flow conditions is necessary for developing and calibrating predictive bedload transport equations.

Gravel-bed streams have some unique features which distinguish them from sand-bed streams and create challenging problems for their analysis. Sand-bed streams often contain a narrow range of particle sizes which allows the use of a single grain size to adequately describe the behavior of the entire streambed

material. Conversely, gravel-bed streams contain a wide range of grain sizes from fine sand to gravel, cobbles, and sometimes even boulders. This mixture of sizes contributes to the complexity of bedload analysis so that a median grain size may not adequately describe the transport behavior. One possible solution to this problem is the use of fractional transport analysis wherein the bed sediment size distribution is separated into distinct size ranges each with a representative grain size.

The bedload transport rate for each size range is determined by multiplying the total bedload discharge by the fraction of material in each size range. Often fractional transport analysis reveals that either the fine grains or coarse grains are relatively more mobile. This selective transport by size is due to bed grain size nonuniformity and is controlled by hiding and relative protrusion. The smaller, and therefore lighter, particles which are naturally the most mobile are often hidden or protected from the flow by the larger particles when in a sediment mixture with many grain sizes. The larger particles on the surface of the streambed protrude farther into the flow, thus subjecting them to greater fluid forces which may compensate in part for their relatively larger weight. The hiding of the smaller particles reduces their transport rate relative to a uniform bed containing the same size particles, while the relative protrusion and exposure of the larger particles increases their transport rate relative to a uniform bed of the same size coarse

particles. Thus, an approximate balance is achieved between the transport rate of the fine and coarse grains, but selective transport may still occur.

Selective transport of the fine particles often leads to a coarse surface layer, which is another distinct feature of gravel-bed streams. The coarse surface layer contains all the particle sizes found in the subsurface but with an over-representation of sizes coarser than the subsurface median grain size. The surface layer thickness is generally defined using the thickness or depth of the largest particles on the bed such as D_{90} (particle size for which 90% of all particles on the bed are smaller).

The degree of coarseness is a function of flow strength and the standard deviation of the bed material size distribution (Diplas, 1987). Commonly, as the stream flow strength increases, the surface layer size distribution coarsens up to some point and then becomes finer approaching the subsurface layer size distribution at the highest flow strengths. Further, a larger standard deviation of the bed sediment size distribution allows for a greater surface coarseness.

The surface layer size distribution is necessary for determining bed roughness used in flow calculations and flood analysis. In addition, the surface layer contains those grains directly available for entrainment. However, the surface layer is tied to the subsurface, which is a source of grains for the surface layer.

Fractional transport analysis requires that the bed size distribution be specified for scaling purposes, however, either the surface or the subsurface size distribution may be used. Traditionally, the subsurface size distribution has been used since it is a known stable distribution that does not vary significantly with flow conditions. Recently, however, researchers such as Parker (1990) and Wilcock and McArdell (1993) have proposed surface based fractional bedload transport approaches claiming that they are more appropriate for the following reasons. First, the surface layer is the place from which grains are entrained and move as bedload. Secondly, it is argued that subsurface scaled fractional transport rates from different data sets are not generally comparable due to differing sediment input conditions (sediment feed and sediment recirculation), but that surface scaled fractional transport rates overcome this problem. A drawback to the surface approach is that it may be necessary to know the continuous change of the surface layer grain size composition with flow conditions. This is typically unknown, especially during flood conditions, when most of the material is transported.

In addition to particle size nonuniformity, particle shape is expected to influence the incipient and sustained motions of particles on the bed. Conflicting field and laboratory results obscure the true nature of the phenomenon. At question is whether flat, disc-like particles are more resistant to initial and sustained motion

than more spherical particles. The answer is crucial for the modeling, maintenance, and design of channels in areas containing a large number of flat particles such as shale.

Studies of bedload transport are based both on laboratory and field data over varying ranges of transport rate and flow strength. Ultimately, it is desirable to describe the relation between bedload discharge and flow strength from initial motion to the highest possible transport rates. This description requires identifying those variables affecting bedload transport such as grain size nonuniformity, grain shape, relative protrusion, selective transport, and surface layer coarseness. Unfortunately, many data sets cover a limited range of the possible flow strengths and transport rates while concentrating on a limited number of variables. Therefore, data sets and studies must be combined in order to achieve an overall picture of bedload transport and to describe the phenomenon accurately.

Once the various effects are accounted for accurately, a predictive bedload relation may be formulated to determine the bedload discharge and its size composition given the flow conditions and initial bed material size distribution. In addition, it is desirable to determine the behavior of the surface layer coarseness and size distribution in response to changing flow conditions. This knowledge may be mandatory if a surface based bedload analysis is used.

1.3 Objectives of the Current Study

The objectives of the current work are threefold and provide an examination of bedload transport phenomena in need of review. First, the effects of particle shape on initial motion will be investigated to determine the relative mobility of disc-like particles versus more spherical particles. Second, the entire transport - flow strength phenomenon from initial motion to the highest transport rates will be investigated. Third, surface and subsurface layer bedload transport analysis approaches will be evaluated and compared.

Using data from Piceance Creek, Colorado, which contains flat shale particles, critical shear stresses will be determined and compared with other data for more spherical particles. This will allow a determination of the relative mobility of discs versus more spherical particles. In addition, the transport rates and corresponding bed shear stresses will be compared. The results will provide information necessary for modifying bedload transport relations to account for grain shape.

Many bedload transport relations are inadequate for predicting transport rates over the entire spectrum of possible transport rates, because they are derived using data ranging only over a portion of the total range of transport rates. Laboratory data of Proffitt (1980) contain both high and low transport rates as well as bed conditions varying from a very low surface coarseness to an armored bed.

Proffitt's data, along with other data, provide the opportunity to investigate the transport phenomenon over a wide range of transport rates. Results of this investigation will allow the development or modification of bedload transport relations which will be valid over a wider range of transport rates and flow conditions.

The presence of a coarse surface layer in most gravel-bed streams produces many difficulties in their analysis. Most bedload transport relations require the specification of bed material characteristics such as a grain size distribution or mean grain size. However, many formulations do not specify whether the bed material refers to the surface layer or the subsurface (bulk) material. Both layers have been used, which has created confusion in the comparison of data and transport relations. The current work will investigate the differences between surface and subsurface approaches and compare their relative merits and inadequacies in an attempt to discern the most suitable approach.

Results of investigating the above objectives will provide researchers and modelers with information necessary for modifying or developing bedload transport relations that account for particle shape effects, wide ranges of transport rates, and surface layer conditions. Prior to these investigations, a review of previous studies on incipient motion, the effects of particle shape, and recent bedload transport relations are provided in the next chapter.

Chapter 2. Review of Incipient Motion and Bedload Transport

2.1 Introduction

Incipient motion of a submerged particle occurs when the particle's resisting forces due to its submerged weight and interaction with surrounding grains is exactly balanced by the fluid lift and drag forces acting on the particle. Many studies have examined this phenomenon to determine the critical fluid conditions such as the critical shear stress necessary for particle movement. A brief overview of some of these studies is provided. More specifically, Shields' analysis and studies on the important parameters that influence the critical shear stress such as grain size nonuniformity, relative protrusion, pivot angle, and particle shape are reviewed.

A logical step after evaluating incipient motion is to estimate how much sediment will be transported. Bedload transport evaluations can be categorized depending on the type of bed, either sand or gravel. The sand size range is 0.06 - 2 mm, the gravel size range is 2 - 64 mm, and cobble and boulder size range is greater than 64 mm (Vanoni, 1975). Sand-bed streams typically exhibit a small range of bed particle sizes including silt, sand, and possibly some gravel. However, gravel-bed streams consist of a wide range of bed particle sizes, and may include a significant amount of sand and some silt. This sometimes causes a

bimodal sediment size distribution. Unlike sand-bed streams, the use of a single particle diameter to describe the bed mobility may not be justified for gravel-bed streams. Another difference between sand and gravel streams is the presence of a thin surface layer that is coarser than the subsurface material in gravel streams. This coarse surface layer (pavement or armor) affects the transport process. As described by Parker, et al. (1982), pavement is a mobile bed phenomenon that tends to equalize the mobility of the coarser and finer portions by over-representing the coarse fraction in the surface layer. A further difference between sand and gravel streams centers on the dependence of the dimensionless critical bed shear stress, τ_c^*, on the grain Reynolds number, R_*. As will be discussed later, τ_c^* varies with R_*, but τ_c^* becomes constant and independent of R_* for $R_* > 500$. For gravel-bed streams with a median particle size, D_{50}, greater than 2 mm τ_c^* is constant and independent of R_*. Following is a review of incipient motion and bedload transport in gravel-bed streams.

2.2 Incipient Particle Motion

2.2.1 Shields Analysis

In their article describing the effect of relative particle protrusion, Fenton and Abbott (1977) reviewed the work of Shields (1936) who considered the forces acting on cohesionless grains on a streambed. The horizontal resisting force due

to the particle's submerged weight was considered proportional to $(\rho_s-\rho)gD^3$ where ρ_s and ρ are the grain and fluid density respectively, g is the acceleration of gravity, and D is a measure of grain size. The drag force was considered proportional to ρD^2u^2 where u is the fluid velocity acting on the grain. The value of u is typically taken at the center of the grain and is estimated by the time mean velocity given by,

$$\frac{u}{u_*} = 5.75 \log\frac{y}{k_s} + f_1(R_*) \tag{1}$$

where k_s is related to particle size and is typically taken as 1 to 2 times D_{90}, and y is the elevation above a zero velocity datum that is typically below the bed surface. The bed shear velocity, u_*, is given by,

$$u_* = \sqrt{\frac{\tau}{\rho}} \tag{2}$$

where τ is the bed shear stress given by,

$$\tau = \rho g R_h S \approx \rho g H S \tag{3}$$

where R_h is the hydraulic radius, S is the downstream slope of the energy grade line, and H is the flow depth. The particle Reynolds number, R_*, is given by,

$$R_* = \frac{u_* D}{\nu} \tag{4}$$

where ν is kinematic viscosity. The physical meaning of u.D/ν is the ratio of particle size to the thickness of the viscous sublayer given by ν/u.. Thus, R. characterizes the roughness of the boundary (smooth to fully rough). Shields assumed y/k_s to be a constant, so,

$$\frac{u}{u_*} = f_2(R_*) \tag{5}$$

The assumption that y/k_s is constant limits the applicability of Shields' procedure to grains of uniform size and shape. Equating forces to determine the initiation of motion and rearranging gives,

$$\frac{\rho u_*^2 D^2}{(\rho_s-\rho)gD^3} \propto \frac{1}{f_2^2(R_*)} \tag{6}$$

This can be rewritten in terms of shear stress as,

$$\tau^* = \frac{\tau}{(\gamma_s-\gamma)D} = f(R_*) \tag{7}$$

where τ^* is the dimensionless bed shear stress, and γ and γ_s are the fluid and sediment specific weights, respectively. Shields used experimental data for nearly spherical or granular uniform sediment laid on flat beds to obtain the Shields curve (Fig. 1).

The data used by Shields were obtained by extrapolating curves of sediment transport rate against shear stress to zero bedload. Contrary to Shields, Paintal (1971) and Taylor and Vanoni (1972) indicated that the incipient or critical shear stress for turbulent flow, $\tau_c^* = 0.06$ gives small, but nonzero sediment discharge. A value of $\tau_c^* = 0.03$ is more representative of initial motion conditions. Neill (1968) also proposed a value of $\tau_c^*=0.03$ for coarse material.

In addition, it should be kept in mind that initiation of motion in turbulent flow is random in nature due to shear and lift force variations caused by the turbulence. For example, Bridge and Bennett (1992), among others, indicated that the time averaged lift force may not act at the same time as the time averaged drag force as the method of force balance implies. Also, the use of a mean shear stress to calculate the critical shear stress, τ_c, results in an underestimation of τ_c for large grains because the large grains may only move during large turbulent fluctuating values of the shear stress.

2.2.2 Modifications of Shields Curve

Modifications to Shields curve have included incorporating the effects of grain size nonuniformity, shape (other than spherical), relative protrusion (other than flat beds), temperature, bed slope, and low ratios of water depth to grain size. The Shields curve in Figure 1 reflects some of these modifications. Yang (1973)

provided a summary of some of the limitations of using Shields curve for incipient motion. Yang's objections to Shields' curve were:

1) The use of the average shear stress, $\tau = \gamma HS$.

2) The fact that Shields used the concept of a laminar sublayer indicating that the laminar sublayer should not have an effect on the velocity distribution when $u_*D/\nu > 70$. However, Shields diagram indicates that τ_c^* varies with u_*D/ν when $R_* > 70$.

3) The straight line extension for $R_* < 3$ indicates that for very fine grains, τ_c is independent of particle size, but White (1940) showed that at small R_*, τ_c is proportional to D, where D is the particle size.

4) It is inappropriate to use τ and u_* as independent and dependent variables respectively because they are related by $u_* = (\tau/\rho)^{1/2}$, causing a trial and error solution for calculating τ_c^*.

5) The consideration only of the tangential drag force acting on the grain with no direct account of the lift force.

2.3 Pivoting Angle Analysis

Pivoting angle analysis was originally investigated by both White (1940) and Bagnold (1941). Komar and Li (1986) presented a pivoting angle analysis to determine the selective entrainment of sediments according to shape and size. Pivot angle analysis examines the forces acting upon a grain resting on and pivoting about grains beneath it. This differs from Shields' flat bed assumption. Figure 2 shows the two main forces, drag and weight, acting on a submerged particle subjected to fluid flowing around it.

Excluding the lift force, when the moment about the pivot point, P, due to the drag force exceeds the moment due to the particle's submerged weight, the particle will pivot about the contact point. The submerged weight of the particle is given by $(\gamma_s-\gamma)V_p$ where V_p is the volume of the particle. The drag force is proportional to τA_p, where τ is the bottom shear stress and A_p is the projected area of the particle normal to the flow direction. At the threshold of motion the balance of moments due to the two forces gives,

$$\tau_c \propto (\gamma_s-\gamma)\frac{V_p}{A_p}\tan\Phi \tag{8}$$

where Φ is the pivoting angle. If the particle shape can be approximated by a triaxial ellipsoid, $V_p = \pi abc/6$ where a, b, and c are the longest, intermediate, and shortest axial diameters respectively. Sediment grains tend to be oriented with their

long axis, a, perpendicular to the flow direction, their intermediate axis, b, in the flow direction, and their shortest axis, c, perpendicular to the bed (Komar and Li, 1986). Therefore, $A_p = \pi ac/4$, so $V_p/A_p \propto b$ and,

$$\tau_c = k(\gamma_s - \gamma)b \tan\Phi \tag{9}$$

or written in terms of the dimensionless critical shear stress,

$$\tau_c^* = \frac{\tau_c}{(\gamma_s - \gamma)b} = k \tan\Phi \tag{10}$$

The above formulation does not take the lift force into account. However, the lift force is not as easily determined as the drag force. Several studies on the lift force produced conflicting results. Ikeda (1982) reviewed previous work on the lift force, including Chepil (1958), Coleman (1967), and Davies and Samad (1978). Coleman (1967) and Davies and Samad (1978) obtained negative lift for particle Reynolds number, $R_* < 15$, and $R_* < 5$ respectively. Coleman (1967) found that for a sphere resting on closely packed hemispheres of the same diameter, the lift force became negative for $R_* < 15$. However, the particle size ranges used later correspond to $R_* >> 15$, so negative lift does not occur.

Komar and Li (1986) indicated that the pivot angle, Φ, is dependent on grain shape and size, with Φ approximately constant for uniform grains. The dependence

of Φ was expressed as,

$$\Phi = e(\frac{b}{K_b})^{-f} \tag{11}$$

where a grain of size b is pivoting over a grain of size K_b, and e and f are empirical coefficients. Li and Komar (1986) indicated that the coefficient f accounts for bed material nonuniformity and that the coefficient e reflects shape effects, with e decreasing as c/b (sphericity) increases. In addition, sliding motion occurred for low values of c/b and pivoting occurred for higher ratios. However, Carling, et. al. (1992) did not observe sliding as the mode of motion for any shapes. The pivot angle, Φ, accounts for particle exposure since Φ is smaller for large grains pivoting over smaller grains and larger for small grains pivoting over larger grains. Komar and Li (1986) demonstrated that values of e increase for imbrication of flat particles (reviewed later) as well as angularity. The increase in e indicates that flat and imbricated particles are harder to mobilize due to an increase in the pivot angle.

The critical shear stress for imbricated grains with a 23° imbrication angle is about 5 to 6 times higher than for spheres and 2 to 3 times greater than for particles lying flat instead of being imbricated. Komar and Li (1986) proposed a series of curves for varying pivot angles due to varying shapes and sizes, which are summarized in Figure 1. Grain top rotation is pivoting directly over the top of the

base grain, while saddle rotation is pivoting between the saddle of two grains. In the sand range the larger particles are removed while in the gravel range the smaller particles are selectively removed which may lead to armoring. Although this analysis only took the effects of pivoting angle on incipient motion into account, Komar and Li (1986) recognized the importance of relative protrusion on incipient motion referring to the work of Fenton and Abbott (1977).

2.4 Relative Protrusion

Relative protrusion refers to the fact that some grains protrude farther into the flow than others, thus being subjected to higher drag forces. This effect is magnified in shallow gravel bed streams (Baker and Ritter, 1975). Shields used uniform material on a 'flat bed,' but as pointed out by Fenton and Abbott (1977), a completely flat bed was probably not obtained by Shields because flat beds are especially difficult to obtain for small particles. This means that some particles may have protruded farther into the flow than others (relative protrusion).

Fenton and Abbott's (1977) experiments consisted of slowly pushing a test grain further into the flow and recording the height of the rod used to push the grain into the flow and determining the shear stress at the time that the particle was first entrained by the flow. They also used different shapes and densities for the grains, and indicated that there is little dependence on the different shapes used.

However, these grains were not imbricated so this finding suggests that imbrication is an important grain stability factor.

Figure 1 demonstrates the importance of relative protrusion on incipient motion. For the case of no protrusion (coplanar bed), p/D = 0, shear stresses are higher than the Shields value. From Figure 1, when p/D = 0, the critical shear stress, τ_c^*, is equal to 0.1 for high particle Reynolds numbers ($R_* > 1000$). Large values of p/D give critical shear stress values lower than those suggested by Shields. Compare the value of $\tau_c^* = 0.01$ for p/D = 0.6 (spheres resting on a hexagonal array of hemispheres), to the widely used values of dimensionless critical shear stress for a coplanar bed, $\tau_c^* = 0.03$, for first displacement, and $\tau_c^* = 0.06$ for a small finite rate of transport. Thus, the dependence of incipient motion on relative particle protrusion is very important. Carling (1983) also found that the Shields stress is inversely related to relative protrusion in shallow streams.

2.5 Effects of Mixture Sorting and Bimodality

Several researchers, including Neill (1968), Andrews (1983), and Wilcock and Southard (1988), have suggested that mixture sorting has little effect on the fractional initial motion conditions.

Wilcock (1992) investigated the effect of sediment mixture properties on bedload transport. The two main aspects of sediment mixtures studied were

mixture sorting and bimodality (size distribution containing two distinct modes). Experiments were conducted to determine the effects of mixtures on incipient motion and established motion of individual size fractions, bed surface texture, and bed configuration. The experiments utilized eight different sediment mixtures. To determine the effect of sorting alone, Wilcock used three sediments with the same mean diameter but different standard deviations. The standard deviations expressed in ϕ units were $\sigma_\phi = 0.2\phi, 0.5\phi, 0.99\phi$, where ϕ is the phi scale representation of particle size given by,

$$\phi = -\log_2 D \tag{12}$$

where D is in millimeters. The geometric standard deviation, σ_g in mm is related to σ_ϕ by,

$$\sigma_g = 2^{\sigma_\phi} \tag{13}.$$

Two sediments were made uniform (fine and coarse) for comparison with the nonuniform sediments, and the other three sediments were bimodal.

Results of the study verified earlier studies and indicated that incipient motion occurred at about the same shear stress for a wide range of unimodal and weakly bimodal mixtures. The critical shear stress for each grain size range was represented by a value a little smaller than a Shields value for D_{50}. Mixture sorting had little effect on the critical shear stress for distributions differing only in their

grain size distribution standard deviation. This suggests that the shape of the grain size distribution does not influence relative particle mobility at near threshold conditions. Further, the experiments verified that equal mobility is achieved at high shear stresses.

For the bimodal mixtures, the size independence of the critical shear stress found with unimodal mixtures was not found. The finer fractions moved at a lower shear stress than the coarser fractions, indicating some selective sorting. Wilcock (1993) reexamined the effect of bimodality and found that the incipient motion of individual fractions in bimodal sediments depends on the absolute and relative sizes, the separation or distance between the modes, and the proportion of sediment in each mode.

Ashworth and Ferguson (1989) also investigated the size selective entrainment of bedload. Their analysis focused on thresholds for entrainment based on mean and maximum particle sizes transported at varying shear stresses, transport rates of different size fractions, and the movement of tracer pebbles in three 'high power streams'. The results indicated that the threshold shear stress for gravel is dependent more on relative size, but does increase with absolute size. Consistent with other studies, they found an increase in median bed load diameter with increasing shear stress, with equal mobility at high shear stresses. The tracer study indicated some size selectivity with the larger particles moving less often and over

shorter distances than smaller particles despite strong relative size effects.

2.6 Shape Effects

2.6.1 Imbrication

As mentioned previously, shape effects influence incipient motion and bedload transport rates. In the review of Komar and Li's (1986) work, it was noted that flat particles were more resistant to movement due to imbrication. Imbrication is demonstrated in Figure 3 where one particle rests on the particle below with one end tilting up in the direction of flow.

The imbricated position is very stable due to the fluid force acting down on the particle as well as a high pivot angle. Carling, et al. (1992) noted that the possibility for imbrication is influenced by particle size, shape, and bed roughness, and found that the shear velocity required to induce imbrication was highest for discs. Li and Komar (1986) found an increase in the pivoting angle due to imbrication. An increased pivot angle provides greater resistance to incipient motion. They also found that the order of increasing entrainment difficulty is as follows: spheres, ellipsoidal grains, angular grains, and imbricated grains. Thus, the imbrication of flat particles plays a dominant role in their ability to be entrained.

2.6.2 Relative Mobility Studies

Lane and Carlson (1954) investigated the effects of shape on the transport of coarse material, including the effects of imbrication. In addition to particle shape measurements, they made hydraulic measurements including flow rate, water surface slope, channel area, width, and depth. The shape measurements included sphericity, Zingg type (Table 1), and visual classifications of roundness. The sphericity measure was given by cb/a^2 and the median sphericity of all the particles was 0.7 with a standard deviation of 0.103. The material in most of the test sections was imbricated.

Lane and Carlson (1954) found that flatter particles are less susceptible to movement than spherical particles of equal weight. On average the flat particles were of the same susceptibility to movement of spheres weighing 2.5 times as much. It should be noted that sampling errors and higher protrusion of spherical particles could contribute to some of these differences between the spherical and flat particles. Another point made by Lane and Carlson is that disc shaped particles may be more readily transported as suspended load than spherical particles because discs have lower settling velocities. Suspension is mainly due to upward turbulent velocities and lift forces, and these forces would be more effective on flat particles than more rounded ones. However, discs appear to be less readily transported as contact load than spherical particles.

Ashworth and Ferguson (1989) found that spherical particles moved farther than flat particles in a tracer pebble study, indicating lower transport rates for flat particles. Further, Mantz (1977) found lower transport rates for flakes compared to fine grains. Similarly, Carling, et al (1992) observed lower particle velocities for discs when compared to spheres for low velocity flows. However, at higher flow velocities over a very rough bed, the trend was reversed. The disc moved faster than a sphere, an ellipse, and a rod. Carling, et al (1992) attribute the disc's high particle velocity to its mode of motion (pivoting) which exposed the particle to higher velocity flows and possibly to enhanced lift due to the shape. In addition, flat particles were observed to move more easily over obstacles on the rough bed, but the sphere meandered around the obstacles, thus lengthening its travelled path and apparent velocity.

Wilcock and McArdell (1993) suggest a bimodal entrainment frequency of partially mobile coarse grains where more spherical particles resting higher above the bed are entrained more frequently than more bladed or disc shaped grains located lower on the bed.

Carling (1983) indicated that shape effects on bedload transport were negligible for a mixture of sizes in Great Eggleshope Beck (23% spheres, 58% discs, 10% blades, and 9 % rods) and Carl Beck (47% spheres, 37% discs, 7% blades, and 11% rods). However, they indicated that this may have been due to

the wide range of shapes.

2.6.3 Mode of Motion

Komar and Li (1986) observed that flat particles slid off the base grains rather than pivoting with a rolling motion. The high pivot angle of flat particles necessitates a higher fluid force to overcome the resistance due to the pivot angle. They suggested the low values of c/b (c/b < 0.6-0.7) that are indicative of flat particles restricted their motion mainly to sliding. Contrary to these findings, Carling, et al (1992) did not observe disc sliding as the mode of motion. Instead, the disc pivoted or rolled, with sliding occurring only as the particle readjusted before pivoting or imbrication. Further, Mantz (1980) in his experiments on discs, observed that the discs tended to "glide" and occasionally were transported at a constant distance above the bed for several seconds which indicates that these particles may have been in suspension.

2.6.4 Bed Stability

Mantz (1980) investigated the effect of bed stability on transport rates over flat beds. In addition, the influence of particle shape on transport was examined by using artificial lightweight discs as sediment. Results of flume experiments indicated that discs traveled more slowly when compared to pea gravel and granite

chippings, of the same nominal diameter, D_N, and $\rho' = \rho_s - \rho$. Although these particles had the same nominal diameter, this does not imply that they had the same sieve diameter.

The bed stability condition provides for different transport - shear relationships. The average critical dimensionless bed shear stress was between 0.024 and 0.04 for the minimum stability beds for grains and discs, and was greater than 0.05 for armored grain beds and 0.10 for imbricated disc beds.

It was mentioned earlier that previous researchers have indicated that the Shields value of $\tau_c^* = 0.06$ for $R_* > 500$ gives small but nonzero transport rates, and that the value of $\tau_c^* = 0.03$ is more indicative of the initial motion condition of most sediments. Mantz's results indicate that the value of $\tau_c^* = 0.03$ describes the initial motion conditions of both non-imbricated discs and more bulky particles. However, imbricated discs are entrained at a critical shear stress 3.33 times higher than more bulky particles. This reinforces the importance of imbrication as a stability factor for flat particles.

Some conclusions from Mantz are that the disc motion was influenced by the shear stress on the disc during impact, and that discs moved more slowly than the more spherical particles. When compared to coarse grain transport rates, changing the disc bed stability from minimum to maximum was equivalent to a 3 fold increase in grain size. Thus, grain imbrication, interlocking, and impact

influence the initiation of motion.

In addition, several investigators, including Johansson (1976), Proffitt (1980), and Carling, et al (1992), have observed that particles frequently reposition themselves to provide maximum resistance to their entrainment.

2.6.5 Shale Study

Magalhaes and Chau (1983) investigated the initiation of motion for shale sediments having a low density (1850 kg/m^3) and platy shape in a laboratory flume. The average Zingg shape was oblate with a b/a ratio of 0.68 and c/b ratio of 0.26. The Corey shape factor (Corey, 1949), CSF, given by,

$$CSF = \frac{c}{\sqrt{ab}} \tag{14}$$

was 0.20 for the shale particles compared to spherical particles which have a Corey shape factor of 1.0. The bed material ranged in size from 1 to 35 mm and was separated into six samples with D_{50} = 1.8, 3.5, 7.5, 11.1, 15.9, and 22.2 mm. A visual observation of the initiation of motion was used for D_{50} = 1.8 and 3.5 mm. Sediment discharge rates were measured for the 5 coarsest samples over periods of 20 to 80 minutes until the bed was "considerably deformed", and a linear regression method was used to estimate the critical shear stresses.

Shields curve predicted critical shear stresses for the shale within 15% when the density is taken into account. The critical dimensionless shear stresses, τ_c^*, increased with grain Reynolds number from about 0.02 at R. = 35 to 0.05 at R. > 1000. Magalhaes and Chau concluded that Neill's recommended Shields parameter, $\tau_c^* = 0.03$, should be satisfactory for shale sediments.

These results are similar to Mantz's results for non-imbricated discs. The reason given by Magalhaes and Chau for the lower critical shear stresses for shale is higher lift forces acting on the thin plates with rounded corners. However, Mantz indicated that the bed stability condition must be considered since it plays a dominant role in determining the critical shear stress for flat particles. The lower shear stresses obtained by Magalhaes and Chau can be attributed to a bed of minimum stability with no imbrication, whereas higher critical shear stresses may have been obtained by providing a bed of higher stability by allowing the particles to become imbricated and then measuring the transport rates and subsequently determining the critical shear stresses.

2.7 Bedload Transport

The previous discussion focused primarily on the effects of size and shape on the inception of motion. A logical step after evaluating incipient motion is to estimate the factors influencing the amount of sediment transported. A key factor

in bedload transport in gravel-bed streams is the presence of a coarse surface layer. Before discussing bedload transport relations, the formation and structure of the surface layer is required.

2.7.1 The Coarse Surface Layer

In the past the coarse surface layer has been described both by the terms armor and pavement interchangeably. In the review and analysis that follows the term armor corresponds to conditions for which the equilibrium transport rate approaches zero. The term pavement corresponds to conditions for which the equilibrium transport rate does not approach zero.

Jain (1990) developed a flow criterion for the formation of armor and pavement layers using a series of conceptual experiments. Jain (1990) argues that a coarse surface layer only forms when the eroded material (EM) is finer than the parent bed material (PBM), and proposed the following definition for armor and pavement: "A coarse surface layer is a pavement or armor, if the flow shear velocity is, respectively, larger or smaller than the transitional shear velocity." The transitional shear velocity, u_{*_t} , corresponds to a bed of maximum surface coarseness, and may be estimated using Chin's (1985) criterion. Jain (1990) suggested that in the armor formation region, $u_* < u_{*_t}$, the bed coarsens with increasing shear velocity, but in the pavement formation region, $u_* > u_{*_t}$, the bed

surface layer becomes finer with increasing shear velocity. For zero sediment influx conditions, Jain (1990) asserts that during armor formation the EM is finer than the PBM, but remains relatively constant in accord with the work of Proffitt (1980) and Mosconi (1988) with the transport rate approaching zero at equilibrium for armored conditions. During pavement development Jain (1990) suggests that the EM is finer than the PBM, but the EM coarsens and is identical to the PBM at equilibrium, with the surface layer as the regulator.

Parker and Klingeman (1982) suggest that the pavement, or coarse surface layer, is present not only at low flows but at higher flows capable of transporting all grain sizes, and that the structure of the pavement is similar at both low and high flows. Parker and Klingeman (1982) argue that the pavement controls the transport of fine and coarse material such that the pavement changes to create near equal mobility conditions. This would imply a bedload size distribution approximating that of the subsurface size distribution as indicated above for a pavement at equilibrium.

2.7.2 Bedload Transport Relations Based on the Bed Subsurface Layer

2.7.2.1 Original Similarity Approach

Parker, et. al. (1982) sparked a renewed interest in bedload transport in gravel streams in their article analyzing the size distribution of bedload in a paved

gravel bed stream using the data from Oak Creek by Milhous (1973). A similarity approach was employed to develop a method for calculating the total bedload as a function of the subpavement D_{50} and bed shear stress. As a first approximation, equality was assumed between the bedload size distribution and the subsurface bed size distribution for shear stresses in excess of the critical shear stress of the pavement. Therefore, it was assumed that equal mobility was achieved once the pavement was broken. Equal mobility is attained when all bed material particle sizes are moved at the same critical shear stress for a given transport rate. As will be discussed in Chapter 4, equal mobility conditions depend on the transport rate so that equal mobility may occur at near threshold conditions or at high transport rates. Equal mobility indicates that only the subsurface D_{50} is required to describe bedload motion. This result would suggest that sand and gravel streams may be treated the same way, and the wide range of sizes in the gravel-bed stream does not complicate the analysis. However, bed surface coarsening would still occur due to size selective entrainment in the surface layer. Assuming equal mobility one can compute the total bedload as a function of the subpavement D_{50}, $q_B = f(\tau, D_{50})$ or in dimensionless terms, $W_i^* = f(\tau_i^*, \bar{D}_i/D_{50})$. A similarity collapse of the data was performed as follows. Curves of the form,

$$W_i^* = \alpha_i \tau_i^{*m_i} \tag{15}$$

were fitted by log - log regression to a plot of the dimensionless bedload transport rate for various size fractions, W_i^*, against dimensionless shear stress, τ_i^*, where,

$$W_i^* = \frac{q_{Bi}^*}{\tau_i^{*1.5}} = \frac{Rq_{Bi}}{f_i\sqrt{g}(HS)^{1.5}} \tag{16}$$

$$\tau_i^* = \frac{\tau}{\rho g R \overline{D}_i} \tag{17}$$

$$q_{Bi}^* = \frac{q_{Bi}}{f_i\sqrt{RgD_i}\,\overline{D}_i} \tag{18}$$

The values of m_i, obtained from regression, increased with grain size, indicating that perfect similarity ($m_1 = ... = m_i$) does not hold. However, a weighted average value of m_i was computed, and regression yielded new values of α_i. These values of α_i were used to calculate τ_{ri}^* for a reference transport value of, W_r^*=0.002. The values of τ_{ri}^* were plotted against $\overline{D}_i/D_{50}$ and a log-log regression of the form,

$$\tau_{ri}^* = \tau_{r50}^* (\overline{D}_i/D_{50})^{-\beta} \tag{19}$$

was performed.

Equal mobility for a given transport rate is achieved for $\beta = 1$. Parker obtained a value of 0.982, and argued that this value was sufficiently close to 1 that equal mobility is roughly achieved. However, since β is slightly less than 1, finer

particles will be more mobile. As will be discussed later, the parameters of Eq. 19 change depending on the value of the reference transport rate, W_r^*. As W_r^* is increased, both β and τ^*_{r50} increase, so that for some sufficiently large value of W_r^*, $\beta = 1$, and equal mobility is achieved.

The Oak Creek data indicated that lower flows correspond to smaller median bedload sizes, while higher flows yielded larger median bedload sizes. Thus, while equality between bedload and subsurface size distributions was approached for Oak Creek it was not attained as indicated by deviations between the bedload and subsurface size distributions with bed shear stress (Milhous, 1973).

A similarity collapse is realized by determining the normalized shear stress for each size range given by the following expression,

$$\phi_i = \frac{\tau_i^*}{\tau_{ri}^*} \tag{20}$$

and plotting W_i^* vs. ϕ_i. The similarity collapse was described by the expression,

$$\frac{W_i^*}{W_r^*} = \phi_i^{m_i} \tag{21}.$$

Parker, et. al. tested their relation with other river data and found that their functional relation was good for gravel streams with moderate to steep slopes without much sand washload. They also found that the Meyer-Peter and Muller

(1948) relation which has often been used for gravel streams did not describe the data well.

2.7.2.2 Modified Similarity Approach

Diplas (1987) provided a new similarity approach using dimensional analysis. Assuming the material is of the same general shape and size distribution with high particle Reynolds number, R. > 1000, and large dimensionless flow depth, H/D_g, where H is flow depth and D_g is the subsurface geometric mean grain size, Diplas (1987) suggested that,

$$W_i^* = f\left(\tau_i^*, \frac{\overline{D_i}}{D_g}, \sigma_g\right) \qquad (22).$$

This implies that the transport rate depends on the grain size distribution. Diplas incorporated the dependence of the transport rate on $\overline{D}_i$ into the similarity approach, and obtained,

$$W_i^* = \alpha_i\left[\tau_i^{*(\overline{D}/D_{50})^b}\right]^{m_i'} \qquad (23)$$

where b = 0.3214. The m_i' values found from the above relation were much less variable than the m_i values from the original formulation by Parker, et. al. (1982) Excluding the coarsest size range, Parker, et. al. (1982) obtained m_i values ranging from 5.51 to 21.45 (290%) typically increasing with $\overline{D}_i$, whereas Diplas (1987)

obtained m_i' values ranging from 12.93 to 14.97 (16%) showing no trend with $\bar{D}_i$. Thus, the inclusion of the size dependence eliminated the increase of m_i with $\bar{D}_i$. A similarity collapse of the data was made, yielding,

$$\frac{W_i^*}{W_r^*} = [\phi_i^{(\bar{D}_i/D_{50})^b}]^{m_i'} \tag{24}$$

where b = 0.3214, m_i' = 13.71, and W_r^* = 0.0025 is a reference value of W_i^*.

Diplas (1987) also accounted for relative protrusion due to a nonuniform mixture, which increases the mobility of the larger particles, by using a hiding function, h. The hiding function was shown to be a function of both $\bar{D}_i/D_{50}$, as well as $\phi_{50} = \tau_{50}^*/\tau_{r50}^*$. Under the old similarity approach, h was assumed to be dependent only on $\bar{D}_i/D_{50}$ suggesting that the composition of the bedload remains unchanged as the bed shear stress varies, and more specifically that the finer grains will always be more mobile than the coarser grains regardless of ϕ_{50}. Since h does depend on ϕ_{50}, a single particle size cannot be used to determine the mobility in nonuniform material, because the representative grain diameter that describes the mobility of the whole bed material will change with bottom shear stress.

Diplas (1987) extended the formulation to cover a wider range of Shields stresses. It has been shown that, at high Shields stresses, the size distribution of bedload coincides with that the bed material (Einstein, 1950), and that the surface

bed layer is equal to the subsurface material (Parker and Klingeman, 1982). This implies that $W_1^* = ... = W_i^* =$ constant at high Shields stresses. At low Shields stresses the surface bed layer material is coarser than the subsurface material.

Results of Diplas' paper reflect the variation of bedload median size with ϕ_{50}. Initially, the bedload is finer than the subsurface and the bedload median size increases with ϕ_{50} and becomes coarser than the subsurface median size up to a certain limiting value of ϕ_{50}. For higher values of ϕ_{50}, the bedload D_{50} decreases and approaches the subpavement D_{50}. Finally, the bed surface material varies with Shields stress. It is coarsest at near critical conditions and at higher shear stresses the bed surface material becomes less coarse approaching the subsurface median size. These results are in agreement with the previous discussion on the pavement layer.

2.7.2.3 Grain Size Distribution Approach

Shih and Komar (1990) also analyzed the bedload data of Oak Creek. However, they used a grain size distribution approach utilizing a Rosin distribution to describe the differential bedload transport rates. Shih and Komar (1990) indicated that in order to use this method, the relation between bedload grain size distributions and bed material distributions at different flow stages must be known. Diplas (1992) suggested that this is a major drawback since the resulting relation

cannot be used as a predictive tool for other streams and, therefore, lacks generality. Such an approach requires extensive data collection for every new river of interest.

2.7.3 Bedload Transport Relations Based on the Bed Surface Layer

The original substrate (subsurface) based bedload relation of Parker (1982) was transformed into one based on the bed surface material (Parker, 1990). This was done to provide a relation that could be inverted to calculate the surface material composition and account for nonequilibrium bedload transport conditions. In addition, Parker asserted that a bedload relation should be based on the surface layer since it is the layer subjected to the fluid forces initiating motion. The Oak Creek data, excluding the sand fraction (D < 2 mm), were used to develop the preliminary surface based relation given by:

$$W_{si}^{*} = 0.00218\ G[\omega\ \phi_{sgo}\ g_o(\delta_i)] = \frac{R\ g\ q_{Bi}}{(\tau/\rho)^{1.5} F_i} \qquad (25)$$

where q_{Bi} is the volumetric bedload transport rate per unit width, F_i is the volume surface fraction in the *ith* size range, and G is determined by one of the following expressions based on the Oak Creek subsurface analysis,

$$G = 5474(1 - 0.853/\phi)^{4.5} \qquad \phi > 1.59 \qquad \textbf{(26a)}$$

$$G = \exp[14.2(\phi - 1) - 9.28(\phi - 1)^2] \qquad 1 < \phi < 1.59 \qquad \textbf{(26b)}$$

$$G = \phi^{14.2} \qquad \phi < 1 \qquad \textbf{(26c).}$$

The parameter g_o denotes a surface-based reduced hiding function,

$$g_o(\delta_i) = \delta_i^{-\beta} \qquad \textbf{(27)}$$

$$\delta_i = \frac{\overline{D_i}}{D_{sg}} \qquad \textbf{(28)}$$

and the parameters β and D_{sg} are given by,

$$\beta = 0.0951; \qquad \ln D_{sg} = \sum F_i \ln \overline{D_i} \qquad \textbf{(29 a, b)}$$

The value of β was determined by a regression of a subsurface based reduced hiding function, g_s, against $\overline{D}_i/D_{50}$, for $\phi_{50} = 1.3$. Thus, it is questionable if the above value of β is valid for ϕ_{50} different than 1.3. The normalized bed shear stress ϕ_{sgo} is given by,

$$\phi_{sg0} = \frac{\tau^*_{sg}}{0.0386}; \qquad \tau^*_{sg} = \frac{\tau}{\rho R g D_{sg}} \qquad \textbf{(30 a, b)}$$

where 0.0386 is the value of τ^*_{rsgo} determined for $\phi_{sgo} = \phi_{sg} = 1$ and $\phi_{50} = 1.035$. The straining parameter for an arbitrary sediment, ω, was determined by assuming

a linear variation of σ_ϕ from a uniform sediment to the Oak Creek sediment, and is given by,

$$\omega = 1 + \frac{\sigma_\phi}{\sigma_{\phi 0}}(\omega_0 - 1) \tag{31}$$

The standard deviation of the surface material on the phi scale, σ_ϕ, is given by,

$$\sigma_\phi^2 = \sum [\frac{(\ln(\overline{D}_i/D_{sg})}{\ln(2)}]^2 F_i \tag{32}$$

and σ_ϕ is related to the geometric standard deviation of the surface layer by,

$$\sigma_{sg} = 2^{\sigma_\phi} \tag{33}$$

The functional relations,

$$\omega_0 = \omega_0 (\phi_{sg0}); \qquad \sigma_{\phi 0} = \sigma_{\phi 0} (\phi_{sg0}) \tag{34 a, b}$$

are found from plots of ω_o and $\sigma_{\phi o}$ versus ϕ_{sgo}.

The above model predicts the bedload transport rate and size distribution for given flow conditions and bed surface size distribution. The model can be inverted so that for given flow conditions, bedload transport rate and composition, one can determine the surface layer composition by solving for F_i,

$$F_i = \frac{p_i \,/\, G[\omega\ \phi_{sg0}\ g_o(\delta_i)]}{\sum p_i \,/\, G[\omega\ \phi_{sg0}\ g_o(\delta_i)]} \tag{35}.$$

Parker's (1990) hiding function will always render the finer particles in the surface layer more mobile than the coarse particles. This implies that hiding is a function only of relative particle size, $\bar{D}_i/D_{50}$. However, Diplas (1987) demonstrated that the hiding function depends both on ϕ_{50} and $\bar{D}_i/D_{50}$,

$$h_1\ (\phi_{50},\ \overline{D_i}/D_{50}) = \phi_{50}^{[(\overline{D_i}/D_{50})^{0.3214}\ -\ 1]}\ [(\overline{D_i}/D_{50})^{-0.057}]^{(\overline{D_i}/D_{50})^{0.3214}} \qquad (36)$$

and that for $\phi_{50} > 1.2$ the coarser grains become more mobile. For $\phi_{50} < 1.2$ the bedload is finer than the subsurface, and coarser than the subsurface for $\phi_{50} > 1.2$. Note that Parker used the singular value of $\phi_{50} = 1.3$ for both the subsurface and surface reduced hiding functions. In addition, the value of β in Parker's hiding function will change depending on the value of ϕ_{50} used to determine it.

Parker's (1990) transformation forced the result that $G(\phi_{50}) = G_T(\phi_{50})$ and equates two equations of different magnitude. The transformation equated a zero*th* order transport function with a first order transport function (Eq. 25). A zero*th* order transport function means that the total transport rate, W^*, is predicted on the basis of D_{50} alone. A first order transport function means that W^* is based on fractional transport rates so that $W^* = \Sigma\ W_i^*$, and $\bar{D}_i$ comes into the equation. The zero*th* order equation is based on an equal mobility condition, while the first order equation can presumably provide varying bedload composition with shear stress. However, Parker uses only one value of ϕ_{50} in defining the hiding function.

A Taylor expansion of $G[g_s(\bar{D}_i/D_{50})\phi_{50}]$ about ϕ_{50} shows that the above is true only if the higher order terms are neglected so that W_i^* is dependent only on $G[\phi_{50}]$ and the slope $G'[\phi_{50}]$ is forced to zero and neglected. Since $G'[\phi_{50}]$ is not zero Parker's reduced hiding function is not actually valid for all ϕ_{50}.

2.7.4 Surface Based Fractional Transport Rates

Wilcock and McArdell (1993) provided coupled flow conditions, bedload transport rates, and bedload and surface size distributions using painted sediment and photographic surface sampling. Wilcock and McArdell (1993) used both a critical shear stress for initial motion and a partial transport shear stress to describe regions of partial and complete mobilization. Complete mobilization is described solely by the amount of material on the surface available for transport. Partial transport is described both by the amount of material available and the amount remaining immobile on the bed surface.

Wilcock and McArdell (1993) suggested that the largest fully mobilized grain may be determined by finding the largest grain for which p_i is greater than or equal to F_i, and that the size of the largest fully mobilized grain increases with shear stress. Wilcock and McArdell (1993) indicated that division between partial and complete mobilization is defined more clearly using surface scaled transport rates, but that the division can also be seen using subsurface scaled transport rates.

The phenomenon of partial and complete mobilization was documented previously by Milhous (1973) and Parker, et al (1982) for Oak Creek, although not using these terms. The data from Oak Creek indicate that, below a certain water discharge, transport rates are determined by sediment availability (unbroken pavement) while at higher discharges (broken pavement) the transport is controlled by hydraulic conditions and not availability.

2.7.5 Fractional Bedload Transport Relation With a Suspension Criterion

Bridge and Bennett (1992) developed a bedload transport model that accounts for the variation of size, density, and shape within a sediment mixture, turbulent fluctuating fluid forces, and the amount of sediment available for transport. Although Bridge and Bennett provide a more sophisticated suspension criterion, a simpler suspension criterion which is applicable to the present study is given by,

$$u_s \geq u_* b \tag{37}$$

where u_s is the grain settling velocity, u_* is the bed shear velocity, and b = 0.8-1.0. To find the maximum particle size in suspension one simply solves for u_s for a given u_* with Eq. 37 and determines the particle size corresponding to u_s. Bridge and Bennett (1992) refer to Dietrich's (1982) equations and curves which account

for particle shape for determining the particle size from settling velocity.

Results of Bridge and Bennett's study indicated that accurate specification of both the pivot angle and size distribution of available sediment must be made. In addition, the pivoting angle was found to have the most influence at incipient motion and negligible effect for large particle sizes (D > 20mm), while the dynamic friction coefficient, μ, has significant effect on the fractional transport rates.

The Bridge and Bennett formulation takes shape effects into account while determining the grain settling velocity, pivoting angle, and relative protrusion. However, this formulation is for a specified shape. It appears that a sediment consisting of mixture of sizes, densities, and shapes could be modelled by a fractional relation accounting not only for size and density ranges but also particle shape ranges.

2.8 Discussion of the Previous Studies

Based on the results of the previous studies on the effects of particle shape, the bed stability condition appears to play a major role in the determination of the initial motion conditions for discs. The discrepancies in the studies are attributed to different bed stability conditions for disc-like particles. Magalhaes and Chau (1983) concluded that the critical shear stress for flat particles is well represented by a value of $\tau_c^* = 0.03$ which is typically used for more bulky particles. However, their flat grains were not imbricated, and their results agree with Mantz's (198) results for non-imbricated grains. Namely, non-imbricated discs are entrianed at critical shear stresses similar to those of other non-imbricated sediments. However, imbricated discs were entrained at critical shear stresses significantly higher than more spherical particles, indicating that imbricated discs are relatively less mobile than more spherical grains.

A major criticism of bedload transport relations is that they are site specific or can only be used for one type of stream. The reason for this criticism is that the relations are usually tested and developed using a limited range of data. As a rule, the range of the various parameters used to obtain a sediment transport expression should be used and followed when the same expression is employed in another stream. Unreasonable results may be obtained when the same expression is used outside its original range without first testing the expression. In addition, the lack

of a wide range of data due to the difficulty in obtaining bedload data further complicates the ability to test the models over a wide range of conditions.

Typically, if the entire $W_i^* - \tau_i^*$ relation from the lowest to the highest possible transport rates is plotted on log - log scales the slope of the relation given by Eq. 15, m_i, varies with transport rate and shear stress. Generally, the slope decreases with increasing transport rate. However, most data sets cover only a portion of the entire transport - shear domain. Therefore, $W_i^* - \tau_i^*$ relations may be approximated locally by linear log-log relations of the form of Eq. 15. However, applying these relations to transport rates and shear stresses outside the data range from which they were derived introduces error since we impose linearity to a curved relation. Note that the reference shear stresses need not be determined from the $W_i^* - \tau_i^*$ regression relations, but may instead be read directly from the graphs of W_i^* vs. τ_i^*. However, this method is also inadequate when trying to determine a reference shear stress, τ_{ri}^*, for a W_r^* value that is outside the given data range. In the similarity approaches a single value of W_r^* is used to provide a similarity collapse of the data. This approach is valid only in the region for which the m_i value is assumed to be constant. A single value for W_r^* for a similarity collapse of the entire $W_i^* - \tau_i^*$ curve would be inappropriate since the m_i value changes along the same $W_i^* - \tau_i^*$ curve. One possible solution to this problem is to divide the entire $W_i^* - \tau_i^*$ curve into sections with nearly constant

m_i and use a different W_r^* value for each of these sections.

In addition, bedload transport data for different streams cover a wide range of transport values. For example, the lowest measured transport rate for stream A may be much different than the lowest measured transport rate for stream B. Problems may arise in choosing a consistent value of W_r^* due to the different range of transport rates for various streams.

2.9 Summary

The previous review provided a framework of the various approaches to incipient motion and bedload transport. The effects of relative protrusion, pivoting angle, sediment mixture nonuniformity, bimodality, and shape on particle entrainment were reviewed. The results of most of these studies generally agree. These results can be summarized as follows:

1. High relative protrusion results in lower critical shear stresses.
2. A large pivot angle, such as that for flat, imbricated grains, results in lower critical shear stresses.
3. For many types of nonuniform sediment mixtures threshold conditions for individual size fractions have been shown to occur at approximately the same shear stress. This indicates equal mobility

at near threshold conditions.

4. Strongly bimodal sediments experience size selective entrainment with the coarser grains moving at lower shear stresses than for a uniform sediment.
5. The mean bedload diameter increases with increasing shear stress, with equal mobility approximated at the highest shear stresses.
6. Non-imbricated discs are entrained at a critical shear stress similar to that of more bulky grains, indicating that non-imbricated discs are of the same mobility as more bulky sediment.
7. Imbricated discs are entrained at a critical shear stress siginificantly higher than more bulky sediments, indicating that imbricated discs are relatively less mobile than more bulky grains.

Conclusions concerning the mode of motion of discs have produced conflicting results. Komar and Li (1986) observed sliding as the mode of motion, while Carling, et al (1992) observed pivoting and rolling. The current study does not include a mode of motion study, but instead focuses on the relative mobility of discs and spheres. To verify the finding that flat, imbricated particles are more difficult to entrain, a relative mobility comparison of discs and spheres is required.

The data from which many of these bedload transport studies are based covers only a portion of the total transport range. Therefore, the bedload transport phenomenon must be studied over a wide range of transport rates. In addition, results from bedload transport analyses using the subsurface and surface based approaches may be in conflict since they are based on different bed material size distributions. Therefore, a comparison of the subsurface and surface based approaches is required.

Table 1. Zingg Classification of Particle Shape.

Class	Shape	b/a	c/b
I	Disks	> 2/3	< 2/3
II	Spherical	> 2/3	> 2/3
III	Blades	< 2/3	< 2/3
IV	Rodlike	< 2/3	> 2/3

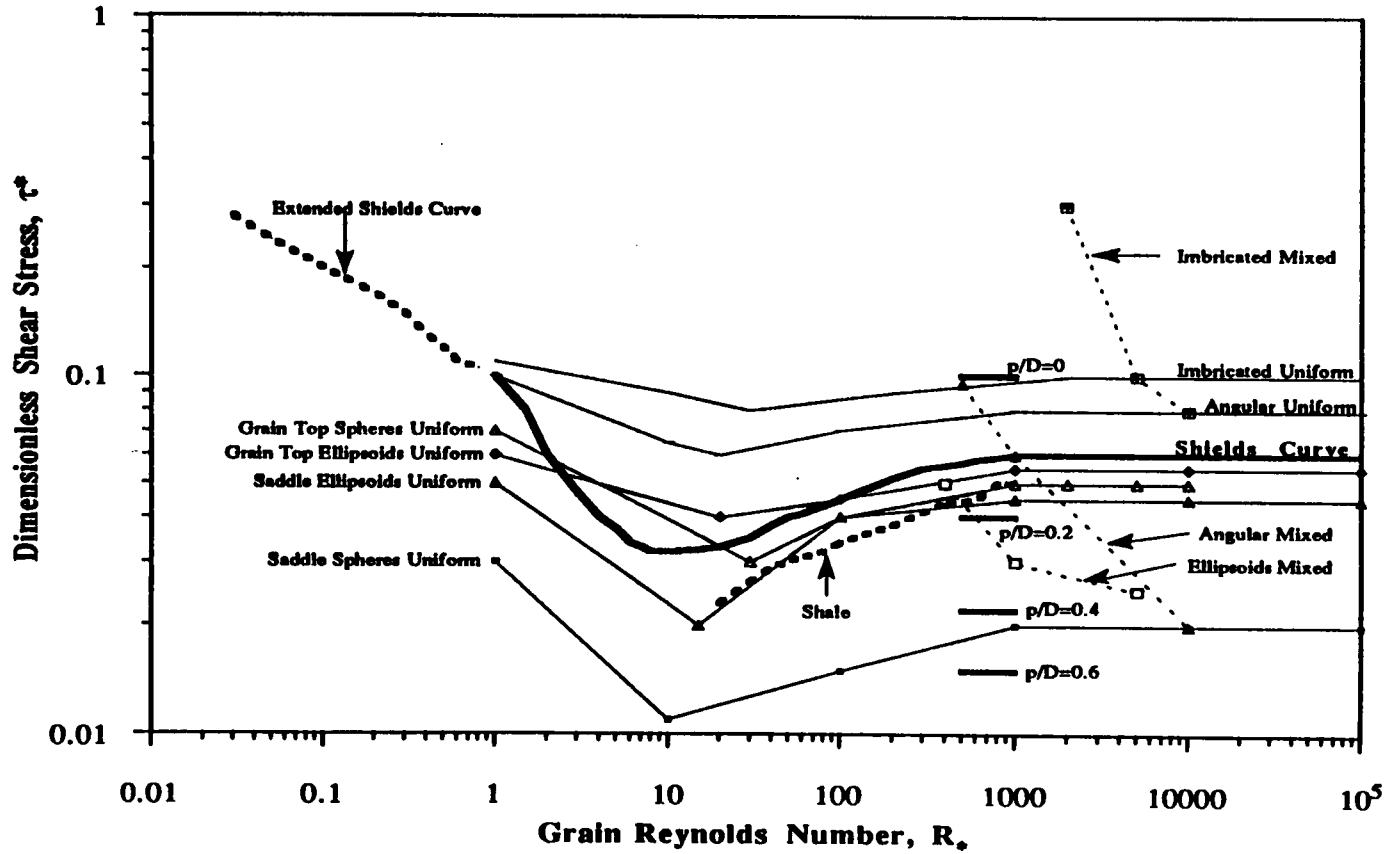

Fig. 1. Modified Shields curve including the extended region for R. < 1 proposed by Mantz (1977) and Yalin and Karahan (1979), the effects of grain size, shape, and imbrication proposed by Komar and Li (1986), the effects of relative protrusion, p/D, proposed by Fenton and Abbott (1977), and the results of a shale study by Magalhaes and Chau (1983).

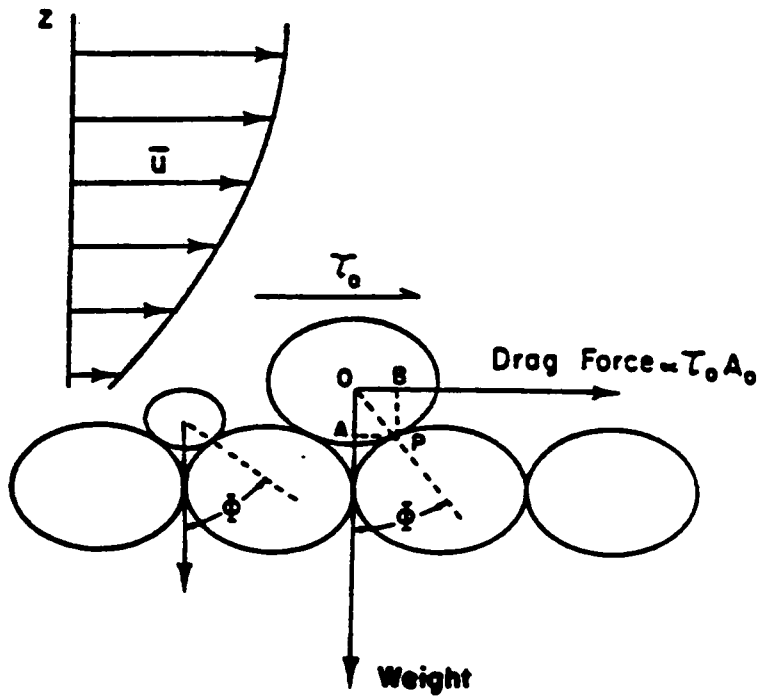

Fig. 2. Pivoting angle analysis for a submerged ellipsoidal grain, from Komar and Li (1986).

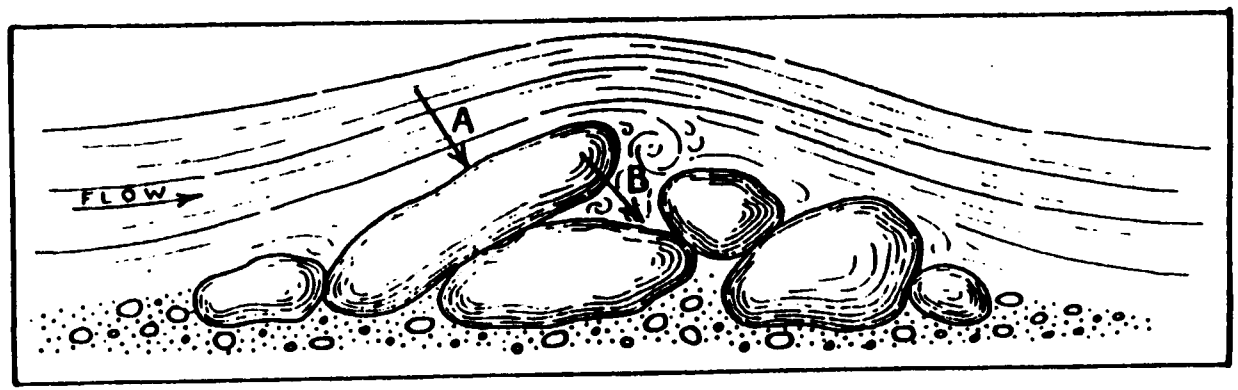

Fig. 3. Illustration of an imbricated grain, from Lane and Carlson (1954).

Chapter 3. Method of Analysis

3.1 Similarity Approach with Fractional Transport Analysis

Fractional transport analysis based on either the bed subsurface or surface layer, in conjunction with the concept of similarity, is suitable for investigating transport rates ranging from initial motion to the highest attainable transport rates. Further, this approach is suitable for investigating the effects of particle shape on bedload transport.

3.1.1 Fractional Transport Analysis

As stated previously, gravel-bed streams typically consist of a variety of particle sizes in the sand and gravel size ranges. Streams exhibiting this grain size nonuniformity require the use of fractional bedload transport rates for their analysis, since a single average particle size may not represent the entire bed material effectively.

Fractional bedload transport analysis consists of dividing the bed material and bedload size distributions into N size ranges. Each size range is then described by a representative particle diameter, $\bar{D}_i$. Volumetric bedload transport rates, q_{bi}, for each size range, may then be calculated from the total volumetric bedload discharge, q_b, with knowledge of the fraction of material in each bedload size range, p_i, by $q_{bi} = p_i q_b$. Transport-shear relations which describe the change in

transport rate with bed shear stress may then be plotted for the fractional transport rates and shear stresses for each size range.

3.1.2 Similarity Approach

The idea behind a similarity analysis for bedload transport is the transformation of fractional bedload transport-shear stress relations so that they can be collapsed into one relation for all size ranges. Parker, et al (1982) used a similarity approach similar to that of Ashida and Michiue (1972) in the analysis of data from Oak Creek. Diplas (1987) then modified this approach to account for the dependence of the transport rate on grain size.

For similarity analysis the fractional transport rates and corresponding bed shear stresses must be expressed in terms of dimensionless transport rates and shear stresses using either the subsurface material size fractions, f_i, or the bed surface size fractions, F_i, sediment properties, and flow conditions. The dimensionless transport rate for each size range, W_i^*, and dimensionless shear stress for each size range, τ_i^*, are given by Eqs. 16 and 17 respectively.

The dimensionless transport rate, W_i^*, may then be plotted against the dimensionless shear stress, τ_i^*, for each size range. Typically, if the total transport-shear relation from the lowest to the highest possible transport rates is plotted on log-log scales the slope of the relation varies with transport rate and

shear stress. Generally, the slope decreases with increasing transport rate. However, most data sets cover only a portion of the entire transport-shear domain. Therefore, W_i^*-τ_i^* relations may be approximated locally by linear log-log relations of the form of Eq. 15 ($W_i^*=\alpha_i\tau_i^{*m_i}$).

These W_i^*-τ_i^* relations for each size range may then be collapsed into a single relation for all size ranges with the aid of a reference dimensionless transport rate, W_r^*. The W_r^* value is the same for all grain size ranges. Using the log-log relations determined previously, for a chosen W_r^*, dimensionless reference shear stresses, τ_{ri}^*, may be obtained. Alternatively, the τ_{ri}^* values may be read directly from the graphs of W_i^*-τ_i^*. These τ_{ri}^* values, for a given W_r^*, are used to compute a normalized shear stress given by Eq. 20 ($\phi_i = \tau_i^*/\tau_{ri}^*$). The similarity collapse is realized when W_i^* is plotted against ϕ_i giving the relation of Eq. 21 ($W_i^*/W_r^*=\phi_i^{m_i}$).

Perfect similarity occurs when the slopes, m_i, of the transport - shear relation given by Eq. 15 are equal, so that $m_1 = ... = m_i$. Parker, et al (1982) indicated that perfect similarity does not occur for Oak Creek. This is demonstrated by a consistent increase in the slope values, m_i, with grain size. Diplas (1987) modified the above similarity approach by introducing a new similarity parameter that accounts for the dependence of W_i^* on $\bar{D}_i$. Log-log relations of the form of Eq. 23 ($W_i^*=\alpha_i[\tau_i^{*(\bar{D}i/D50)^{\wedge}b}]^{mi'}$), are used to describe the data. The exponent b is

obtained by a linear log-log relation between the original m_i values and $\bar{D}_i/D_{50}$. When the above relation between W_i^* and τ_i^* is regressed for Oak Creek, the m_i' values are nearly constant and do not increase with grain size. As W_i^* increases the exponent b in Eq. 23 decreases and approaches zero at very high transport rates. In addition, as W_i^* increases the m_i values decrease and the m_i' values approach the m_i values. The proposed new similarity collapse is described by an equation of the form of Eq. 24 ($W_i^*/W_r^*=[\phi_i^{(\bar{D}i/D50)^{\wedge}b}]^{mi'}$).

3.1.3 Reference Transport Critical Shear Stresses

The reference shear stresses described above may be determined for any given reference transport rate ranging from near initial motion conditions to very high transport rates. Recall that a critical shear stress describes the initial motion condition for a particle. Therefore, when the reference transport rate is chosen to correspond to near initial motion conditions the reference shear stress may be thought of as a critical shear stress for initial motion. These are termed the reference transport critical shear stresses and correspond to the same W_r^* value. The critical shear stresses may then be compared to other data to describe the relative mobility of grains. Specifically, the effects of particle shape and surface coarseness on bedload transport may be investigated.

A relation between the reference shear stress, τ_{ri}^*, and relative grain size, $\bar{D}_i/D_{50}$, of the form of Eq. 19 ($\tau_{ri}^*=\tau_{r50}^*(\bar{D}_i/D_{50})^{-\beta}$), where τ_{r50}^* is the reference shear stress for the median grain size, provides valuable information on the relative mobility and selective transport of the fine and coarse particles for a given transport rate. For a particular value of W_r^* a value of $\beta = 1$ indicates equal mobility wherein all particles are mobilized at the same dimensional bed shear stress. Values of β different than 1 indicate conditions of selective transport. Values of $\beta < 1$ indicate that the finer particles are mobilized at critical shear stresses smaller than those for coarse particles, whereas when $\beta > 1$, the coarse particles are mobilized first.

Further, the value of the reference critical shear stress for the median grain size, τ_{r50}^*, for one data set may be readily compared to other data sets. This comparison can provide the relative initial mobility of particles of different shape and from different bed conditions.

3.1.4 Subsurface and Surface Scaled Dimensionless Transport Rates

In the previously given expression for the dimensionless transport rate, Wi*, either the bed subsurface fraction, f_i, or the bed surface fraction, F_i may be used. The remaining analysis is identical for both the subsurface and surface approaches. The use of both approaches in the similarity analysis will allow comparison of the

results of the two approaches.

3.2 Discussion of Perfect Similarity and Equal Mobility

To provide a clarification of the concepts of perfect similarity and equal mobility, a brief discussion is provided. Equal mobility at near threshlod conditions occurs when all grain sizes are entrained at the same dimensional critical shear stress. Equal mobility implies that the median bed grain size adequately describes the mobility of the entire sediment. Perfect similarity occurs when the slopes, m_i, of Eq. 15 are constant for all size ranges, so that $m_1 = ... = m_i$, and therefore the slopes of the transport - shear relations are parallel. Perfect similarity does not imply equal mobility where the exponent of Eq. 19, $\beta = 1$. However, perfect similarity does imply that β remains constant for any value of the reference transport rate, W_r^*, used to define Eq. 19. Note that Eq. 19 does not describe the overall mobility of the bed material, but it does describe the relative mobility of various grain sizes for a given bedload transport rate, W_r^*.

If m_i varies with grain size, then β changes with W_r^*. Typically m_i increases with grain size and β increases with W_r^*. This implies that equal mobility ($\beta = 1$) may be achieved for some value of W_r^*. The Oak Creek data demonstrate these trends as shown by Diplas (1992) so that for W_r^*=0.0025, $\beta <$ 1, and for $W_r^* = 0.04$, $\beta > 1$, and equal mobility ($\beta = 1$) occurs at a W_r^* value

between $W_r^* = 0.0025$ and 0.04 for Oak Creek.

Following is a discussion of the implications of perfect similarity and equal mobility for several cases. First, when perfect similarity and equal mobility occur simultaneously, the m_i values for all size ranges are equal, and β has a constant value of unity for all W_r^*. However, the value of τ_{r50}^* will increase with W_r^*. This implies that Eq. 19 describes the overall mobility of the bed material for all transport rates. Second, when perfect similarity occurs without equal mobility, the m_i values are again equal for all size ranges and β is again constant for all W_r^*. However, in this case since equal mobility does not occur β is different than unity. For the second case Eq. 19 again describes the overall mobility of various grain sizes for all W_r^*. Third, when perfect similarity does not occur, the m_i values vary with grain size, and therefore the β values vary with W_r^*, and equal mobility occurs only for a unique value of W_r^*. For this case, Eq. 19 does not describe the overall mobility of the bed material, but instead describes the relative mobility of various grain sizes for a given transport rate. Fourth, if both perfect similarity and equal mobility do not occur then the m_i values vary with grain size and equal mobility is not achieved for any value of W_r^*.

3.3 Suspension Criteria

Depending on the manner in which bedload transport rates are measured in the laboratory or the field, a portion of the measured rates may consist of particles which are in suspension. Therefore, a procedure is required to determine the maximum size of particles in suspension at the time of measurement. This procedure for determining particle sizes in suspension is especially critical when the bedload capturing device extends above the bed, and, therefore, may collect sediment moving in suspension (e.g. Helley-Smith bedload sampler). The measured transport rates may then be corrected to more accurately reflect the transport rate consisting of particles moving as bedload only. It should be noted that bedload in gravel-bed streams does not necessarily consist only of gravel, but may also contain some sand. Although the assumption that all the gravel moves as bedload may be a valid assumption in most cases, the assumption that all sand moves in suspension is not valid. Therefore, if bedload is assumed to consist only of gravel, that part of the bedload which consists of sand may be neglected. A determination of the maximum particle size in suspension is required for a more accurate determination of the minimum bedload particle size.

Bridge and Bennett (1992) provided a suspension criterion given by Eq. 37 ($u_s \geq u_*b$). The settling velocity is determined using Dietrich's (1982) curve based on experimental data and incorporating the effects of particle shape. The

procedure to find the maximum particle size in suspension for a given bed shear velocity is to equate the relation of Eq. 37 to obtain the particle settling velocity, u_s, and then determine the corresponding particle diameter for a given particle shape. It is assumed that all particles equal to and smaller than this size are in suspension. This procedure is applied to the given range of shear velocities, which yields a range of maximum particles sizes in suspension. An average particle size may then be computed, and all particle sizes smaller than this value can then be dropped from the bedload analysis which provides a more accurate representation of the actual bedload.

3.4 Summary of Method of Analysis

Given the bed material and bedload size distributions and corresponding flow conditions, fractional bedload transport rates are calculated. A suspension criterion is used to determine the maximum particle size in suspension so that the particle sizes moving predominately in suspension may be eliminated from the bedload analysis.

The fractional transport rates and corresponding bed shear stresses are then rendered dimensionless for use in similarity analysis. In an attempt to correlate the transport rate and shear stress, the dimensionless transport rate, W_i^*, is plotted against the dimensionless shear stress, τ_i^*, for each size range and linear log-log

relations of the form of Eq. 15 ($W_i^*=\alpha_i\tau_i^{*mi}$) are obtained.

The similarity approach attempts to collapse these relations for each size range into a single curve. This is accomplished using a dimensionless reference transport rate, W_r^*, corresponding to near initial motion conditions and determining the corresponding dimensionless reference shear stress, τ_{ri}^*. The similarity collapse is realized by plotting the dimensionless transport rate, W_i^*, against the normalized shear stress, $\phi_i = \tau_i^*/\tau_{ri}^*$. The modified similarity approach is then used to provide a better collapse by accounting for the dependence of the transport rate on grain size.

The dimensionless reference transport critical shear stresses, τ_{ri}^*, determined above are used to compare initial motion conditions for various bed sediments. Specifically, the effects of particle shape and surface layer coarseness on bedload transport may be investigated.

Finally a comparison between surface and subsurface approaches is obtained by scaling the dimensionless transport rate by the bed surface fraction, F_i, and subsurface size fraction, f_i. Using the similarity approach for both subsurface and surface scaled transport rates allows a comparison of the two approaches.

The above methods will be employed to investigate the effects of particle shape on bedload transport and a wide range of transport rates using both surface and subsurface based approaches.

Chapter 4. The Effects of Particle Shape on Bedload Transport

4.1 Introduction

The experiments on which the widely used Shields curve for incipient motion is based are for nearly spherical, uniform grains on a flat bed. Since most bedload transport relations do not specifically account for the effects of particle shape on grain motion these effects must be studied for streams containing either a variety of particle shapes or an abundance of a particular shape. The effects of particle shape on bedload transport in gravel-bed streams are examined in this report using a similarity approach and fractional transport analysis for data from Piceance Creek, Colorado.

Piceance Creek is a gravel-bed stream located in northwestern Colorado on the western slope of the Rocky Mountains. Its bed material consists mostly of flat shale particles with a specific gravity of about 2.1. The bed material data is from a bulk (volumetric) sample that includes both surface and subsurface material. The pavement data is from a grid sample (pebble count) and therefore may be biased against the smaller sized particles (Fripp and Diplas, 1993). A comparison of the bed bulk and surface sizes is provided in Table 2, and the bed sediment size distributions are plotted in Figure 4.

The bulk (subsurface and surface material) median grain size, D_{50}, is 5.05 mm. The actual subsurface median grain size is unknown since a bulk bed

material sample was taken. The surface median grain size, D_{50s}, is 14 mm. The surface coarseness may be described by the ratio of D_{50s} to D_{50} which gives a value of surface coarseness equal to 2.77. However, the surface coarseness would actually be higher if the surface portion of the bulk sample is disregarded in some way.

The given data is used to calculate fractional bedload transport rates and provides information for calculating a corrected bedload value accounting for suspended particles that are part of the measurements taken with the bedload sampler. More importantly, the influence of particle shape on bedload transport rates is investigated in this analysis for the flat, platy particles in Piceance Creek.

4.2 Size Ranges

The bedload measurements in Piceance Creek were made with a Helley-Smith beldoad sampler, which is a direct measuring pressure difference sampler that traps sediment within a small region (typically 76.2 mm) of the total streambed width. The limitations of this device must be addressed before analyzing the data. Emmett (1980) provides a good summary of the characteristics of the Helley-Smith bedload sampler as well as a field calibration of the sampler.

The main deficiency of the Helley-Smith sampler is that it traps some suspended load because the nozzle through which the bed material passes must

protrude into the flow, and typically suspended sediment concentrations are highest near the bed. Thus, one must determine the maximum particle size in suspension at the time of measurement in order to determine a more accurate representation of the bedload. In addition, because the sampler covers only a small portion of the total width, the coarsest size ranges tend not to be sampled effectively.

Emmett (1980) found that the Helley-Smith bedload sampler had a near 100% sediment trapping efficiency for particles ranging in size from 0.50 - 16 mm. Sediment trapping efficiency is defined as the ratio of the weight of sediment accumulated per sampling time to the weight of sediment per sampling time that would have passed through the nozzle area had the sampler not been present. For particles less than 0.50 mm, the sampler had high trapping efficiency due to suspended particles. Note that the typical mesh size on the sampler is 0.2-0.25 mm, so the data for these size fractions should not be used to calculate the bedload, however suspended particles larger than 0.2-0.25 mm may still contribute to the measured bedload. For particles larger than 16 mm, Emmett found low trap efficiencies because these sizes seldom moved, and the likelihood of trapping a large particle is very small because of the sampler nozzle width (typically 76.2 mm) to stream width ratio is also small. It would be unrealistic to expect to capture particles 64 mm in 76 mm opening in a representative way. Thus, the lack of representative samples of large particle sizes prevents accurate conclusions

concerning the bedload contribution for the largest size fractions.

4.2.1 Upper Size Range

Conclusions concerning the nature of the bedload transport in Piceance Creek do not include particles larger than 32 mm due to the small number of bedload measurements for the largest sizes and the limitations of the Helley-Smith bedload sampler for the largest sizes mentioned previously. The cumulative bedload size fractions for sizes coarser than 32 mm are less than 8% for all samples.

4.2.2 Lower Size Range

The suspension criteria of Bridge and Bennett (1990) indicates that the maximum particle size in suspension for the given flow conditions ranges from 1 to 2 mm for a Corey Shape Factor, CSF, of 0.3 and a sediment specific gravity of 2.1. Therefore, the size range 1.4 - 2.0 mm is used as the lower limit for subsequent evaluations. The cumulative bedload size fractions for sizes finer than 1.4 mm is less than 23% for all samples.

4.2.3 Size Ranges used in the Analysis

Originally, geometric mean particle sizes for each size range, $\overline{D}_i$, varying by a factor of 1.4 (the square root of 2) were used to provide the maximum number of size ranges for the given data. The quantity $\overline{D}_i$ is calculated by the following equation,

$$\overline{D_i} = \sqrt{D_i * D_{i+1}} \tag{38}$$

where D_i and D_{i+1} are the sieve diameters which are smaller and larger than $\overline{D}_i$ respectively. However, a similarity analysis using these size ranges indicates that the slope of the $W_i^* - \tau_i^*$ regression relations, m_i, show a significant drop at $\overline{D}_i/D_{50}$ = 1.33 to 1.86. This is demonstrated in Table 3. A similarity analysis using $\overline{D}_i$ values varying by a factor of 2 decreases the number of size ranges but eliminates the problem with the m_i values.

In order to provide the maximum number of size ranges while avoiding the above problem with the m_i values, a combination of the above size ranges is used. That is, $\overline{D}_i$'s varying by a factor of 2 are used for the large grains and $\overline{D}_i$ values varying by a factor of 1.4 for the smaller grains. Table 4 includes the size ranges for Piceance Creek used in calculating the fractional transport rates and performing the similarity analysis.

4.3 Bedload Transport Rates and Bed Shear Stresses

The total corrected volumetric bedload transport rates per unit width, q_B, range from about 1.45×10^{-6} to 4.24×10^{-5} m^2/s for $1.7 < \bar{D}_i < 23$ mm compared to the total measured range of 6.33×10^{-6} to 7.19×10^{-5} m^2/s for all sizes. The dimensionless transport rates, W_i^*, vary from about 0.01 to 0.6 for $\bar{D}_i$ = 1.7 to 23 mm. The bed shear stresses, τ, range from 15.276 to 17.214 N/m^2 for Samples 18 through 43. The dimensionless bed shear stresses range from about 0.06 to 1.0 for $\bar{D}_i$ = 1.7 to 23 mm. The dimensionless bed shear stresses for the median grain size, τ_{50}^*, range from 0.28 to 0.32.

4.4 Transport - Shear Relations

Plots of the dimensionless transport rate, W_i^*, against the dimensionless shear stress, τ_i^*, for each size range are provided in Figures 5 and 6. Log-Log regression results of these plots are given in the next section. Separate plots for each size range are used to determine samples that are inconsistent with the rest of the data. Typically samples that do not follow the general trend have measured bedload values that are much lower than other samples taken under similar hydraulic conditions. Samples 23, 29, 30, 42, and possibly 21, 22, and 43 appear to be inconsistent with the rest of the data over all the size ranges. The samples which are excluded from the analysis are samples 21, 23, 29, 30, 36, 37, and 42.

4.5 Transport - Shear Relation Regression Results

4.5.1 Original Similarity Approach

Tables 4 and 5 give the size ranges and corresponding log-log regression results of W_i^* vs. τ_i^* fitted to equations of the form of Eq. 15 ($W_i^* = \alpha_i \tau_i^{*mi}$). The first regression was performed using all samples from 18 through 43, and the second regression was performed for samples 18 through 43 excluding samples 21, 23, 29, 30, 36, 37, and 42. The slopes of the transport - shear relation, m_i, increase by -2 to +10% when eliminating these samples but the correlation coefficients, r^2, are typically doubled. Thus, it is reasonable to eliminate these samples from the analysis.

The first regression results have m_i values that gradually increase with $\bar{D}_i$. The second regression results show a similar behavior except at $\bar{D}_i$ = 23 mm where the m_i values decrease. The m_i values appear to approach a constant value at high $\bar{D}_i/D_{50}$. Possible explanations are shape effects or sampling problems for large grain sizes. Constant m_i values would indicate no dependence of W_i^* on size. It has been suggested that the dimensionless shear stress also reaches a constant value at $\bar{D}_i/D_{50}$ values greater than 4.2 - 5.0 (Andrews, 1983).

4.5.2 Modified Similarity Approach

The dependence of the transport rate, W_i^*, on particle size was demonstrated for Oak Creek by increasing values of the transport - shear relations, m_i, with grain size. Diplas (1987) accounted for the dependence of the transport rate on grain size for the Oak Creek data by considering the parameter, $\tau_i^{*(\bar{D}i/D50)^{\wedge}b}$, where the exponent b is from the regression of $m_i = a(\bar{D}_i/D_{50})^b$. A plot of m_i vs. $\bar{D}_i/D_{50}$ is given in Fig. 8. Regression of m_i - $\bar{D}_i/D_{50}$ for Piceance Creek yields:

Samples 18 to 43 (all)

$\bar{D}_i$ = 1.7 - 23 mm: $m_i = 13.87(\bar{D}_i/D_{50})^{0.087}$ $r^2 = 0.89$ **(39a)**

$\bar{D}_i$ = 1.7 - 11 mm: $m_i = 13.97(\bar{D}_i/D_{50})^{0.106}$ $r^2 = 0.88$ **(39b)**

Samples 18 to 43 (excluding samples 21, 23, 29, 30, 36, 37 and 42)

$\bar{D}_i$ = 1.7 - 23 mm: $m_i = 14.79(\bar{D}_i/D_{50})^{0.0592}$ $r^2 = 0.54$ **(40a)**

$\bar{D}_i$ = 1.7 - 11 mm: $m_i = 15.23(\bar{D}_i/D_{50})^{0.116}$ $r^2 = 0.95$ **(40b).**

The expressions for the regression of all samples from 18 to 43 given by Eqs. 39a and 39b are provided for comparison with Eqs. 40a and 40b. However, the relations of Eq. 40 are used in the subsequent analysis for the reasons stated previously. In addition, the relation for $\bar{D}_i$ = 1.7 - 11 mm, Eq. 40 b, provides a

higher correlation coefficient and is used in the subsequent analysis.

Regression of W_i^*-$\tau_i^{*(\bar{D}i/D50)^b}$ for Oak Creek yielded m_i values showing no dependence on $\bar{D}_i/D_{50}$, and a reduced range of m_i values from 289% to just 15.8% (Table 6). Since the m_i values of Piceance Creek show a general increase with size, a similar analysis is provided for various size ranges and the results are given in Tables 4 and 5. The value m_i' refers to the slope of the W_i^*-$\tau_i^{*(\bar{D}i/D50)^b}$ power relation ($W_i^*=\alpha_i(\tau_i^{*(\bar{D}i/D50)^b})^{mi'}$). Note that the intercepts, α, and r^2 are the same as for the original regression of W_i^*-τ_i^*.

The modified similarity approach provides some improvement for the Piceance Creek data (excluding the previously indicated samples) as evidenced by the decrease in the m_i value range from 24% to 13%. However, the usefulness of the modified approach in this case is questionable since the m_i value range is initially low (24%). Similar results are obtained without excluding some samples.

The m_i and m_i' values show a similar trend of increasing with $\bar{D}_i/D_{50}$ up to high values of $\bar{D}_i/D_{50}$ for the data excluding the questionable data points. The m_i' values for all samples from 18-43 decrease at high $\bar{D}_i/D_{50}$ unlike the m_i values.

4.6 Reference Transport Rates

A reference transport rate and corresponding reference shear stresses are needed in order to perform a similarity collapse of the transport-shear relations. As discussed earlier, if the reference transport rate, W_r^*, corresponds to very low bedload transport rates near initial motion, the corresponding reference shear stresses may be considered as critical shear stresses. A value of $W_r^* = 0.04$ appears suitable for Piceance Creek, however for comparison with Oak Creek a value of $W_r^* = 0.0025$ is also used in the analysis.

4.7 Reference Shear Stresses

Values of the dimensionless reference shear stress for each size range, τ_{ri}^*, are calculated for $W_r^* = 0.0025$ and 0.04 from the W_i^*-τ_i^* regression relations for samples 18-43 excluding the samples indicated previously. The τ_{ri}^* values are given in Table 7 and plotted against $\bar{D}_i/D_{50}$ in Fig. 9.

Note that the τ_{ri}^* values calculated based on the regression equations of W_i^* vs. τ_i^* are biased and may provide spurious correlation of τ_{ri}^* and $\bar{D}_i/D_{50}$. Therefore, values of τ_{ri}^* are also read visually from the graphs of W_i^* vs. τ_i^* and are given in Table 7 and plotted against $\bar{D}_i/D_{50}$ in Fig. 9.

A relation of the so determined τ_{ri}^* values with $\bar{D}_i/D_{50}$ of the form of Eq. 19 ($\tau_{ri}^* = \tau_{r50}^*(\bar{D}_i/D_{50})^{\beta}$) yields the value of the reference transport critical shear stress

for the median grain size, τ_{r50}*, which can be used to determine the relative initial mobility of discs and spheres. Values of τ_{ri}* (for W_r* = 0.0025 and 0.04) calculated using the above methods are plotted against $\bar{D}_i/D_{50}$ in Figure 9 and yield the following expressions for Piceance Creek:

- τ_{ri}* determined from W_i*-τ_i* regression relations

$W_r^* = 0.0025$; $\tau_{ri}^* = 0.2228(\bar{D}_i/D_{50})^{-0.9517}$; $r^2=0.9999$ **(41a)**

$W_r^* = 0.04$; $\tau_{ri}^* = 0.2689(\bar{D}_i/D_{50})^{-0.9629}$; $r^2=0.9999$ **(41b)**

- τ_{ri}* read by eye from W_i*-τ_i* graphs

$W_r^* = 0.0025$; $\tau_{ri}^* = 0.2598(\bar{D}_i/D_{50})^{-1.0071}$; $r^2=0.9978$ **(42a)**

$W_r^* = 0.04$; $\tau_{ri}^* = 0.2837(\bar{D}_i/D_{50})^{-0.9930}$; $r^2=0.9999$ **(42b).**

Thus, slightly higher τ_{r50}* and β values are obtained for τ_{ri}* values read visually from graphs of W_i* vs. τ_i*. This may be due to error in reading the values by eye from the graphs or by introducing some curvature in the W_i*-τ_i* relations where the W_i*-τ_i* linear log-log relations provide no curvature. Curvature in the relations should lead to slightly higher τ_{ri}* values as seen above.

The above values of τ_{ri}* and τ_{r50}* were based on a bulk based approach wherein the dimensionless transport rate for each size range, W_i*, is scaled by the

fraction of material in the same bulk size range. However, since the surface is the layer from which grains are entrained and various streams have a different surface layer coarseness it is appropriate to determine a critical shear stress based on the surface layer. The above subsurface based τ_{r50}^* values may be scaled to account for surface coarseness by dividing the subsurface value of τ_{r50}^* by the surface coarseness. This conversion aids in the comparison of critical shear stresses from different data sets.

For a surface coarseness of 2.77 and $W_r^* = 0.04$, the above subsurface based values of $\tau_{r50}^* = 0.2689$ and 0.2837 convert to surface based critical shear stress values of $\tau_{r50s}^* = 0.0971$ and 0.1024. Similarly the surface values for $W_r^* = 0.0025$ are $\tau_{r50s}^* = 0.0804$ and 0.0906.

As indicated previously, values of β different from unity indicate that selective transport occurs, while when $\beta = 1$ equal mobility occurs wherein all particle sizes are mobilized at the same dimensional shear stress value. If $\beta < 1$, particle sizes finer than D_{50} are more mobile. Conversely, if $\beta > 1$, the larger sizes are mobile. The β value for Piceance Creek are all less than or approximately equal to unity indicating that near equal mobility conditions occur for both $W_r^* = 0.0025$ and 0.04.

4.8 Comparison with Other Data

4.8.1 Transport - Shear Relations

The regression of $m_i = a(\bar{D}_i/D_{50})^b$ for Piceance Creek is given by Eq. 40b and the Oak Creek relation determined by Diplas (1987) is given by:

$$\text{Oak Creek:} \qquad m_i = 13.71(\bar{D}_i/D_{50})^{0.3214} \qquad (43).$$

The constants of Eqs. 40b and 43 are similar with a slightly higher value for Piceance Creek, and the exponent for Piceance Creek is slightly lower than Oak Creek's indicating less size dependence than Oak Creek.

The correlation coefficients for the W_i^*-τ_i^* regression relations for Piceance Creek are much lower than Oak Creek, which can partly be attributed to the bedload sampling technique. The vortex sampler used in Oak Creek provides a much more accurate bedload measurement than does the Helley-Smith sampler since the vortex trough samples continuously over the entire channel width and provides a longer record of measurements. Also note that the W_i^* values cover a smaller range of values (2 orders of magnitude) compared with Oak Creek (3 orders of magnitude), but the W_i^* values for Piceance Creek are consistently higher than those of Oak Creek for similar size ranges (See Figures 5 and 7). This may influence the regression coefficients (m_i and α_i) for the power relation $W_i^* = \alpha_i \tau_i^{*m_i}$.

The incorporation of $\bar{D}_i/D_{50}$ into the Piceance Creek W_i^*-τ_i^* relations does not eliminate the increase in m_i with $\bar{D}_i/D_{50}$ but does decrease the range of m_i values, but not as dramatically as for Oak Creek. Note that the range of m_i values for Piceance Creek is much smaller than for Oak Creek, which perhaps limits the effectiveness of incorporating $\bar{D}_i/D_{50}$ into the W_i^*-τ_i^* relation. However, the lowered range of m_i values indicates that $\bar{D}_i/D_{50}$'s influence on W_i^* is accounted for to some degree. Also note that the Picenace Creek $\bar{D}_i/D_{50}$ values range from 0.337 to 4.55 while the Oak Creek $\bar{D}_i/D_{50}$ values range from 0.0446 to 4.445. Thus, Piceance Creek has a much narrower range of $\bar{D}_i/D_{50}$ values which coincide with the upper range of $\bar{D}_i/D_{50}$ values for Oak Creek.

4.8.2 Equal Mobility and Selective Transport

The Piceance Creek τ_{ri}^*-$\bar{D}_i/D_{50}$ relations are given by Eqs. 41 and 42 and the Oak Creek relations are given by,

$$W_r^* = 0.0025: \qquad \tau_{ri}^* = 0.0876(\bar{D}_i/D_{50})^{-0.982} \qquad r^2 = 0.9997 \quad \textbf{(44a)}.$$

$$W_r^* = 0.04: \qquad \tau_{ri}^* = 0.1097(\bar{D}_i/D_{50})^{-1.070} \qquad r^2 = 0.9996 \quad \textbf{(44b)}.$$

The Oak Creek and Piceance Creek β values for $W_r^* = 0.0025$ are similar and close to unity so that approximately similar transport conditions are present in both

streams. The β values are slightly less than unity indicating that the finer particles are slightly more mobile at $W_r^* = 0.0025$.

The regression results of τ_{ri}^* vs $\bar{D}_i/D_{50}$ indicate that the exponents, β, approach unity as W_r^* is increased for τ_{ri}^* based on regression, but at a slower rate than for Oak Creek. The very gradual increase in β as W_r^* is increased may be due to the small range of m_i values for Piceance Creek. The exponent β reaches a value of 1 at about $W_r^* = 10\text{-}20$ and $W_r^* = 0.02$ for Piceacne Creek and Oak Creek respectively.

4.8.3 Relative Mobility

Comparison of the Oak Creek data and Piceance Creek data is attempted using values of reference shear stresses, τ_r^*. Parker (1982) uses reference values of the dimensionless bedload parameter, $W_r^* = 0.002$ and $W_r^* = 0.0025$ to determine the values of τ_{ri}^* from Eq. 15 ($W_i^* = \alpha_i \tau_i^{*mi}$), where the values of α_i and m_i were obtained from log-log regression. Parker used a weighted mean value of $m_i = 13.38$ for Oak Creek, whereas the individual values from log-log regression for each size range are used for Piceance Creek.

Diplas' (1992) plot of reference shear stress versus grain size for Oak Creek indicates that $\tau_{r50}^* = 0.1097$ and $\tau_{r50s}^* = 0.0442$ for $W_r^* = 0.04$. Parker, et al (1982) indicate that $\tau_r^* = 1.183\tau_c^*$ (for $W_r^* = 0.0025$) for Oak Creek, and that for

a surface coarseness of 2.48 the subsurface value of $\tau_r^* = 0.0876$ converts to a surface $\tau_c^* = 0.0299$. The surface based value of $\tau_c^* = 0.0299$ for Oak Creek corresponds closely to the value of $\tau_c^* = 0.03$ proposed by Neill (1968) based on a surface layer D_{50}.

The Piceance Creek τ_{r50s}^* values from the regression relations and read by eye for $W_r^* = 0.04$ are 2.2 and 2.3 times higher than the corresponding Oak Creek value respectively. The Piceance Creek τ_{r50s}^* values from the regression relations and read by eye for $W_r^* = 0.0025$ are 2.7 and 3.0 times higher than the corresponding Oak Creek value, respectively. If it is assumed that the dimensionless critical shear stress value, $\tau_c^* = 0.03$, is a good indicator of the critical conditions for coarse gravel-bed streams, as Oak Creek and many other data sets indicate, then the Piceance Creek critical shear stress values, when adjusted for surface coarseness, are 2 to 3 times higher than most gravel-bed streams.

These findings are supported by Mantz's (1980) results for imbricated discs which had a critical shear stress 3.33 times higher than more bulky non-imbricated sediment. Further, this supports Lane and Carlson's (1954) results that imbricated discs were less mobile than spheres and of equal susceptibility to motion as spheres weighing 2.5 times as much.

4.9 Summary of Piceance Creek Data Analysis and Results

Using Piceance Creek measured bedload transport rates, fractional bed material transport rates were calculated. An attempt to account for the influence of particle size, $\bar{D}_i$, on the dimensionless transport rate, W_i^*, revealed that the slope values, m_i of the power relation, $W_i^* = \alpha_i \tau_i^{*mi}$, approached a constant value at high $\bar{D}_i$ or $\bar{D}_i/D_{50}$. This may be due to sampling problems for large grain sizes or perhaps shape effects.

A relative mobility investigation revealed that the disc-like shale particles of Piceance Creek require 2 to 3 times the normal dimensionless critical shear stress for gravel-bed streams to initiate their motion, which may lead to lower transport rates for discs relative to spheres for given flow conditions. This finding is in support of previous studies on imbricated discs.

Table 2. Comparison of Bulk Bed Material and Surface Material (Pavement) for Piceance Creek, Colorado

	Bulk Bed Material mm	Pavement mm
d_5	0.284	-
d_{16}	0.574	4.0
d_{25}	1.06	6.8
d_{35}	2.11	10
d_{50}	5.05	14
d_{65}	10.1	23
d_{75}	16.2	30
d_{84}	23.8	43
d_{95}	39.7	60

Table 3. Piceance Creek W_i^*-τ_i^* Regression Results for the Original and Modified Similarity Approaches for Di values varying by a factor of 1.4.

Samples 18-43 (all)

Size Range, (mm)	$\bar{D}_i$ (mm)	$\bar{D}_i/D_{50}$	m_i	m_i'	α_i	r^2
1.4 - 2.0	1.7	0.337	12.15	13.36	8.04×10^{-1}	0.21
2.0 - 2.8	2.4	0.475	12.80	13.66	7.01×10^{1}	0.20
2.8 - 4.0	3.3	0.653	13.79	14.31	8.07×10^{3}	0.22
4.0 - 5.6	4.7	0.931	14.95	15.04	3.72×10^{6}	0.24
5.6 - 8.0	6.7	1.33	14.13	13.77	1.83×10^{8}	0.21
8.0 - 11	9.4	1.86	13.59	12.86	8.03×10^{9}	0.22
11 - 16	13	2.57	16.43	15.10	2.40×10^{14}	0.29
16 - 23	19	3.76	16.83	14.95	2.26×10^{17}	0.37
23 - 32	27	5.35	14.78	12.73	1.47×10^{17}	0.27
	Range		12.2-16.8	12.7-15.1		
			38.52%	18.62%		
	Average m_i =		14.38	13.98		

Table 4. Piceance Creek W_i^*-τ_i^* Regression Results for the Original and Modified Similarity Approaches.

Samples 18-43 (all)

Size Range (mm)	$\bar{D}_i$ (mm)	$\bar{D}_i/D_{50}$	m_i	m_i'	α_i	r^2
1.4 - 2.0	1.7	0.337	12.15	13.36	8.04×10^{-1}	0.21
2.0 - 2.8	2.4	0.475	12.80	13.66	7.01×10^{1}	0.20
2.8 - 4.0	3.3	0.653	13.39	14.31	8.07×10^{3}	0.22
4.0 - 8.0	5.6	1.11	14.54	14.41	2.73×10^{7}	0.22
8.0 - 16	11	2.18	14.76	13.79	6.3×10^{11}	0.26
16 - 32	23	4.55	15.43	13.52	1.11×10^{17}	0.40
	Range		12.15-15.43	13.36-14.41		
			27.0%	7.86%		
	Average m_i =		13.92	13.84		

Table 5. Piceance Creek W_i^*-τ_i^* Regression Results for the Original and Modified Similarity Approaches.

Samples 18-43 (Excluding 21,23,29,30,36,37,42)

Size Range	$\bar{D}_i$ (mm)	$\bar{D}_i/D_{50}$	m_i	m_i'	α_i	r^2
1.4 - 2.0	1.7	0.337	13.18	14.06	1.26	0.41
2.0 - 2.8	2.4	0.475	13.89	14.51	1.64×10^{2}	0.42
2.8 - 4.0	3.3	0.653	14.91	15.29	2.78×10^{4}	0.44
4.0 - 8.0	5.6	1.11	15.60	15.50	1.60×10^{8}	0.46
8.0 - 16	11	2.18	16.40	15.62	2.10×10^{13}	0.50
16 - 32	23	4.55	15.10	13.82	5.80×10^{16}	0.57
	Range		13.18-16.4	13.82-15.62		
			24.43%	13.02%		
	Average m_i =		14.85	14.80		

Table 6. Oak Creek W_i^* - τ_i^* Regression Results for the Original and Modified Similarity Approaches (values from Diplas (1987)).

Size Range (mm)	$\bar{D}_i$ (mm)	$\bar{D}_i/D_{50}$	m_i	m_i'	α_i	r^2
0.59 -1.2	0.892	0.0446	5.51	14.97	0.166×10^{-3}	0.72
1.2 - 2.4	1.79	0.0895	5.95	12.93	0.691×10^{-2}	0.67
2.4 - 4.8	3.57	0.1785	7.49	13.03	0.100×10^{1}	0.64
4.8 - 9.5	7.14	0.3570	9.85	13.72	0.428×10^{4}	0.65
9.5 - 19	14.3	0.715	12.28	13.68	0.535×10^{9}	0.66
19 - 25	22.2	1.11	14.18	13.71	0.158×10^{14}	0.73
25 - 38	31.8	1.59	15.87	13.67	0.150×10^{18}	0.78
38 - 51	44.4	2.22	16.81	13.01	0.474×10^{21}	0.82
51 - 76	63.5	3.175	21.45	14.8	0.121×10^{31}	0.86
76 - 102	88.9	4.445	15.49	9.59	0.214×10^{24}	0.64
	Range		5.51 - 21.45	12.93 - 14.97		
			289%	15.8%		
	Average m_i =		12.15	13.72		

Table 7. Values of the dimensionless reference shear stress, τ_{ri}^*, for Piceance Creek determined for $W_r^* = 0.0025$ and $W_r^* = 0.04$ from the W_i^*-τ_i^* regression relations and read directly from W_i^*-τ_i^* graphs.

$\bar{D}_i$ mm	$\bar{D}_i/D_{50}$	$W_r^*=0.0025$ W_i^*-τ_i^* Regression	W_i^*-τ_i^* Graph	$W_r^*=0.04$ W_i^*-τ_i^* Regression	W_i^*-τ_i^* Graph
1.7	0.337	0.624	0.80	0.770	0.84
2.4	0.475	0.450	0.55	0.549	0.59
3.3	0.653	0.337	0.40	0.406	0.43
5.6	1.11	0.203	0.23	0.243	0.26
11	2.18	0.107	0.11	0.127	0.13
23	4.55	0.052	0.06	0.063	0.063

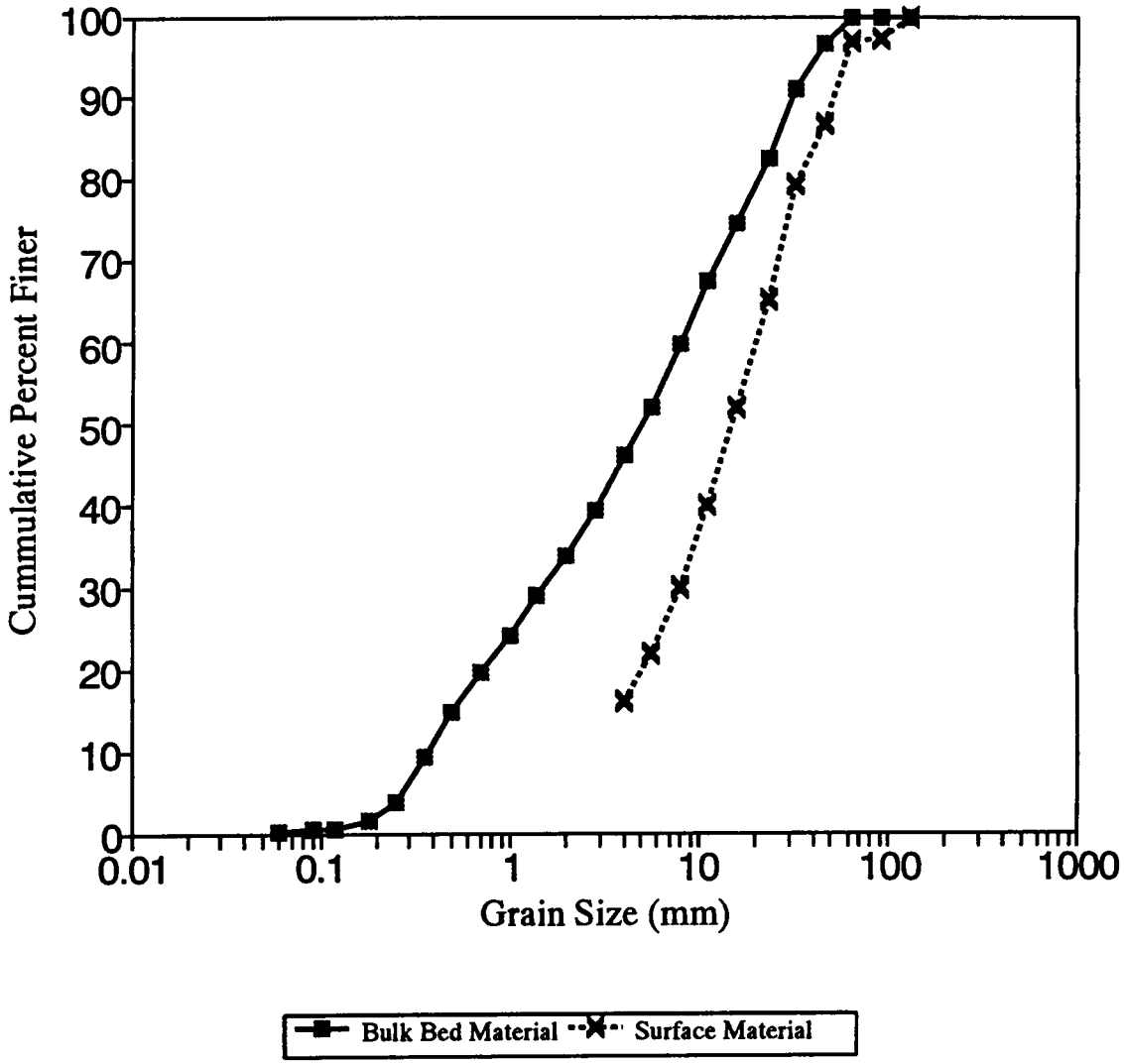

Fig. 4. Piceance Creek Bulk Bed and Surface Material Size Distributions.

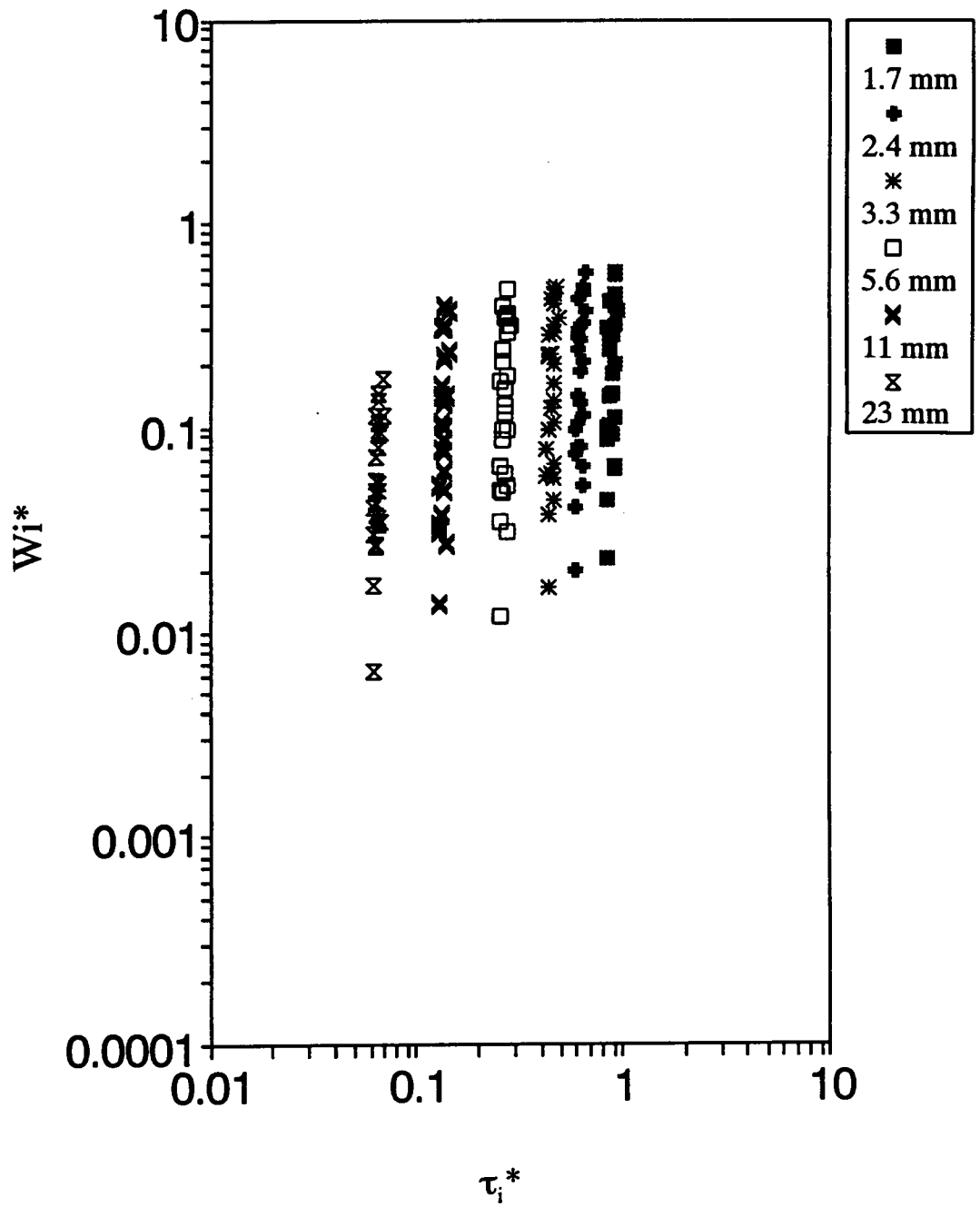

Fig. 5. Plot of W_i^* vs. τ_i^* for Piceance Creek for All Samples 18 to 43.

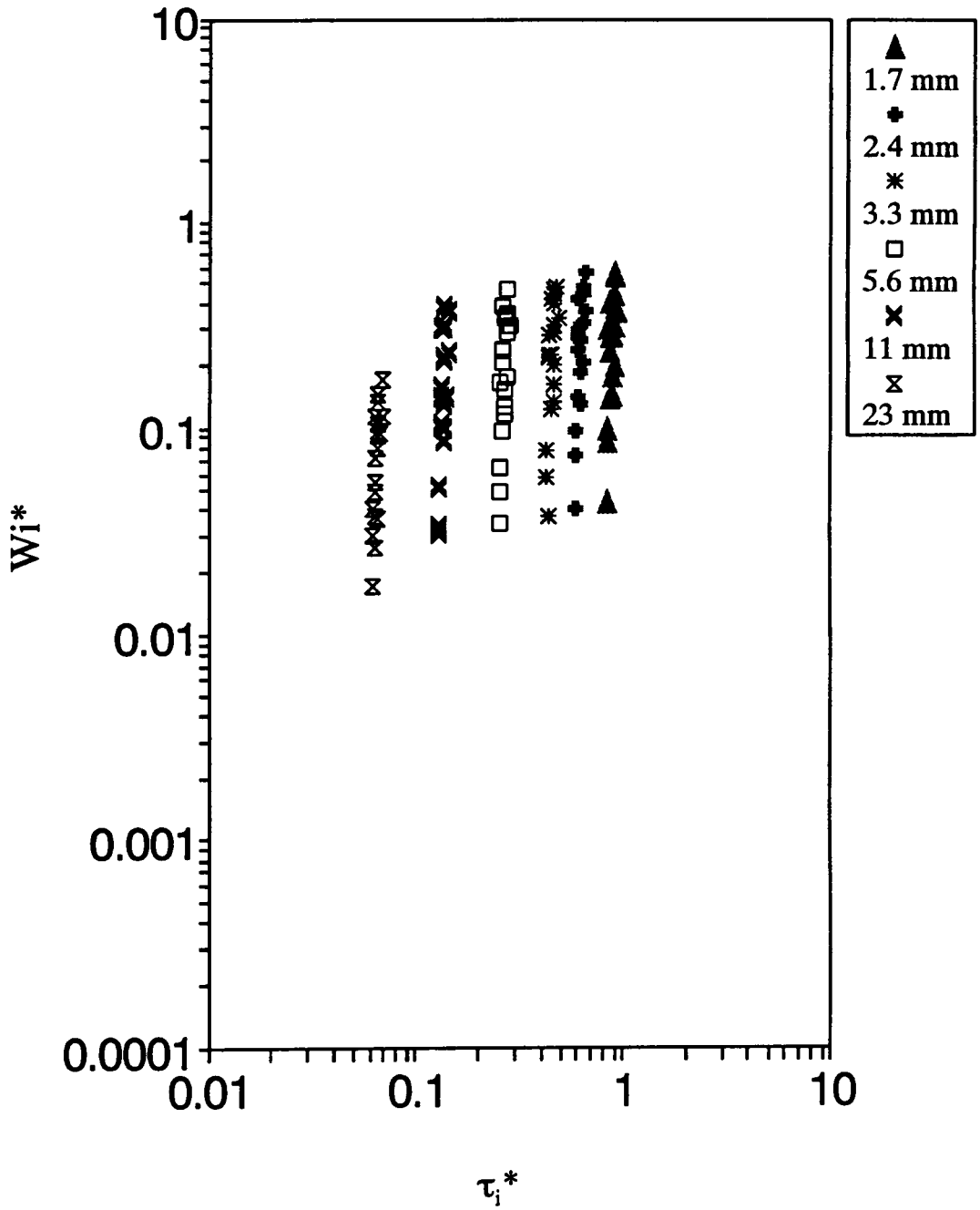

Fig. 6. Plot of W_i^*-τ_i^* for Piceance Creek, Samples 18 to 43, Excluding Samples 21, 23, 29, 30, 36, 37, and 42.

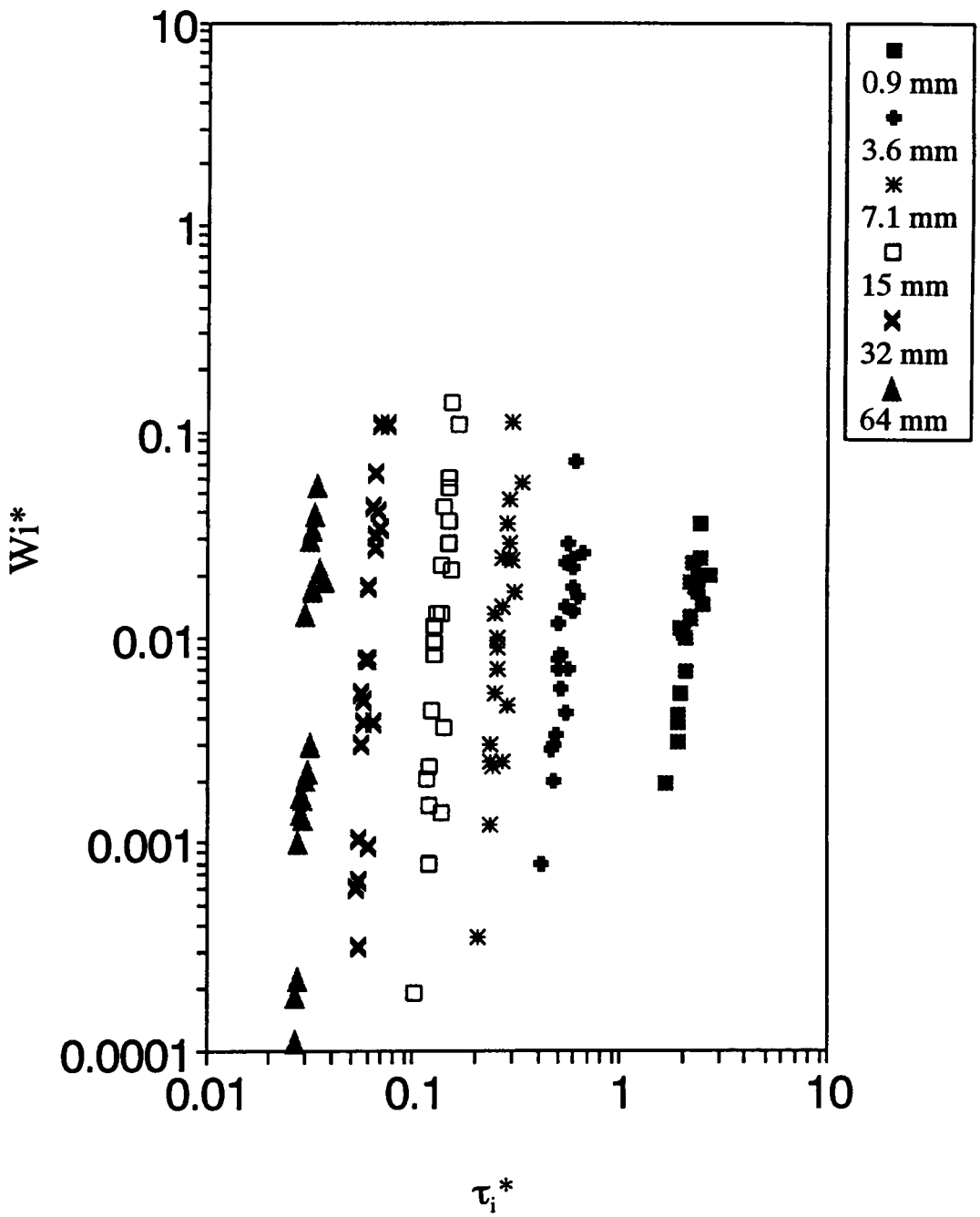

Fig. 7. Plot of W_i^* vs. τ_i^* for Oak Creek for six size ranges.

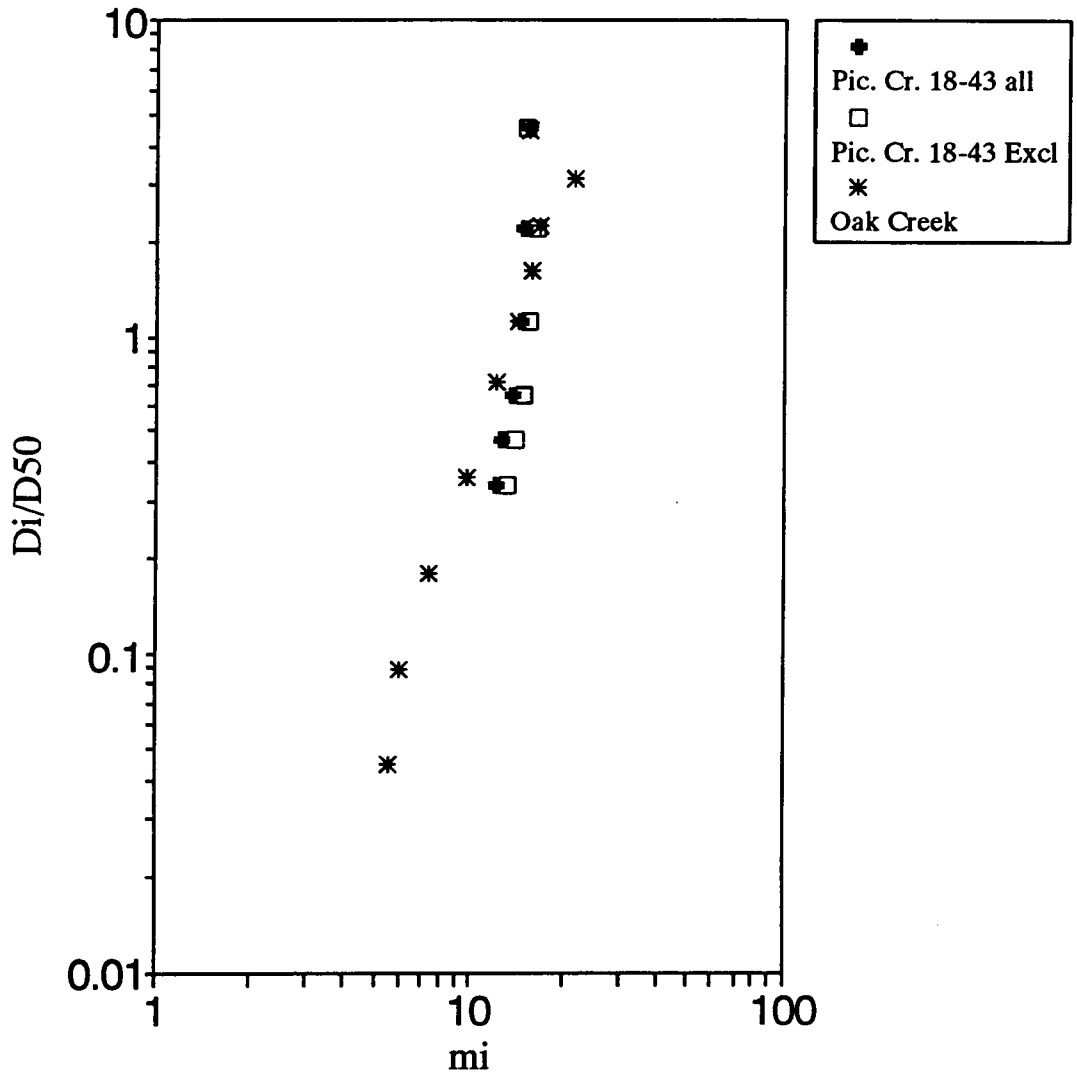

Fig. 8. Plot of m_i vs. $\bar{D}_i/D_{50}$ for Oak Creek and Piceance Creek, for all samples 18 to 43, and excluding (Excl) samples 21, 23, 29, 30, 36, 37, and 42.

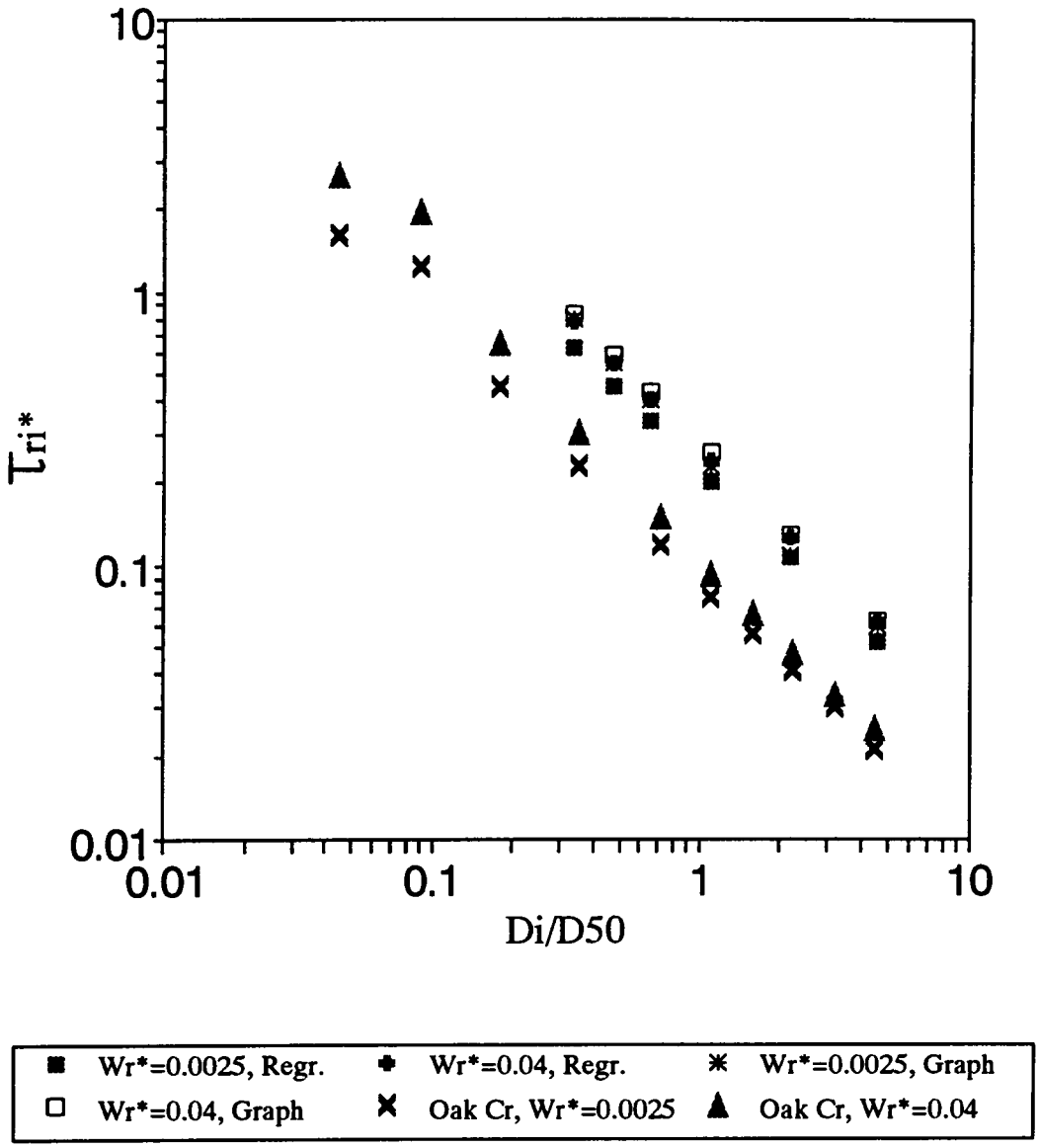

Fig. 9. Plot of τ_{ri}^* vs. $\bar{D}_i/D_{50}$ for Piceance Creek for $W_r^*=0.0025$ and $W_r^*=0.04$ where τ_{ri}^* is determined both from the W_i^*-τ_i^* regression relations and read directly from the W_i^*-τ_i^* graphs and for Oak Creek where τ_{ri}^* is from the W_i^*-τ_i^* regression relations.

Chapter 5. Investigation of a Wide Range of Transport Rates

5.1 Description of Proffitt's Experiments

The experimental data obtained by Proffitt are suitable for investigating a wide range of transport rates. Proffitt (1980) conducted experiments in a non-recirculating sediment flume to study armoring due to selective transport of nonuniform sediments. The bed material and bedload size distributions, bedload transport rates, and corresponding hydraulic data are given in Appendix I, and are suitable for fractional transport analysis using a similarity approach analogous to that of Parker, et al (1982) and Diplas (1987) for Oak Creek.

Proffitt used four nearly log-normal bed sediment gradings, with similar but different median grain sizes, D_{50}, geometric mean sizes, D_g, and standard deviations, σ_g, for each (Table 8). The initial bed sediment size distributions are plotted in Figure 10. Note that the fourth bed sediment (series 4) differs from the other series and is not lognormally distributed, since D_{50} does not equal D_g. However, Wilcock (1988) indicates that the bed size distribution of nonuniform sediments does not greatly influence incipient motion conditions, so series 4 is analyzed together with the other series.

In addition to providing four sediment gradings, Proffitt made four experimental runs for each sediment. Each experiment is designated by two numbers. The first number refers to the bed material series, and the second refers

to experimental run made for that series. For example, the number 1-4 refers to the fourth experimental run using sediment series 1.

In general, an experimental run started by first mixing and laying the bed sediment so that little or no coarse surface layer existed initially. Water was then introduced into the flume and a flow established. The measured friction slopes were different for each experimental run, and varied from 0.27 to 0.43 %. Bedload transport rates, bedload size distributions, and hydraulic conditions were measured over an extended period of time while keeping the bed shear stress nearly constant by adjusting the flume slope until the final transport rates were 1-5% of the initial transport rates. The initial phase measurements were averaged over the first hour when the transport rate was very high (0.108 to 2.486 N/s-m), while the final phase measurements were taken 20 to 95 hours later depending on the flow conditions and bed material series being used. This procedure was repeated for different hydraulic conditions and bed material.

The so determined bedload transport rates cover a wide range. The initial measured transport rates are very high (0.108 to 2.486 N/s-m) due to an initially unstable bed with little or no coarse surface layer. The final transport rates (over the same range of shear stresses) are very low (0.0016 to 0.0403 N/s-m) and correspond to an armored bed.

5.2 Size Ranges

5.2.1 Proffitt's Size Ranges

Proffitt used bed sediments ranging in size from 0.075 mm to 38 mm. The sediment was initially divided into 17 size ranges with geometric mean sizes for each range, $\bar{D}_i$, varying by a factor of 1.4 and ranging from 0.11 mm to 32 mm. The $\bar{D}_i$ value for each size range is calculated using Eq. 38 ($\bar{D}_i = (D_i * D_{i+1})^{1/2}$). For fractional transport and similarity analysis it is necessary to use relative particle sizes described by the ratio, $\bar{D}_i/D_{50}$. Since each of the bed sediment series have slightly different D_{50} values an average D_{50} value of 3.3 mm is used for collectively analyzing all series. The armor layer D_{50s} values increase with bed shear stress and range from 4.65 mm to 11.7 mm and are provided in Table 9. An average D_{50s} value of 7.25 mm is used in the analysis.

5.2.2 Upper Size Range

The bedload size distributions for both the initial and final transport phases indicate that all particles in the bedload are finer than 27 mm, and with the exception of experiments 1-3, 3-1, and 3-3, all particles in the bedload are finer than 19 mm. Therefore, the upper size range used in the bedload analysis is 12.7 - 19 mm with a corresponding $\bar{D}_i$ value of 15.6 mm.

5.2.3 Lower Size Range

The lower size range used in the analysis was partially determined using the suspension criterion of Bridge and Bennett (1990) described earlier. Proffitt used a sediment trap with a settling basin, so it is conceivable that some particles moving in suspension could have settled and subsequently included with the bedload measurements. In addition, Proffitt noted that fine material consisting of between 0.2 and 1.7% of the total for a run was carried over the top of the trap. Afterwards, the weights and size distributions were then adjusted in proportion to the total amount collected. Thus, it is necessary to determine the size ranges carried in suspension so that they may be eliminated from the fractional bedload analysis.

Using the Bridge and Bennett suspension criterion, a sediment submerged specific gravity of 1.7, and an assumed Corey Shape Factor, CSF, of 0.7 for Proffitt's sediment, the maximum particle size in suspension for both the initial and final phases ranged from 0.3 to 0.5 mm. Therefore, particles smaller than 0.5 mm were frequently or always in suspension. The cumulative bedload fractions for $\bar{D}_i$ values less than 0.5 mm range from 0.21 to 5.31 % for both the initial and final phases. This indicates that sizes smaller than 0.5 mm do not contribute greatly to the total measured bedload.

It was mentioned earlier that the slopes, m_i, of the transport-shear relation given by Eq. 15 ($W_i^*=\alpha_i\tau_i^{*mi}$) typically increase with grain size. For the final transport phase $\bar{D}_i$ values less than 1.0 mm, the m_i values show a decrease with grain size. This could possibly be due to the frequent suspension of these smaller particles. Therefore, in an attempt to simplify the analysis $\bar{D}_i$ values less than 1.0 mm are not used. This eliminates the four finest size ranges corresponding to $\bar{D}_i$ = 0.25, 0.35, 0.50, and 0.72 mm.

The cumulative percent of bedload size fractions, p_i, for $\bar{D}_i$ < 1.0 mm range from 1.15 to 11.3 % for the initial phase and from 1.42 to 20 % for the final phase. In the majority of experiments the cumulative p_i values are less than 12% for both the initial and final phases. It should be noted that possible problems with accurately sampling the smallest size ranges provided uncertainty about the p_i values for the smallest size ranges. The size ranges used in this analysis are given in Table 10, and the corresponding $\bar{D}_i$ values range from 1.0 mm to 15.6 mm.

5.3 Bedload Transport Rates

Volumetric bedload transport rates per unit width for each size range, q_{bi}, are determined for Proffitt's data. The total volumetric transport rates for the initial phase range from $4.07\text{x}10^{-6}$ to $9.37\text{x}10^{-5}$ m^2/s and from $6.03\text{x}10^{-8}$ to $1.52\text{x}10^{-6}$ m^2/s for the final phase. The q_{bi} values range from $3.66\text{x}10^{-9}$ to $1.94\text{x}10^{-5}$ m^2/s for the

initial phase and from $3x10^{-10}$ to $3.86x10^{-7}$ m^2/s for the final phase. In addition, dimensionless transport rates for each size range scaled using the bulk bed material size fractions, W_i^*, are determined for the initial and final phases. Dimensionless transport rates for each size range scaled using the surface size fractions, W_{si}^*, are determined for the final phase to provide a surface vs. subsurface approach comparison. A surface based approach is not used for the initial phase because the initial surface layer composition is unknown. The W_i^* values approximately range from 0.01 to 4 for the initial phase and from 0.001 to 0.1 for the final phase. The W_{si}^* values for the final phase data range from 0.00016 to 0.16.

5.4 Bed Shear Stresses

Proffitt maintained nearly constant bed shear stresses for the same run over the initial and final phases by adjusting the flume slope. The bed shear stresses range from 2.79 to 7.22 N/m^2 for both the initial and final phases. Dimensionless shear stresses for each size range, τ_i^*, are calculated using Eq. 17. The τ_i^* values range from about 0.01 to 0.4 for the initial and final phases for $\bar{D}_i$ = 1.0 mm to $\bar{D}_i$ = 15.6 mm. The highest and lowest τ_i^* values correspond to $\bar{D}_i$ = 1.0 mm and $\bar{D}_i$ = 15.6 mm respectively.

5.5 Transport - Shear Relations

In an attempt to correlate the transport rate with the bed shear stress, the subsurface scaled dimensionless transport rate, W_i^*, is plotted against the dimensionless bed shear stress, τ_i^*, in Figures 11a and 11b for the initial and final transport phase data. Similarly, the surface scaled dimensionless transport rates, W_{si}^*, are plotted against τ_i^* for the final phase data in Figure 12. A linear log-log relation between W_i^* or W_{si}^* and τ_i^* of the form of Eq. 15 ($W_i^*=\alpha_i\tau_i^{*mi}$) is determined by regression for each size range.

The regression was performed for individual bed sediment series as well as for combinations of the series. Performing the regression individually for each series was typically based on only four data points since Proffitt conducted four runs for each bed sediment series. The use of only four pairs of points in a regression analysis may provide questionable results, since the influence of one outlying point increases as the number of points is decreased. The data for series 1 and 4 and for series 2 and 3 show similar trends. Therefore, regression is performed for series 1 and 4 and for series 2 and 3. This regression based on two series is based on 8 rather than 4 data points so the results are more meaningful. However, it is most useful to regress all of the series together since this provides the most data points.

The objective here is to correlate the transport rate with the shear stress, so the use of many data points provides more general results which reflect the transport - shear relation for a variety of conditions. Therefore, the approach of performing regression for individual series is not taken. Instead, regression is performed both for all series collectively, series 1 through 4, and for series 1 through 3, using an average value of D_{50}. The reason series 1 through 3 are regressed collectively is that the data for series 4 typically plot higher than the other values. That is, for a given shear stress, the series 4 data have higher transport rates than the other series. Recall that the series 4 bed sediment differs slightly from the other sediment series.

5.6 Transport - Shear Relation Regression Results

5.6.1 General Information

Regression results for the subsurface and surface scaled dimensionless transport - shear relations for the initial and final phases are given in Tables 11 through 14. The slope of the linear log-log transport-shear relation, m_i, provides information on the nature of the relationship between transport rate and shear stress. Recall that m_i typically decreases with increasing transport rate. Therefore, it is anticipated that the m_i values for the high transport rate initial phase should be lower than the m_i values for the lower transport rate final phase.

5.6.2 Initial Phase Regression Results

The initial phase W_i^*-τ_i^* regression results are given in Table 11. For the initial transport phase, the m_i values range from 2.06 to 4.03 (96% range) for Series 1 through 4 and from 1.68 to 4.26 (154% range) for series 1 through 3. The highest m_i values correspond to $\bar{D}_i$ = 11 mm. When the m_i values for $\bar{D}_i$ = 11 mm are dropped the m_i values range from 2.06 to 2.31 (12% range) for series 1 through 4 and from 1.68 to 2.12 (26% range) for series 1 through 3.

The initial phase m_i values show little correspondence with grain size, which indicates that the transport rate is not dependent on the grain size. This is a reasonable result due to the high initial transport rates resulting from an unstable bed with no coarse surface layer. Note that the correlation coefficients, r^2, for the initial phase are generally quite good and range from 0.26 to 0.86 for series 1 through 4 and from 0.25 to 0.93 for Series 1 through 3.

Since the initial phase m_i values show little variation with grain size, a weighted average m_i value was computed, $\bar{m}_i$ = 2.24 for series 1 through 4 and $\bar{m}_i$ = 2.06 for series 1 through 3, and the regression of $W_i^*=\alpha_i\tau_i^{*mi}$ was performed to determine new intercepts, α_i. The results are given in Table 12. Thus, perfect similarity is assumed for the intial phase by using the same m_i value for all size ranges.

5.6.3 Final Phase Regression Results

The final phase W_i^*-τ_i^* and W_{si}^*-τ_i^* regression results are given in Tables 13 and 14. The subsurface scaled final transport phase data have m_i values ranging from 0.73 to 2.79 (282% range) for series 1 through 4 and from 1.09 to 3.92 (260% range) for series 1 through 3. The surface scaled final phase data m_i values range from 1.37 to 3.00 (119% range) for series 1 through 4 and from 1.49 to 3.85 (158% range) for series 1 through 3. The subsurface and surface final phase m_i values show similar trends and increase with grain size.

The subsurface based final phase correlation coefficients, r^2, range from 0.052 to 0.43 for series 1 through 4 and from 0.14 to 0.82 for series 1 through 3. The surface scaled final phase r^2 values range from 0.15 to 0.55 for series 1 though 4 and from 0.23 to 0.87 for series 1 though 3. The final phase r^2 values are lower than the initial phase r^2 values because the final phase transport-shear data is quite scattered. Note that the surface scaled regression lines have higher r^2 values than the subsurface regression lines for series 1 through 4. However, the r^2 values are approximately the same for the surface and subsurface regression lines for series 1 through 3.

The final phase m_i values are typically lower or approximately equal to the initial phase m_i values. As pointed out earlier, the final phase m_i values should be higher than the initial phase values since the final phase values have lower

transport rates. It is the nature of the regression technique used that causes the final phase m_i values to be lower than the initial phase m_i values.

5.6.4 Modified Regression Technique

By plotting the final phase W_i^*-τ_i^* regression lines and comparing them with the observed data it can be observed that the regression technique fits lines with slopes that are lower than anticipated (Figure 13). A typical least squares regression technique fits a line that minimizes the distance (error) between the dependent variable (W_i^*) and the best fit line. This method assumes there is no error in the measurement of the independent variable (τ_i^*). This reasoning is valid in some sense since τ_i^* is the predictor for W_i^*. However, applying this technique to plots of W_i^*-τ_i^* may produce best fit lines with slopes that do not describe the data trend effectively. Typically, the slopes are lower than expected, as is the case here.

One solution to the above problem is to fit lines to the data by eye. However, a modified regression technique which accounts for error in both W_i^* and τ_i^* produces best fit lines that describe the data adequately, while avoiding the subjectiveness of fitting lines by eye. The modified regression technique coefficients for Eq. 15 ($W_i^*=\alpha_i\tau_i^{*mi}$), α, and m, are given by,

$$m^2 [n\overline{xy} - \Sigma x_i y_i] + m[\Sigma y_i^2 - \Sigma x_i^2 + n(\overline{x^2} - \overline{y^2})] + [\Sigma x_i y_i - n\overline{xy}] = 0 \quad (45)$$

$$\alpha = \overline{y} - m\overline{x} \quad (46)$$

where n is the number of observations, $x_i = \log(\tau_i^*)$, and $y_i = \log(W_i^*)$. The modified regression results are given along with the corresponding original regression results in Tables 13 and 14.

Using this modified regression technique produces final phase m_i values which are higher than the initial phase m_i values. In addition, the final phase m_i values still show a trend of increasing with grain size for $\overline{D}_i \geq 2.84$ mm, while the initial phase m_i values do not show any trend with grain size. Note that the high final phase values of m_i for $\overline{D}_i$ = 1.0, 1.42, and 2.0 mm may be due to low correlation coefficients. The correlation coefficients, r^2, remain the same for both regression techniques and as r^2 approaches a value of 1, the two techniques produce the same results. Since the initial phase r^2 values are relatively high, the original and modified regression techniques produce similar results.

Using the modified regression technique the initial phase m_i values for series 1 through 4 range from 2.37 to 7.85 (231% range) over all $\overline{D}_i$ values. However, when the m_i values for $\overline{D}_i$ = 7.78, 11 and 15.6 mm are dropped, the m_i values range from 2.37 to 3.02 (27% range) for $1.0 \leq \overline{D}_i \leq 7.78$ mm.

The subsurface final phase m_i values determined using the modified regression technique range from 4.00 to 12.80 (222% range) for series 1 through 4. The m_i values for $2.84 \leq \bar{D}_i \leq 15.6$ mm range from 4.00 to 8.7 (118%) for series 1 through 4. The surface scaled final phase modified regression m_i values range from 4.06 to 8.31 (105% range) for series 1 through 4.

5.7 Modified Similarity Approach

The final phase m_i values show an increase with grain size, which indicates a dependence of the transport rate, W_i^*, on grain size, $\bar{D}_i$. Diplas (1987) provided a modified similarity approach which takes this dependence on $\bar{D}_i$ into account. The new similarity approach utilizes and equation of the form of Eq. 23 ($W_i^*=\alpha_i[\tau_i^{*(\bar{D}i/D50)^{\wedge}b}]^{mi'}$). The modified similarity approach is not used for the initial phase data since the initial phase m_i values do not show an increase with grain size. This indicates that the initial phase transport rates are not dependent on grain size.

The first step in using the new similarity approach is to obtain the exponent b by determining a relation of m_i and the relative grain size, $\bar{D}_i/D_{50}$ of the form $m_i=a(\bar{D}_i/D_{50})^b$. Plots of m_i vs. $\bar{D}_i/D_{50}$ are given in Figures 14 and 15. The m_i values for the modified regression technique are quite variable and only show a trend of increasing with grain size $\bar{D}_i$ for $\bar{D}_i$ = 2.84 to 11 mm. However, the m_i values for the original regression technique generally increase over all $\bar{D}_i$. To

avoid problems connected with the variability of the modified regression m_i values, the original regression m_i values are used in the modified similarity approach. The m_i - $\bar{D}_i/D_{50}$ relations determined using the original regression determined m_i values for the subsurface and surface scaled final transport phases (P.F.P.) for series 1 through 4 and $\bar{D}_i$ = 1.0 to 15.6 mm are given by,

P.F.P. Subsurface Approach: $m_i = 1.376(\bar{D}_i/D_{50})^{0.504}$ $r^2=0.9796$ **(47)**

P.F.P. Surface Approach: $m_i = 2.549(\bar{D}_i/D_{50s})^{0.292}$ $r^2=0.8583$ **(48).**

Using Eq. 23 ($W_i^*=\alpha_i[\tau_i^{*(\bar{D}i/D50)\hat{}b}]^{mi'}$), which is the modified similarity expression for the relation between W_i^* and τ_i^*, new slope values, m_i', are determined and given in Tables 13 and 14. Note that the intercepts, α_i, and correlation coefficients, r^2, are the same as for the original similarity approach.

The values of m_i' do not show a significant steady increase with grain size as the m_i values did. Further, the range of the m_i' values is much lower than the m_i values. Table 15 provides a comparison of the initial and final phase m_i and m_i' value ranges. The m_i' values differ at most by 23% and 43% for the final phase subsurface and surface approaches, respectively for $1.0 \leq \bar{D}_i \leq 15.6$ mm. Recall that the m_i values differ at most by 220% and 105% for the final phase subsurface and surface approaches respectively for $1.0 \leq \bar{D}_i \leq 15.6$ mm. The range of the

initial phase m_i values for $1.0 \leq \bar{D}_i \leq 15.6$ mm is quite substantial (96% and 231% for the original and modified regressions respectively). However, when the m_i value for $\bar{D}_i = 11$ mm is dropped the m_i range is reduced considerably (11% and 27% for the original and modified regressions respectively) and has a much smaller range than the final phase m_i values. Further, the final phase m_i' value ranges are comparable to the initial phase m_i value ranges for $1.0 \leq \bar{D}_i \leq 7.78$ mm. The subsurface and surface m_i' values differ at most by 18% and 28% repsectively, while the initial phase m_i values differ at most by 11% and 27% for the original and modified regressions respectively.

In summary, the modified similarity approach accounts for the dependence of the transport rate on grain size indicated by m_i values which increase with grain size by using a modified relation between W_i^* and τ_i^*. When applied to the final phase data which show an increase in m_i with grain size, new slope values, m_i', are produced which show little variation with grain size and have a much smaller range of values.

5.8 Reference Transport Rates

The initial phase dimensionless transport rates, W_i^*, range from about 0.1 to 4, while the final phase W_i^* values range from about 0.0001 to 0.1. Therefore, different reference transport rates, W_r^*, which represent conditions near initial

motion are needed for the initial and final phases. The W_r^* value chosen for the initial phase is W_r^*=0.4. The W_r^* value chosen for the final phase is W_r^*=0.0025 which corresponds to the value used in the analysis of the Oak Creek data and aids in comparison of the final phase data with the Oak Creek data.

5.9 Reference Shear Stresses

5.9.1 Methods for Determining the Reference Shear Stress

Reference dimensionless transport rates, τ_{ri}^*, are determined using the W_i^*-τ_i^* regression relations for the initial phase and for the W_i^*-τ_i^* and W_{si}^*-τ_i^* regression relations for the final phase. The process of determining τ_{ri}^* is essentially the same for both the initial and final phases. For a given W_r^* the transport-shear regressions are used to determine values of τ_{ri}^*. Various values of W_r^* were used to determine τ_{ri}^* for the initial and final phases to aid in equal mobility analysis and to identify the correct value of W_r^* to use.

The τ_{ri}^* values for the initial phase data are determined from W_i^*-τ_i^* relations of the form of Eq. 15 ($W_i^*=\alpha_i\tau_i^{*m_i}$) for both the original and modified regression relations where m_i is averaged . The values of τ_{ri}^* for the final phase may be determined using either the original similarity W_i^* - τ_i^* relations of the form of Eq. 15 or the modified similarity W_i^*-τ_i^* relations of the form of Eq. 23 ($W_i^*=\alpha_i[\tau_i^{*(\bar{D}i/D50)^{\wedge}b}]^{mi'}$) for both the original and modified regression relations. In

an attempt to simplify the analysis, the original similarity $W_i^* - \tau_i^*$ and $W_{si}^* - \tau_i^*$ relations similar to Eq. 15 are used to determine the τ_{ri}^* values for the final phase subsurface and surface approaches respectively.

The so determined τ_{ri}^* values are given in Tables 16 and 17 and plotted in Figures 17 and 18 and decrease with grain size for $\bar{D}_i$ = 1.0 to 7.78 or 11 mm. The τ_{ri}^* values at $\bar{D}_i$ = 11 to 15.6 mm ($\bar{D}_i/D_{50}$ = 3.34 to 4.73) appear to approach a constant value. This supports Andrew's (1983) finding of constant τ_{ri}^* at $\bar{D}_i/D_{50}$ greater than about 4. However, more τ_{ri}^* values at higher $\bar{D}_i/D_{50}$ values, which are not available, would be required to further verify this for Proffitt's data. The τ_{ri}^* values for $\bar{D}_i$ = 11 and 15.6 mm are not used in the subsequent analysis since they typically do not show the same trend as the other values. As an aid in the similarity analysis, the τ_{ri}^* values are regressed against relative grain size, $\bar{D}_i/D_{50}$, for $\bar{D}_i$ = 1.0 to 7.78 mm using the relation of Eq. 19 ($\tau_{ri}^* = \tau_{r50}^* (\bar{D}_i/D_{50})^{-\beta}$). Plots of τ_{ri}^*-$\bar{D}_i/D_{50}$ are given in Figures 17 and 18 and the regression relations are given in Table 18.

5.9.2 Equal Mobility and Selective Transport

The β values for the initial phase are less than unity, indicating that selective transport of the finer grains occurs. This is a necessary condition for the development of a coarse surface layer. Recall that perfect similarity was assumed

for the initial phase by using a single value of m_i for all size ranges, so that $m_1 = ... = m_i$. As mentioned in Chapter 3, perfect similarity produces β values that are constant for all values of W_r^*. This is demonstrated in Table 18, where the β values for both the original and modified intial phase regressions are the same for both $W_r^* = 0.0025$ and 0.4. However, the τ_{r50}^* values increase with W_r^*. Note that the value of $W_r^* = 0.0025$ is well below the range of the initial phase data, so that the nature of the transport - shear relation and, therefore, the m_i values, would be different in this region. It is emphasized that although perfect similarity is assumed for the intial phase equal mobility does not occur because the β values are constant and less than unity for all W_r^*.

The β values for the subsurface final phase are less (larger) than one for the original (modified and graph) regression analyses. The β values for the surface final phase are larger (less) than unity for the original (modified and graph) regression analysis. Thus, the subsurface and surface approaches predict different transport conditions depending on the method of determining the values of τ_{ri}^*.

If it is assumed that the τ_{ri}^* values determined from the modified regression relations and graphical analysis are more accurate, then the final phase subsurface and surface approaches predict different transport conditions. The subsurface approach predicts selective transport of the coarse grains, while the surface approach predicts selective transport of the finer grains. This occurs because the

the reference material for the two approaches (subsurface vs. surface) is different. The final phase bedload is typically coarser than the subsurface and finer than the surface approach.

5.9.3 Reference Shear Stresses for the Median Grain Size

In addition to the β values, the values for the dimensionless reference shear stress for the subsurface and surface median grain sizes, τ_{r50}^*, and τ_{r50s}^*, respectively, provide useful information on the initial motion conditions and aid in the comparison of various data sets. The initial phase values of τ_{r50}^* for $W_r^*=0.4$, $1.0 \leq \bar{D}_i \leq 7.78$ mm, series 1 through 4 are 0.04346 and 0.05022 for the τ_{ri}^* values determined using the original regression and modified regression W_i^*-τ_i^* relations respectively.

The values of τ_{r50}^* for the subsurface final phase data for $W_r^*=0.0025$, $1.0 \leq \bar{D}_i \leq 7.78$ mm, series 1 through 4 are 0.02158 and 0.05827 for the original and modified regression relations respectively. The corresponding values for the surface approach are 0.02341 and 0.02613 for the original and modified regression relations respectively.

5.9.4 Validity of Regression Determined Reference Shear Stresses

In an attempt to determine the validity of using regression relations to determine τ_{ri}^*, values of τ_{ri}^* were read by eye from graphs of W_i^*-τ_i^*. The values are given in Tables 16 and 17. The technique used is to choose a value of W_r^* and from individual graphs of W_i^*-τ_i^* for each grain size read the value of τ_{ri}^*. When several data points fell near the W_r^* value an average value of τ_{ri}^* is chosen. The major weakness of this technique for determining τ_{ri}^* is that it is quite subjective when there are no data points near the reference transport rate.

For the initial phase and $W_r^* = 0.4$ the values of τ_{ri}^* read from graphs of W_i^*-τ_i^* are nearly identical to the values determined from the regression relations. The τ_{ri}^* values determined from the graph and the modified regression relations are much closer than the values determined from the original regression relations. In either case the corresponding graph and regression determined τ_{ri}^* values differ at most by only 25% for W_r^*=0.4. However, for W_r^*=0.0025, the values differ by as much as an order of magnitude. This occurs because there is no data in this region for the initial phase. Therefore, the regression relations are inadequate for determining τ_{ri}^* for W_r^*=0.0025.

For the final phase subsurface and surface approaches where W_r^*=0.0025, the values of τ_{ri}^* determined from the graphs and modified regression relations are similar, and typically differ by less than 10%. However, the graph values often

differ substantially with the original regression relation values. The values from the graph are typically higher than the corresponding original regression values due to the nature of the original regression relations. The original regression relations have rather low m_i values which results in lower τ_{ri}^* values than is observed in the graphs. The modified regression relations appear to fit the final phase data more accurately, and, therefore, the τ_{ri}^* values predicted using the modified regression method are much closer to the τ_{ri}^* values determined visually.

Thus, it is reasonable to determine τ_{ri}^* from the linear log-log W_i^*-τ_i^* relations as long as the value of W_r^* is within the range of the given data from which the regression relations were created. However, when W_r^* falls well outside the given range of data the linear relations become inadequate. In addition, if regression is to be used for determining τ_{ri}^* values the modified regression relations are preferable since they reflect the data trends more accurately.

5.9.5 Reference Transport Relations

The τ_{ri}^* - $\bar{D}_i/D_{50}$ regression relations are given in Table 19. The relations determined for the final phase original regression technique conflict with the relations determined for both the modified regression and graphical procedures. It is proposed that the modified regression procedure reflects more accurately the actual conditions because it produces W_i^*-τ_i^* relations which fit the data accurately

and is in agreement with the graphical procedure. Therefore, the τ_{ri}^* relations proposed for the initial (P.I.P.) and the final phases (P.F.P.) are:

P.I.P (W_r^*=0.4): $\tau_{ri}^* = 0.05022(\bar{D}_i/D_{50})^{-0.9590}$ **(49)**

P.F.P. Subsurface (W_r^*=0.0025): $\tau_{ri}^* = 0.05827(\bar{D}_i/D_{50})^{-1.0577}$ **(50)**

P.F.P. Surface (W_r^*=0.0025): $\tau_{ri}^* = 0.02613(\bar{D}_i/D_{50s})^{-0.9197}$ **(51).**

5.10 Similarity Collapse

A similarity collapse of the W_i^*-τ_i^* relations for each grain size into a single curve for all grain sizes can be realized by plotting W_i^* against a normalized shear stress, ϕ_i, defined by Eq. 20 ($\phi_i=\tau_i^*/\tau_{ri}^*$). Using the modified similarity approach W_i^* is plotted against $\phi_i^{(\bar{D}i/D50)^{\wedge}b}$. The original regression results are used for the intial and final phase similarity collapses for the reason stated previously. The similarity collapses or plots of W_i^* vs. ϕ_i are given in Figures 19 through 24.

The initial phase data collapse nicely into a relation described by,

Initial Phase Series 1 through 4: $W_i^*/W_r^*=\phi_i^{2.24}$ **(52a)**

Initial Phase Series 1 through 3: $W_i^*/W_r^*=\phi_i^{2.06}$ **(52b)**

where W_r^* = 0.4. Some scatter is evident for the largest grain sizes, $\bar{D}_i$ = 11 and

15.6 mm. However, the final phase data for series 1 through 4 using the original similarity approach do not collapse nicely into a single curve, but instead show singinificant scatter. The original similarity (O.S.) approach collapses for series 1 through 4 are given by,

P.F.P. O.S. Subsurface: $W_i^*/W_r^*=\phi_i^{1.66}$ (53)

P.F.P. O.S. Surface: $W_i^*/W_r^*=\phi_i^{2.22}$ (54)

where $W_r^* = 0.0025$. The scatter is reduced for the final phase when series 4 is dropped and series 1 through 3 are analyzed collectively (Fig. 23).

Some of the scatter using the original similarity approach is due to the dependence of the transport rate on grain size. Using the modified similarity approach for the final phase for series 1 through 4 and series 1 through 3 reduces the scatter significantly. The subsurface final phase modified similarity collapses are described by,

P.F.P. Subsurface Series 1 though 4: $W_i^*/W_r^*=[\phi_i^{(\bar{D}i/D50)\text{^}0.504}]^{1.376}$ (55a)

P.F.P. Subsurface Series 1 though 3: $W_i^*/W_r^*=[\phi_i^{(\bar{D}i/D50)\text{^}0.531}]^{1.820}$ (55b)

where $W_r^* = 0.0025$. The corresponding surface based relations for the final phase

are,

P.F.P. Surface Series 1 through 4: $W_{si}^*/W_r^* = [\phi_i^{(\bar{D}i/D50s)^{\wedge}0.292}]^{2.549}$ **(56a)**

P.F.P. Surface Series 1 through 3: $W_{si}^*/W_r^* = [\phi_i^{(\bar{D}i/D50s)^{\wedge}0.377}]^{3.136}$ **(56b)**

where $W_r^* = 0.0025$.

5.11 Predictive Ability of Transport - Shear Relations

In an attempt to verify the validity of the regression relations obtained from similarity analysis, total calculated and observed transport rates are plotted against shear stress in Figure 25. The original regression relations for series 1 through 4 are used for the intial phase while the modified regression relations for series 1 through 4 are used for the final phase. As expected, the plots indicate that the regression relations provide an accurate description of the measured transport rates from which they are derived.

5.12 Surface Coarseness

The final phase corresponds to an armored bed with a surface coarsness (SC) that generally increases with bed shear stress. As mentioned previously, the surface coarseness may be defined by the ratio of the median surface grain size, D_{50s}, to

the subsurface median grain size, D_{50}. Jain (1990) provided criteria for the development of the surface layer (armor or pavement) based on the transitional shear velocity, u_{*_t}. Chin (1985) provided a relation for the determination of u_{*_t} so that the surface coarseness may be determined. The value of u_{*_t} for the final phase is 0.1 m/s.

The predicted surface coarseness using Jain and Chin's criteria is compared with the actual surface coarseness in Table 19. The predicted SC is coarser than the actual SC by 0.532 to 2.165 mm. The average predicted SC is 3.37 compared to the average actual SC of 2.24. Thus, based on Jain and Chin's criteria, the final phase armor layer is not at its equilibrium value.

5.13 Comparison of Proffitt and Oak Creek Data

5.13.1 Background Information

Parker, et al (1982) and Diplas (1987) applied a similarity approach analogous to that used above for Proffitt's data to bedload data from Oak Creek, Oregon. The Oak Creek data correspond more closely to the Proffitt final phase data than to the initial phase data in terms of bedload transport rates. The Oak Creek and final phase subsurface scaled dimensionless transport rates range from 0.0001 to 0.20 and 0.00035 to 0.07 respectively. The Oak Creek and final phase dimensionless shear stresses range from 0.02 to 2.7 and 0.015 to 0.42 respectively.

A comparison of the Oak Creek and final phase subsurface scaled dimensionless transport rates for each size range is given in Table 20. Although the $\bar{D}_i/D_{50}$ values do not match exactly for the two data sets, the transport rates for similar $\bar{D}_i/D_{50}$ values correspond nicely. In a similar fashion the dimensionless shear stresses for each size range are given in Table 20. Much like the dimensionless transport rates the dimensionless shear stresses correspond well for similar $\bar{D}_i/D_{50}$ values. Therefore, a comparison of the Oak Creek and final phase subsurface based similarity results is provided.

5.13.2 Comparison of Transport-Shear Relations

Both Oak Creek and the final phase m_i values increase with grain size, which indicates grain size dependence of the transport rate. The Oak Creek m_i and m_i' values are given in Table 6. The Oak Creek m_i values are typically much larger than both the original regression and modified regression m_i values. Although the Oak Creek values are larger than the final phase m_i values, the percentage difference between the smallest and largest m_i values is similar for the two data sets. The subsurface final phase m_i values differ at most by 282% and 220% for the original and modified regression respectively, while the Oak Creek m_i values differ at most by 290%. The log-log regression relation for Oak Creek determined by Diplas (1987) is given by Eq. 43, while the relations for the

subsurface and surface final phase are given by Eqs. 47 and 48 respectively.

Using the modified similarity approach the dependence of the transport rate on grain size is accounted for to some degree. The modified similarity approach produces m_i' values which vary by 16% for Oak Creek and about 22% for the subsurface final phase original regression, which is a considerable reduction from the m_i value ranges.

5.13.3 Comparison of Reference Shear Stresses

Relations for the dimensionless reference shear stresses, τ_{ri}^*, for Oak Creek provided by Parker, et al (1982) and Diplas (1987) are compared to the subsurface and surface based relations for the final phase (series 1 through 4). Both relations are determined for a reference transport rate, $W_r^* = 0.0025$, which falls at the lower range of measured transport rates for both Oak Creek and the final phase. The τ_{ri}^* relations for $W_r^* = 0.0025$ are given by Eqs. 50 and 51 for the Proffitt final phase subsurface and surface approaches respectively and Eq. 44a for Oak Creek. The exponents, β, which are all greater than 0.9 indicate that the Oak Creek data and Proffitt subsurface based final phase correspond to near equal mobility at near threshold conditions.

The value of the dimensionless reference shear stress for the subsurface median grain size, τ_{r50}^*, for Oak Creek is 0.0876 determined by Parker, et al (1982)

and 0.0873 determined by Diplas (1987). The value of τ_{r50}* for the subsurface final phase is 0.05827. These values may be scaled by the surface coarseness.

A comparison of the surface coarseness defined as the ratio of the surface median size, D_{50s}, to the subsurface median size, D_{50}, is provided for Oak Creek and the final phase. Oak Creek has a surface coarseness of about 2.7, while the final phase data have an average surface coarseness of 2.24.

Therefore, the reference shear stresses for the surface median grain size, τ_{r50s}* become approximately 0.032 for Oak Creek and 0.026 for the subsurface final phase. The τ_{r50s}* value determined from the surface based approach is also 0.026. These values of τ_{r50s}* are close to the value of 0.03 proposed by Niell (1968) for coarse material (gravel-bed streams).

5.13.4 Comparison of Similarity Collapses

A comparison of the equations describing the subsurface and surface original similarity (O.S.) and modified similarity (M.S.) collapses are given by Eqs. 53 through 45, and the expressions for Oak Creek are given by,

Oak Creek O.S.: $$W_i^*/W_r^* = \phi_i^{13.38} \quad (57)$$

Oak Creek M.S.: $$W_i^*/W_r^* = [\phi_i^{(\bar{D}i/D50)\text{^}0.3214}]^{13.71} \quad (58).$$

The m_i exponents for Oak Creek are 13.38 and 13.71 for the original and modified similarity approaches respectively. The m_i exponents for the final phase original regression are about 2 to 3 and much lower than the Oak Creek values. The modified regression m_i exponents would be higher than 2 to 3, but still lower than the values for Oak Creek. This reflects the lower m_i values for the final phase compared to Oak Creek.

5.13.5 Comparison of Oak Creek and Initial Phase Data

The initial phase transport rates are higher than the bulk of the Oak Creek transport rates, which limits direct comparison of the two data sets. However, in an attempt to verify the magnitude of the initial phase m_i values, Diplas' (1987) relation derived from Oak Creek given by,

$$\frac{W_i^*}{W_r^*} = 4 \times 17^{2.625b} \qquad (59)$$

where, $W_r^* = 0.0025$ and,

$$b = 1 - 1.205\,\phi_i^{-1.843\,(D_i/D_{50})^{0.3214}} \qquad (60)$$

is used to calculate W_i^* values for a range of ϕ_i (τ_i^*) values. The Oak Creek data correspond to $\phi_i = 0.9$ to 1.4 and $W_i^* = 0.0001$ to 0.20. For $\phi_i = 0.9$ to 1.4 the corresponding initial phase W_i^* values range from 0.1 to 1.5, which does not cover

the entire intial phase data. Therefore, Diplas' relation is used to predict m_i values at transport rates higher than those observed in Oak Creek, which correspond to the transport rates of the initial phase data. Log-log regression of Eq. 15. gives m_i values over the same range of transport rates as the initial phase (Table 20). Using Diplas's relation for ϕ_i = 1.7 to 1.9 gives W_i^* = 0.0327 to 4.51, and an average m_i value of 4.63. This ϕ_i range corresponds to W_i^* = 0.5 to 3.5 for the initial phase, and an average m_i of 2.24. Thus, the m_i values determined from Diplas' Oak Creek relation are slightly higher than the initial phase values over nearly the same transport rates, but do verify the magnitude of the initial phase m_i values.

As seen in Table 20, Diplas' relation predicts m_i values that decrease with increasing bed shear stress and transport rate. This is in agreement with both the Oak Creek data and Proffitt data. Further, it has been hypothesized that the m_i values reach a constant value at high bed shear stresses and transport rates. This is observed in Table 20, where the predicted m_i values not only decrease with increasing ϕ_i and W_i^*, but also the range of m_i values decreases with increasing ϕ_i and W_i^* so that m_i approaches a constant value at high ϕ_i and W_i.

In addition to the m_i values a comparison of the initial phase and Oak Creek data β values indicates that similar conditions exist for both cases. The β values for the initial phase original and modified similarity approaches are 0.9316 and 0.9590 respectively for W_r^* = 0.4. These values are similar to the value of

β = 0.943 for W_r^* = 0.0025 obtained by Diplas (1987) for Oak Creek using the modified similarity approach, but lower than the value of β = 0.982 for W_r^* = 0.0025 obtained by Parker, et al (1982) using the original similarity approach.

5.14 Summary of Proffitt Data Analysis and Results

Proffitt's flume data allowed the use of a similarity approach employing fractional transport rates to analyze the bedload transport rates both for the initial phase high transport rates and the final phase low transport rates. The high intial transport rates were due to an initially unstable bed, while the low final phase transport rates (typically 1 - 5% of the initial rates) were due to an armored bed.

Proffitt used four different bed sediments and conducted four experimental runs for each bed sediment. The fourth bed sediment (series 4) is not lognormally distributed as the other bed sediments, and the transport rates for series 4 are typically higher than the others for a given bed shear stress.

The analysis was performed for all the series collectively (series 1 through 4), and for series 1 through 3, using an average subsurface D_{50} = 3.3 mm and a surface D_{50s} = 7.25 mm. Similar results were obtained for the analysis of series 1 through 4 and series 1 through 3, which supports previous findings that the shape of the bed sediment grain size distribution does not significantly influence transport

conditions.

The upper size range used in the analysis was determined by the bedload size fractions, p_i. The majority of grains in the bedload are finer than 19 mm, so an upper size range of 12.7 to 19 mm with a corresponding $\bar{D}_i$ = 15.6 mm was used. The lower size range was determined from a suspension criterion and a preliminary analysis of the transport -shear relations. The suspesnion criterion indicated that particles smaller than 0.5 mm were frequently in suspension. The preliminary analysis indicated that for $\bar{D}_i$ sizes smaller than 1.0 mm, the m_i values decreased with grain size, which conflicts with previous findings. Therefore, the lower size range used in the analysis was 0.853 - 1.20 mm with a corresponding $\bar{D}_i$ value of 1.0 mm.

Analysis of the initial phase data resulted in transport-shear relations with high correlation coefficients, r^2, and relatively constant m_i values. Since the m_i values were nearly constant, perfect similarity was assumed for the initial phase. The average m_i values for the initial phase were 2.24 and 2.67 for the original and modified regressions respectively. The magnitude of these m_i values was approximately verified by applying a bedload relation, derived from Oak Creek by Diplas (1987), over nearly the same range of transport rates. Diplas' relation predicted an average m_i value of 4.63. Although the m_i value predicted by the relation is higher, it roughly verifies the magnitude of the initial phase m_i values.

The high correlation coefficients and the assumption of perfect similarity led to an excellent similarity collapse of the initial phase data.

A reference transport rate, W_r^*, equal to 0.4 was used for the initial phase since this value falls at the lower end of the given intial phase data range. The initial phase data correspond to conditions of selective transport as evidienced by β values less than unity (0.9316 and 0.9590 for the original and modified regressions respectively) in the τ_{ri}^* - $\bar{D}_i/D_{50}$ relation. Further, since perfect similarity was assumed and selective transport occured, the β values remained constant and less than unity for all values of the reference transport rate, W_r^*. For the initial phase modified regression the reference bed shear stress for the median grain size, τ_{r50}^*, was equal to 0.05002 for $W_r^* = 0.4$.

The final phase data were analyzed using both subsurface and surface based approaches. The final phase correlation coefficients, r^2, were lower than the initial phase r^2 values. Both the subsurface and surface m_i values showed similar trends and generally increased with grain size indicating some dependence of the transport rate on grain size. The modified similarity approach took this dependence into account as evidenced by m_i' values that did not increase with grain size and had a significantly smaller range than the m_i values.

Using a standard regression technique for the final phase to correlate W_i^* and τ_i^* produced m_i values that were lower than the initial phase data. This trend

is not in agreement with traditional transport - shear relations. However, using a modified regression technique, the final phase m_i values were higher than the initial phase m_i values in agreement with observed data. The modified regression m_i values showed some variability, but increased with $\bar{D}_i$ for $\bar{D}_i$ = 2.84 to 11 mm.

Original similarity collapses for the final phase showed considerable scatter, and were much poorer than the initial phase collpses. However, the final phase modified similarity collpases reduced the scatter. The scatter in the final phase collapses was attributed to low correlation coefficients in the transport - shear relations due to scatter in the final phase data.

The final phase reference shear stresses for W_r^* = 0.0025 were determined from the original and modified regression relations and read directly from graphs of W_i^* vs. τ_i^*. The τ_{ri}^* values determined from the modified regression relations and the graphs were in agreement, but not in agreeemnt with the original regression relations. It is suggested that the modified regression technique more accurately reflects the actual conditions and should be used to determine values of the reference shear stress.

Comparison of the final phase data and the Oak Creek data indicated that the final phase data and the Oak Creek data have similar transport rates and bed shear stresses for corresponding $\bar{D}_i/D_{50}$ values. In addition, both Oak Creek and the final phase data have m_i values that increase with grain size. Both the original and

modified regression m_i values were lower than those for Oak Creek. However, both the final phase and Oak Creek m_i values were higher than the initial phase values. The initial phase data had m_i values that did not vary significantly with grain size indicating that the transport rate is not dependent on grain size in this region. This result verifies that the dependence of the transport rate on grain size diminishes with increasing transport rate, and constant m_i values are obtained at high tranpsort rates.

Table 8. Summary of Proffitt Data Bed Sediment Properties

	Series 1	Series 2	Series 3	Series 4	Average
D_{50}, mm	2.9	3.25	3.07	4.2	3.3
D_g, mm	2.95	3.3	3.28	2.83	
σ_g, mm	2.26	3.24	2.78	1.95	

Table 9. Surface Coarseness (D_{50s}/D_{50}) for the Proffitt final phase data.

Experiment	Bed Shear Stress N/m^2	Surface D_{50s} mm	Subsurface D_{50} mm	Surface Coarseness
1-2	4.304	6.85	2.90	2.36
1-3	2.937	4.68	2.90	1.61
1-4	3.727	5.70	2.90	1.97
1-7	3.293	5.00	2.90	1.72
2-1	3.672	6.40	3.25	1.97
2-2	4.331	6.90	3.25	2.12
2-3	5.128	8.70	3.25	2.68
2-4	6.819	11.7	3.25	3.60
3-1	5.592	8.30	3.07	2.70
3-2	6.101	10.7	3.07	3.49
3-3	7.216	11.7	3.07	3.81
3-4	4.827	9.00	3.07	2.93
4-1	3.642	4.95	4.20	1.18
4-2	3.066	4.65	4.20	1.11
4-3	3.992	5.30	4.20	1.26
4-4	4.488	5.45	4.20	1.30
	Average =	7.25	3.33	2.24

Table 10. Proffitt Size Ranges and Corresponding $\bar{D}_i$ and f_i values.

Size Range, mm	$\bar{D}_i$, mm	Series 1 f_i, %	Series 2 f_i, %	Series 3 f_i, %	Series 4 f_i, %
0.853 - 1.20	1.0	6.65	7.67	7.86	6.33
1.20 - 1.68	1.42	11.68	9.29	10.46	8.60
1.68 - 2.41	2.0	15.68	12.55	14.48	11.95
2.41 - 3.35	2.84	16.04	9.31	11.80	7.04
3.35 - 4.76	4.0	12.10	13.26	17.87	20.75
4.76 - 6.35	5.6	13.65	12.25	8.15	31.96
6.35 - 9.52	7.78	7.38	5.76	5.28	3.22
9.52 - 12.7	11.0	5.01	5.00	5.47	2.66
12.7 - 19.0	15.6	2.43	6.42	7.10	2.48

Table 11. Proffitt Initial Phase W_i^*-τ_i^* Regression Results.

		Series 1 through 4					Series 1 through 3		
		Original Regression		Modified Regression			Original Regression		
$\bar{D}_i$, mm	$\bar{D}_i/D_{50}$	m_i	α_i	m_i	α_i	r^2	m_i	α_i	r^2
0.25	0.076	4.42	0.239			0.62	3.94	0.276	0.58
0.35	0.106	4.02	1.28			0.61	3.52	1.26	0.59
0.50	0.152	3.10	4.62			0.55	2.52	3.57	0.55
0.72	0.219	2.38	12.0			0.59	1.84	7.62	0.69
1.0	0.304	2.12	27.1	3.02	91.84	0.67	1.68	16.2	0.88
1.42	0.432	2.18	67.5	2.77	185	0.76	1.85	41.4	0.91
2.0	0.608	2.12	137	2.60	365	0.79	1.84	82.8	0.93
2.84	0.864	2.09	272	2.53	785	0.80	1.83	155	0.91
4.0	1.216	2.06	495	2.37	1156	0.85	1.87	299	0.92
5.5	1.672	2.22	1320	2.54	3507	0.86	2.04	796	0.90
7.78	2.366	2.31	2586	2.86	$1.71X10^4$	0.78	2.12	1360	0.79
11	3.345	4.03	$1.54X10^6$	6.70	$3.47X10^{10}$	0.59	4.26	3.30x106	0.58
15.6	4.729	2.10	883	7.85	$1.21X10^{13}$	0.26	2.10	884	0.25
Weighted Average m_i = for $1.0 \leq \bar{D}_i \leq 15.6$ mm		2.24		2.67			2.06		

Table 12. Proffitt Initial Phase new α_i values using an average m_i value from the original and modified regression techniques for Series 1 through 4.

		Original Regression		Modified Regression	
$\bar{D}_i$, mm	$\bar{D}_i/D_{50}$	$\bar{m}_i$	α_i	$\bar{m}_i$	α_i
1.0	0.304	2.24	31.6	2.67	49
1.42	0.432	2.24	74.2	2.67	132
2.0	0.608	2.24	176	2.67	356
2.84	0.864	2.24	390	2.67	920
4.0	1.216	2.24	800	2.67	2200
5.5	1.672	2.24	1410	2.67	4630
7.78	2.366	2.24	2060	2.67	8690
11	3.345	2.24	1825	2.67	1.44×10^4
15.6	4.729	2.24	1550	2.67	1.09×10^4

Table 13. Proffitt Subsurface Final Phase W_i^*-τ_i^* Regression Results

		Series 1 through 4						Series 1 through 3			
		Original Regression		Modified Regression		Modified Similarity		Original Regression		Modified Similarity	
$\bar{D}_i$ (mm)	$\bar{D}_i/D_{50}$	m_i	α_i	m_i	α_i	m_i'	r^2	m_i	α_i	m_i'	r^2
0.25	0.076	2.44	0.00182				0.37	2.39	0.00152		0.49
0.35	0.106	2.49	0.00920				0.38	2.37	0.00773		0.48
0.50	0.152	1.88	0.0297				0.28	1.85	0.0251		0.38
0.72	0.219	1.28	0.0424				0.15	1.68	0.0493		0.29
1.0	0.304	0.73	0.036	12.8	3.53×10^{5}	1.34	0.052	1.12	0.0478	2.03	0.14
1.42	0.432	0.89	0.060	8.23	1.48×10^{4}	1.38	0.096	1.09	0.0684	1.64	0.19
2.0	0.608	1.06	0.133	4.83	278	1.37	0.19	1.24	0.160	1.56	0.37
2.84	0.864	1.32	0.401	4.00	233	1.44	0.29	1.64	0.673	1.71	0.57
4.0	1.22	1.45	0.894	4.76	7140	1.33	0.28	1.94	2.50	1.68	0.65
5.5	1.67	1.95	5.30	4.96	4.96×10^{4}	1.52	0.37	2.53	22.2	1.86	0.74
7.78	2.37	2.40	26.3	5.33	5.33×10^{5}	1.57	0.43	2.94	117	1.80	0.82
11	3.34	2.38	35.2	8.70	5.28×10^{11}	1.31	0.26	3.77	3670	1.91	0.64
15.6	4.73	2.79	179	7.49	1.88×10^{10}	1.28	0.36	3.92	1.17×10^{4}	1.80	0.64
Average m_i = (1.0 ≤ $\bar{D}_i$ ≤ 15.6 mm)		1.66		6.78		1.39		2.24		1.78	

Table 14. Proffitt Surface Final Phase W_{si}^*-τ_i^* Regression Results.

		Series 1 through 4						Series 1 though 3		
		Original Regression		Modified Regression		Modified Similarity		Original Regression		
$\bar{D}_i$ (mm)	$\bar{D}_i/D_{50}$	m_i	α_i	m_i	α_i	m_i'	r^2	m_i	α_i	r^2
0.25	0.034	3.30	0.010				0.35	3.52	0.008	0.38
0.35	0.048	2.50	0.009				0.38	3.50	0.037	0.42
0.50	0.069	2.47	0.109				0.30	2.73	0.110	0.37
0.72	0.099	1.87	0.142				0.22	2.23	0.170	0.32
1.0	0.138	1.37	0.146	8.31	1530	1.94	0.15	1.66	0.178	0.23
1.42	0.196	1.44	0.312	5.60	339	1.85	0.23	1.49	0.30	0.30
2.0	0.276	1.76	1.10	4.17	144	2.04	0.39	1.76	1.10	0.39
2.84	0.392	1.96	3.05	4.06	454	2.04	0.45	1.96	3.05	0.45
4.0	0.552	2.38	15.4	4.47	4610	2.24	0.51	2.79	36.2	0.77
5.5	0.759	2.74	67.6	5.59	3.81×10^5	2.36	0.47	3.47	413	0.84
7.78	1.073	2.92	83.4	5.24	2.14×10^5	2.27	0.54	3.53	459	0.87
11.0	1.517	2.38	35.1	7.46	1.88×10^9	1.65	0.26	3.34	323	0.50
15.6	2.152	3.00	106	5.26	7.53×10^5	1.91	0.55	3.85	2480	0.78
Average m_i =		2.22		5.57		2.03		2.65		
($1.0 \leq \bar{D}_i \leq 15.6$ mm)										

Table 15. Comparison of m_i and m_i' ranges for the Proffitt Initial and Final Phases.

	Series 1 through 4			Series 1 through 3	
	Original Regression	Modified Regression	Modified Similarity	Original Regression	Modified Similarity
Size Range	m_i	m_i	m_i'	m_i	m_i'
$1.0 < \bar{D}_i < 15.6$mm					
Intial Phase	96%	231%		154%	
Subsurface Final	282%	220%	23%	260%	30%
Surface Final	120%	105%	43%	160%	
$1.0 < \bar{D}_i < 7.78$mm					
Initial Phase	11%	27%		26%	
Subsurface Final	230%	220%	18%	170%	30%
Surface Final	113%	105%	28%	137%	
$2.84 < \bar{D}_i < 15.6$mm					
Initial Phase	96%	231%		133%	
Subsurface Final	111%	118%	23%	139%	14%
Surface Final	53%	84%	43%	96%	

Table 16. Values of τ_{ri}^* for Proffitt Initial Phase determined from W_i^*-τ_i^* regression relations and directly from graphs of W_i^*-τ_i^* for $W_r^* = 0.0025$ and $W_r^* = 0.4$.

		$W_r^* = 0.0025$			$W_r^* = 0.4$		
$\bar{D}_i$ mm	$\bar{D}_i/D_{50}$	τ_{ri}^* from Original Regression Using m_i	τ_{ri}^* from Modified Regression Using m_i	τ_{ri}^* from W_i^*-τ_i^* Graphs	τ_{ri}^* from Original Regression Using m_i	τ_{ri}^* from Modified Regression Using m_i	τ_{ri}^* from W_i^*-τ_i^* Graphs
1.0	0.304	0.01475	0.02469	0.1	0.1422	0.1652	0.15
1.42	0.432	0.01008	0.01703	0.08	0.0971	0.1140	0.12
2.0	0.608	0.00685	0.01174	0.05	0.0661	0.0786	0.08
2.84	0.864	0.00480	0.00823	0.04	0.0463	0.0551	0.055
4.0	1.22	0.00349	0.00594	0.03	0.0336	0.0397	0.035
5.5	1.67	0.00271	0.00449	0.02	0.0261	0.0301	0.030
7.78	2.37	0.00228	0.00355	0.015	0.0220	0.0238	0.025
11.0	3.34	0.00241	0.00294	0.015	0.0232	0.0196	0.020
15.6	4.73	0.00260	0.00326	0.01	0.0251	0.0218	0.020

Table 17. Values of τ_{ri}^* for Proffitt Final Phase determined from W_i^*-τ_i^* regression relations and directly from graphs of W_i^*-τ_i^* for $W_r^* = 0.0025$.

		Subsurface				Surface		
$\bar{D}_i$ mm	$\bar{D}_i/D_{50}$	τ_{ri}^* from Original Regression	τ_{ri}^* from Modified Regression	τ_{ri}^* from W_i^*-τ_i^* Graphs	$\bar{D}_i/D_{50s}$	τ_{ri}^* from Original Regression	τ_{ri}^* from Modified Regression	τ_{ri}^* from W_{si}^*-τ_i^* Graphs
1.0	0.304	0.0259	0.2308	0.23	0.138	0.0514	0.2012	0.20
1.42	0.432	0.0281	0.1504	0.16	0.196	0.0350	0.1212	0.15
2.0	0.608	0.0235	0.0902	0.10	0.276	0.0315	0.0722	0.08
2.84	0.864	0.0214	0.0572	0.056	0.392	0.0266	0.0507	0.06
4.0	1.22	0.0173	0.0440	0.045	0.552	0.0256	0.0396	0.04
5.5	1.67	0.0197	0.0338	0.035	0.759	0.0241	0.0344	0.035
7.78	2.37	0.0211	0.0274	0.025	1.073	0.0282	0.0306	0.028
11.0	3.34	0.0181	0.0226	0.023	1.517	0.0181	0.0256	0.025
15.6	4.73	0.0182	0.0191	0.011	2.152	0.0287	0.0244	0.023

Table 18. Proffitt Initial and Final Phase τ_{ri}^* - $\bar{D}_i/D_{50}$ relations for $1.0 < \bar{D}_i < 7.78$ mm.

Proffitt Initial Phase		
$W_r^* = 0.0025$		
Original Regression	$\tau_{ri}^* = 0.004509(\bar{D}_i/D_{50})^{-0.9316}$	$r^2 = 0.9877$
Modified Regression	$\tau_{ri}^* = 0.007505(\bar{D}_i/D_{50})^{-0.9590}$	$r^2 = 0.9953$
Graph (Fig. 11b)	$\tau_{ri}^* = 0.03389(\bar{D}_i/D_{50})^{-0.9380}$	$r^2 = 0.9932$
$W_r^* = 0.04$		
Original Regression	$\tau_{ri}^* = 0.04346(\bar{D}_i/D_{50})^{-0.9316}$	$r^2 = 0.9877$
Modified Regression	$\tau_{ri}^* = 0.05022(\bar{D}_i/D_{50})^{-0.9590}$	$r^2 = 0.9953$
Graph (Fig. 11b)	$\tau_{ri}^* = 0.04962(\bar{D}_i/D_{50})^{-0.9395}$	$r^2 = 0.9820$
Proffitt Subsurface Final Phase		
$W_r^* = 0.0025$		
Original Regression	$\tau_{ri}^* = 0.02158(\bar{D}_i/D_{50})^{-0.1720}$	$r^2 = 0.5931$
Modified Regression	$\tau_{ri}^* = 0.05827(\bar{D}_i/D_{50})^{-1.0577}$	$r^2 = 0.9773$
Graph (Fig. 11b)	$\tau_{ri}^* = 0.05870(\bar{D}_i/D_{50})^{-1.0991}$	$r^2 = 0.9825$
Proffitt Surface Final Phase		
$W_r^* = 0.0025$		
Original Regression	$\tau_{ri}^* = 0.02341(\bar{D}_i/D_{50s})^{-0.2891}$	$r^2 = 0.6788$
Modified Regression	$\tau_{ri}^* = 0.02613(\bar{D}_i/D_{50s})^{-0.9197}$	$r^2 = 0.9372$
Graph (Fig. 12)	$\tau_{ri}^* = 0.02580(\bar{D}_i/D_{50s})^{-0.9958}$	$r^2 = 0.9692$

Table 19. Comparison of the final phase predicted equilibrium surface coarseness (PSC_e) and the actual surface coarseness (SC), where u_{*t} = 0.1 m/s and PSC_{max} = 6.3 mm.

Run	Bed Shear Velocity				
	u_*, m/s	u_*/u_{*t}	PSC_e/PSC_{max}	PSC_e	SC
1-2	0.066	0.66	0.53	3.339	2.36
1-3	0.054	0.54	0.34	2.142	1.61
1-4	0.061	0.61	0.45	2.835	1.97
1-7	0.057	0.57	0.37	2.331	1.72
2-1	0.061	0.61	0.45	2.835	1.97
2-2	0.065	0.65	0.51	3.213	2.12
2-3	0.071	0.71	0.60	3.780	2.68
2-4	0.082	0.82	0.75	4.725	3.60
3-1	0.075	0.75	0.65	4.095	2.70
3-2	0.078	0.78	0.70	4.410	3.49
3-3	0.085	0.85	0.83	5.229	3.81
3-4	0.069	0.69	0.57	3.591	2.93
4-1	0.060	0.60	0.43	2.709	1.18
4-2	0.056	0.56	0.36	2.268	1.11
4-3	0.063	0.63	0.47	2.961	1.26
4-4	0.067	0.67	0.55	3.465	1.30

Table 20. Comparison of Proffitt Final Phase and Oak Creek τ_i^* and W_i^* Ranges

Oak Creek				Proffitt Subsurface Final Phase Data			
$\bar{D}_i$ (mm)	$\bar{D}_i/D_{50}$	τ_i^* Range	W_i^* Range	$\bar{D}_i$ (mm)	$\bar{D}_i/D_{50}$	τ_i^* Range	W_i^* Range
88.9	4.445	0.02 -0.025	0.0011 - 0.022	15.6	4.73	0.015-0.027	0.00035 - 0.012
63.5	3.175	0.027-0.035	0.0001 - 0.06	11.0	3.34	0.017-0.03	0.00065 - 0.038
44.4	2.22	0.038-0.055	0.00035 - 0.10	7.78	2.37	0.022-0.055	0.001 - 0.045
31.8	1.59	0.055-0.075	0.0003 - 0.10	5.50	1.67	0.031-0.079	0.002 - 0.067
22.2	1.11	0.075- 0.11	0.00075 - 0.20	4.00	1.22	0.045-0.11	0.004 - 0.07
14.3	0.715	0.12 - 0.17	0.0008 - 0.13	2.84	0.864	0.06 - 0.15	0.006 - 0.067
7.14	0.357	0.24 - 0.33	0.001 - 0.10	2.00	0.608	0.09 - 0.12	0.006 - 0.06
3.57	0.1785	0.48 - 0.68	0.002 - 0.07	1.42	0.432	0.12 - 0.31	0.0043 - 0.062
1.79	0.0895	0.95 - 1.4	0.003 - 0.055	1.00	0.304	0.18 - 0.42	0.0023 - 0.07
0.89	0.0445	1.9 - 2.7	0.0035 - 0.038				
		0.02 - 2.7	0.0001 - 0.20			0.015 - 0.42	0.00035 - 0.07

Table 21. Regression of $W_i^* = \alpha_i \tau_i^{*m_i}$ for Oak Creek using Diplas's relation.

	ϕ_i= 0.9 - 1.4		ϕ_i= 0.9 - 1.175		ϕ_i= 1.2 - 1.4		ϕ_i= 1.5 - 1.9		ϕ_i = 1.7- 1.9	
Oak Cr.	W_i^* = 0.0001 - 0.20		W_i^* = 0.001 - 0.066		W_i^* = 6.18×10^{-3} - 0.20		W_i^* = 0.020-4.51		W_i^*=0.0327-4.51	
P.I.P.	W_i^* = 0.1 - 1.5		W_i^* = 0.1 - 1.0		W_i^* = 0.2 - 1.5		W_i^* = 0.5 - 3.5		W_i^* = 0.5 - 3.5	
P.F.P.	W_i^* = 0.001 - 0.04		W_i^* = 0.001 - 0.03		W_i^* = 0.002 - 0.0		W_i^* = 0.002 - 0.05		W_i^* = 0.002 - 0.05	
$\bar{D}_i/D_{50}$	m_i	α_i	m_i	α_i	m_i	α_i	m_i	α_i	m_i	α_i
0.0446	5.62	1.35×10^{-4}	5.97	1.13×10^{-4}	5.10	1.97×10^{-4}	4.27	4.08×10^{-4}	4.08	4.98×10^{-4}
0.0896	6.89	6.59×10^{-3}	7.43	7.14×10^{-3}	6.10	7.03×10^{-3}	4.88	9.15×10^{-3}	4.62	1.03×10^{-2}
0.1785	8.41	1.995	9.23	3.83	7.22	1.012	5.47	0.472	5.10	0.436
0.357	10.21	6772	11.45	41182	8.42	759	5.95	51.4	5.46	33.6
0.715	12.33	4.80×10^{8}	14.21	2.52×10^{10}	9.67	3.22×10^{6}	6.27	8523	5.63	3190
1.11	13.85	3.67×10^{12}	16.28	1.69×10^{15}	10.44	1.48×10^{9}	6.34	2.10×10^{5}	5.59	4.93×10^{4}
1.59	15.19	1.87×10^{16}	18.18	9.81×10^{19}	11.04	3.33×10^{11}	6.31	2.44×10^{6}	5.48	3.65×10^{5}
2.22	16.52	1.52×10^{20}	20.14	1.52×10^{25}	11.55	6.52×10^{13}	6.20	1.88×10^{7}	5.29	1.77×10^{6}
3.175	18.04	8.23×10^{24}	22.48	4.91×10^{31}	12.03	2.17×10^{16}	6.00	1.17×10^{8}	5.01	6.54×10^{6}
4.445	19.55	8.23×10^{29}	24.91	6.8×10^{38}	12.39	5.16×10^{18}	5.71	4.22×10^{8}	4.67	1.44×10^{7}
Average m_i=	12.66		15.03		9.40		5.74		4.63	
m_i Range	248%		317%		143%		48.5%		38.0%	

Proffitt Initial Phase m_i = 2.24

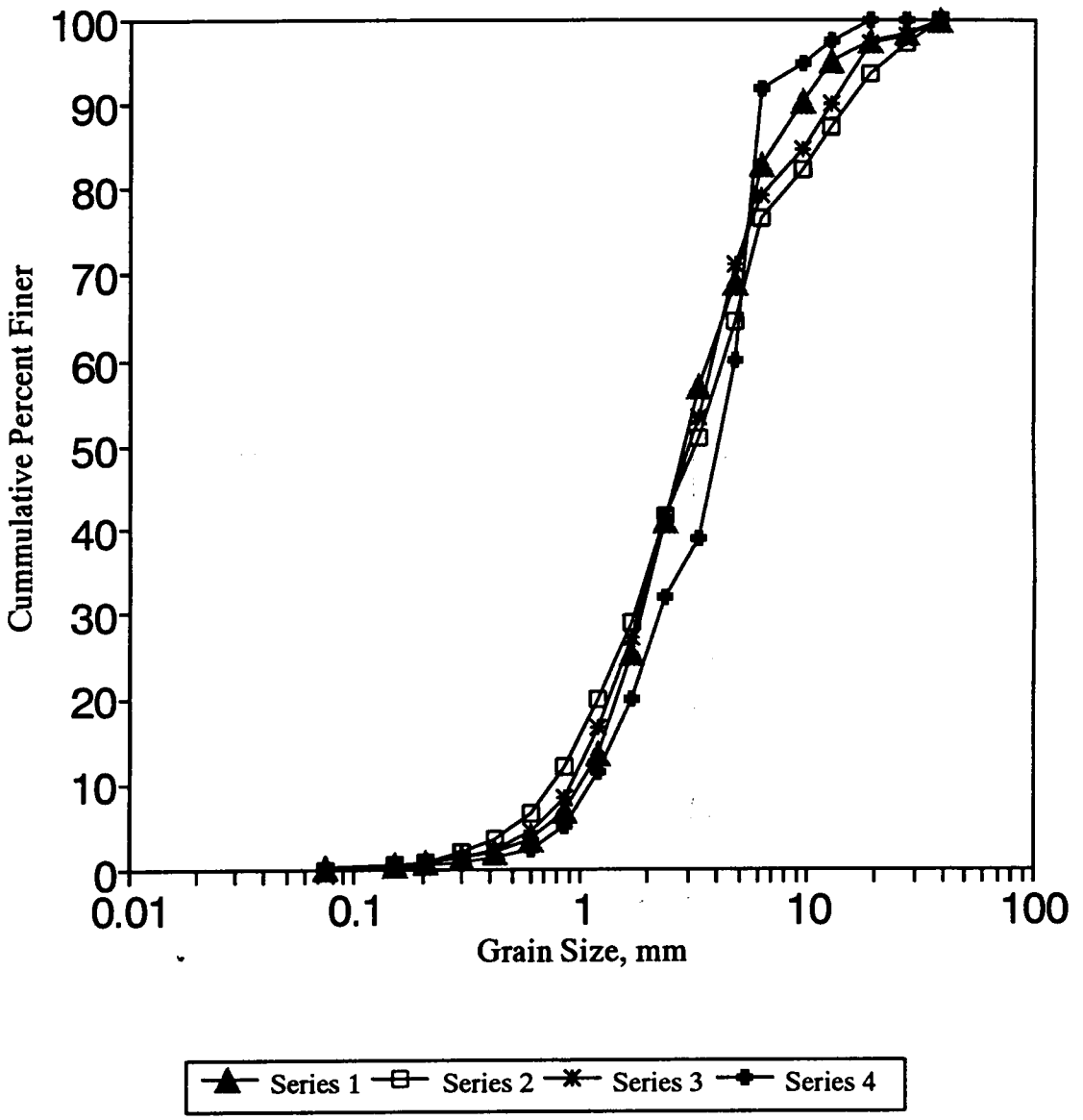

Fig. 10. Proffitt Initial Bed Material Size Distributions for Series 1 through 4.

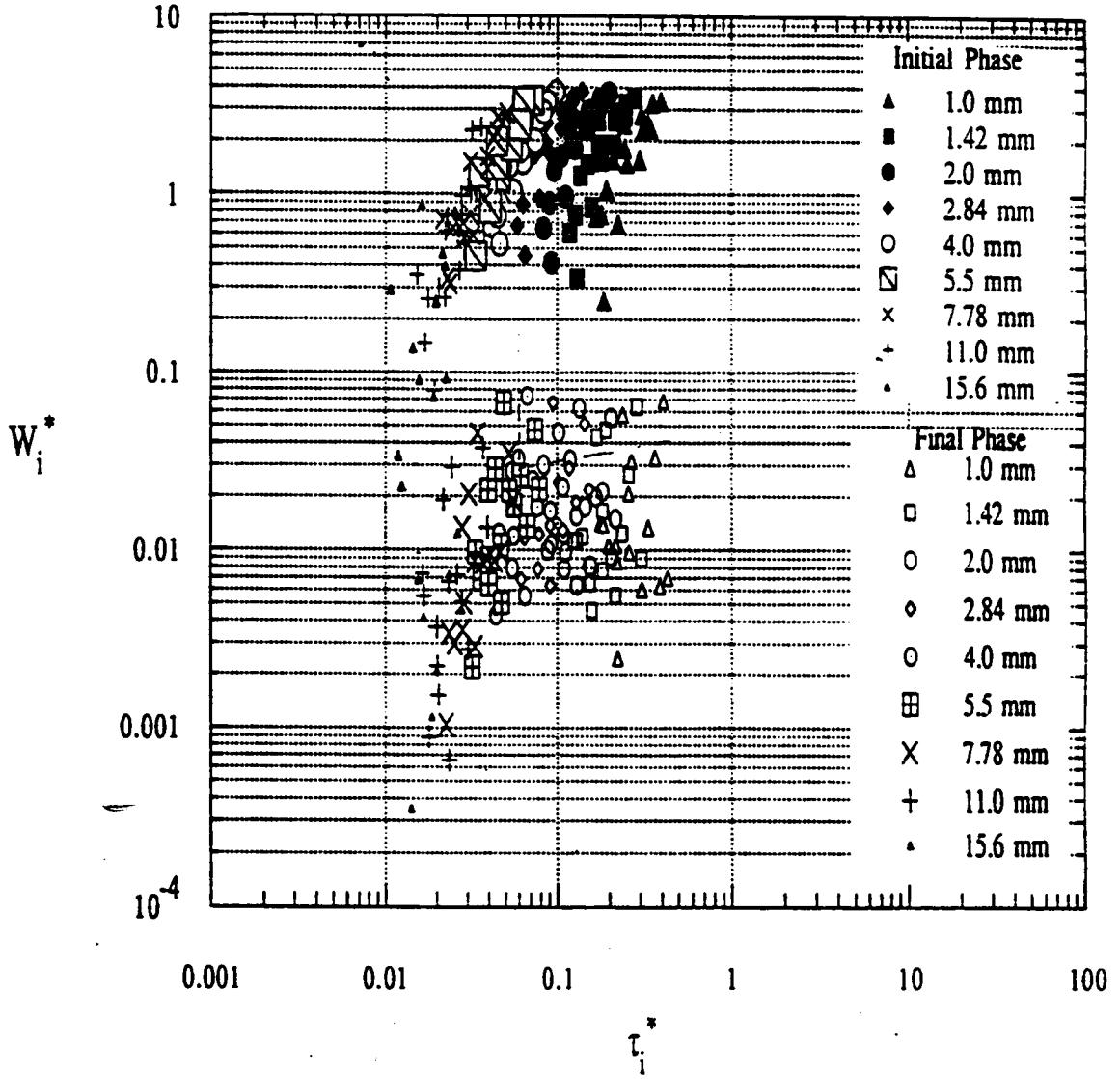

Fig. 11a. Plot of W_i^* vs. τ_i^* for Proffitt Initial and Final Phase Data.

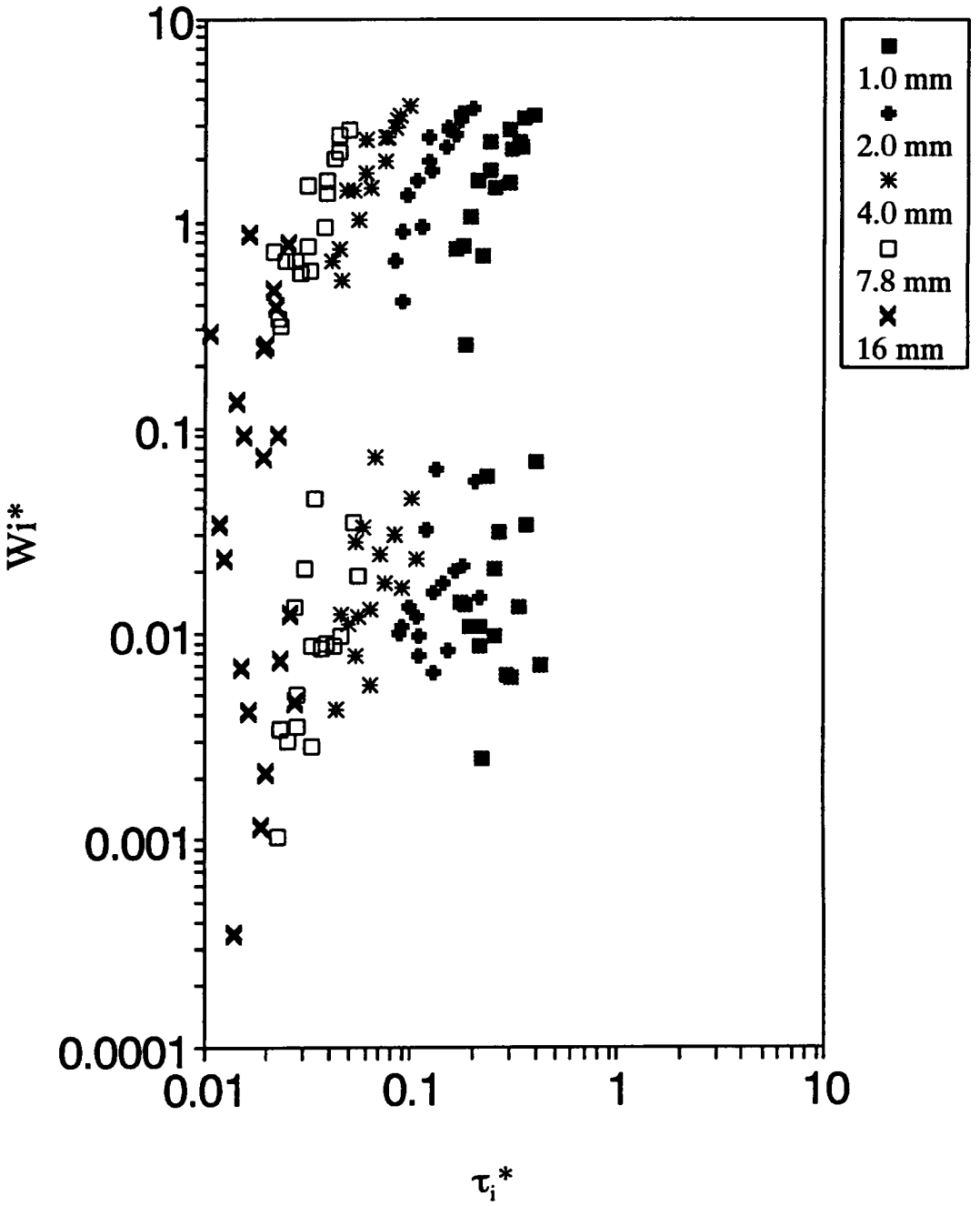

Fig. 11b. W_i^* vs. τ_i^* for selected sizes for Proffitt Initial and Final Phases.

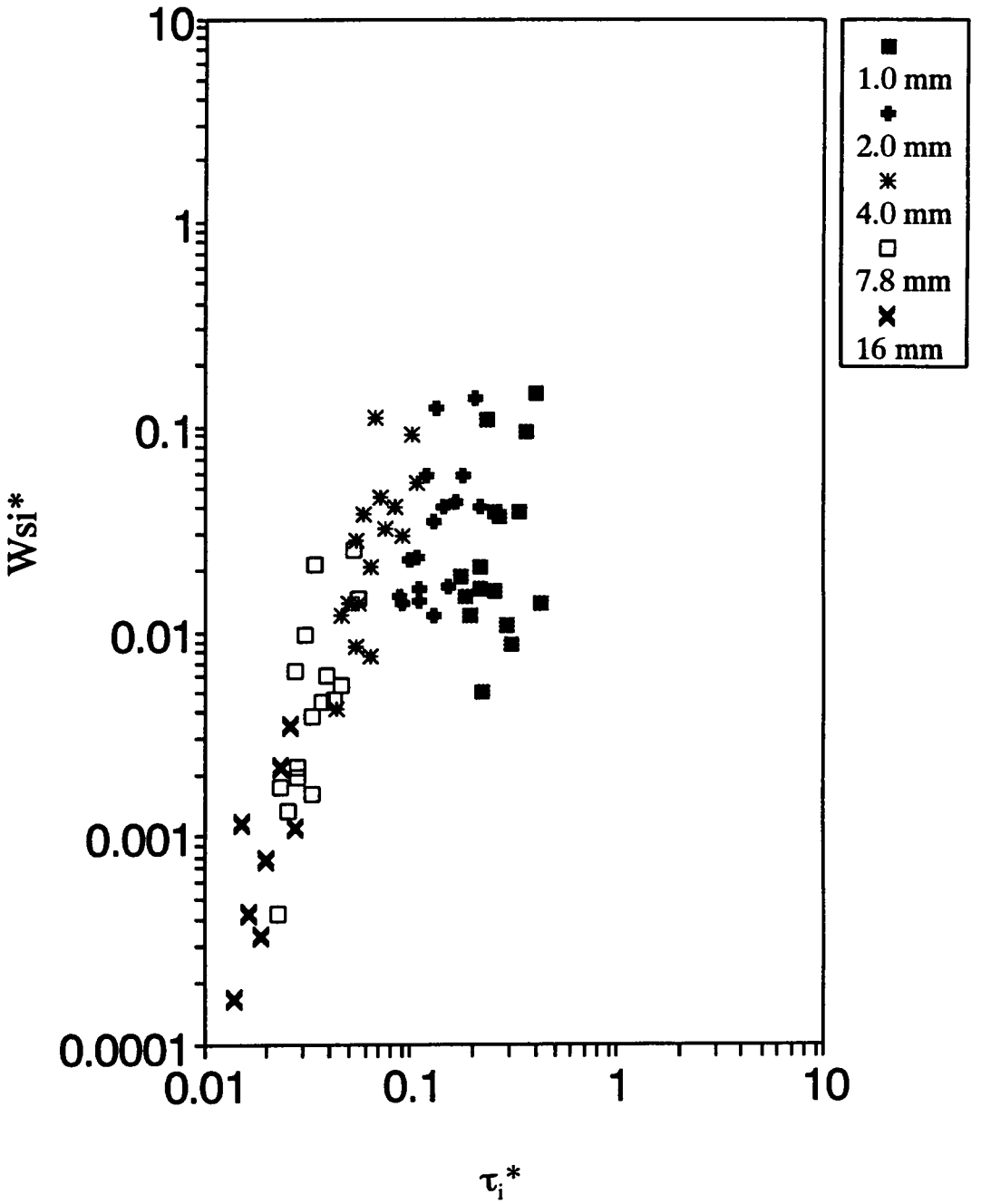

Fig 12. W_{si}^* vs. τ_i^* for selected sizes for the Proffitt Final Phase Surface Approach.

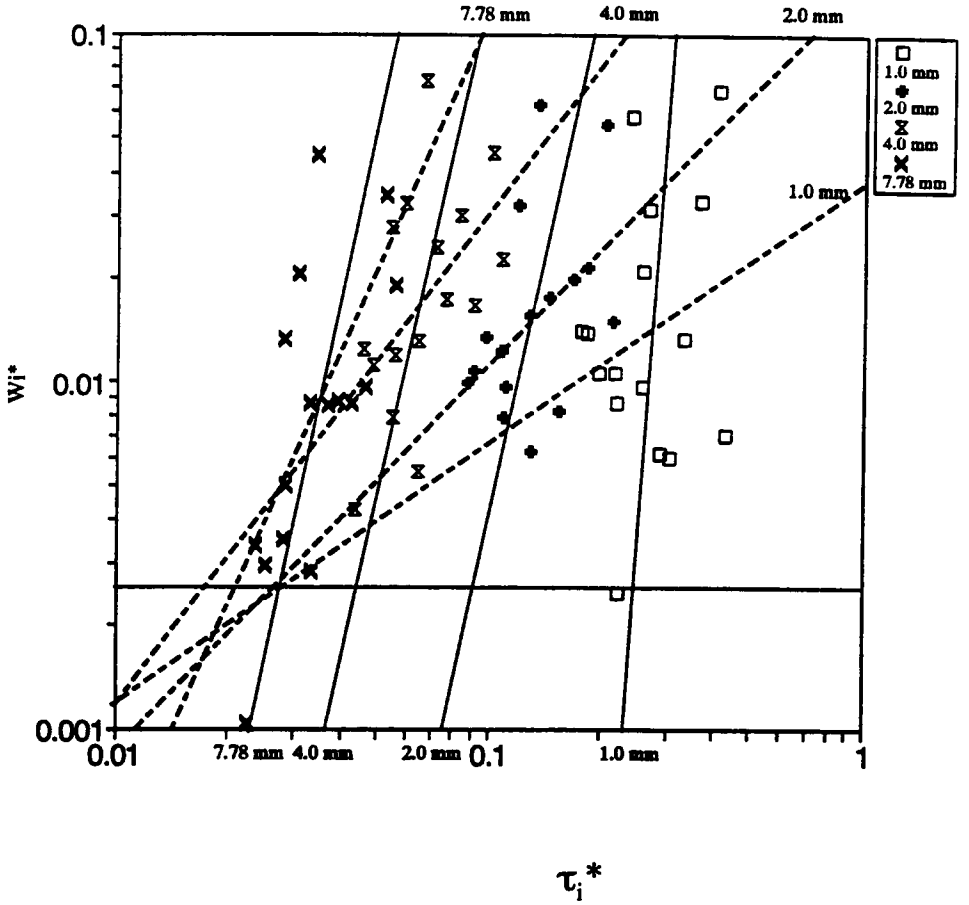

Fig. 13. Plot of W_i^* vs. τ_i^* for Proffitt Final Phase Data with the Original Regression (dashed) and Modified Regression (solid) lines included.

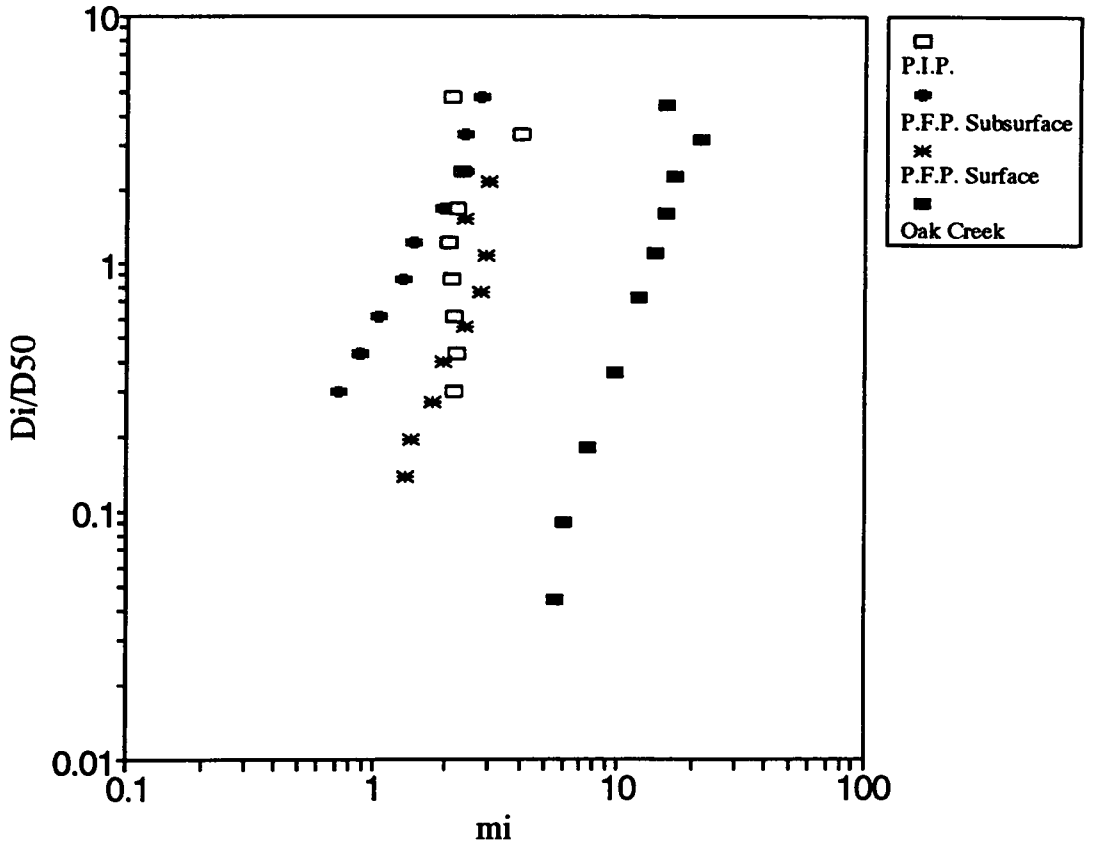

Fig. 14. Plot of m_i vs. $\bar{D}_i/D_{50}$ for the original regression technique m_i values for the Proffitt Initial Phase (P.I.P.), Proffitt Final Phase (P.F.P.) Subsurface and Surface, and Oak Creek.

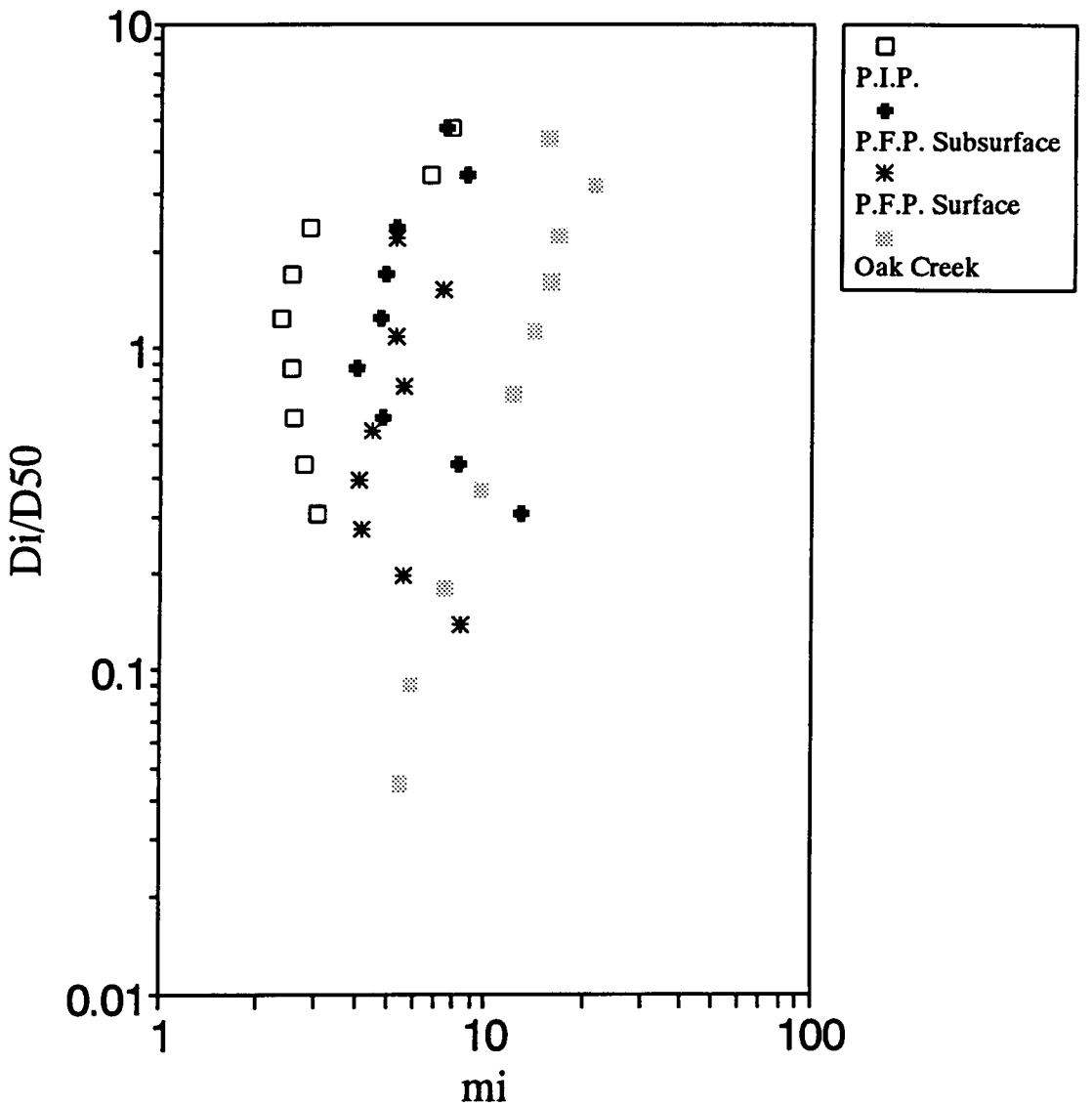

Fig. 15. Plot of m_i vs. $\bar{D}_i/D_{50}$ for the modified regression technique m_i values for the Proffitt Initial Phase (P.I.P.), Proffitt Final Phase (P.F.P.) Subsurface and Surface, and Oak Creek.

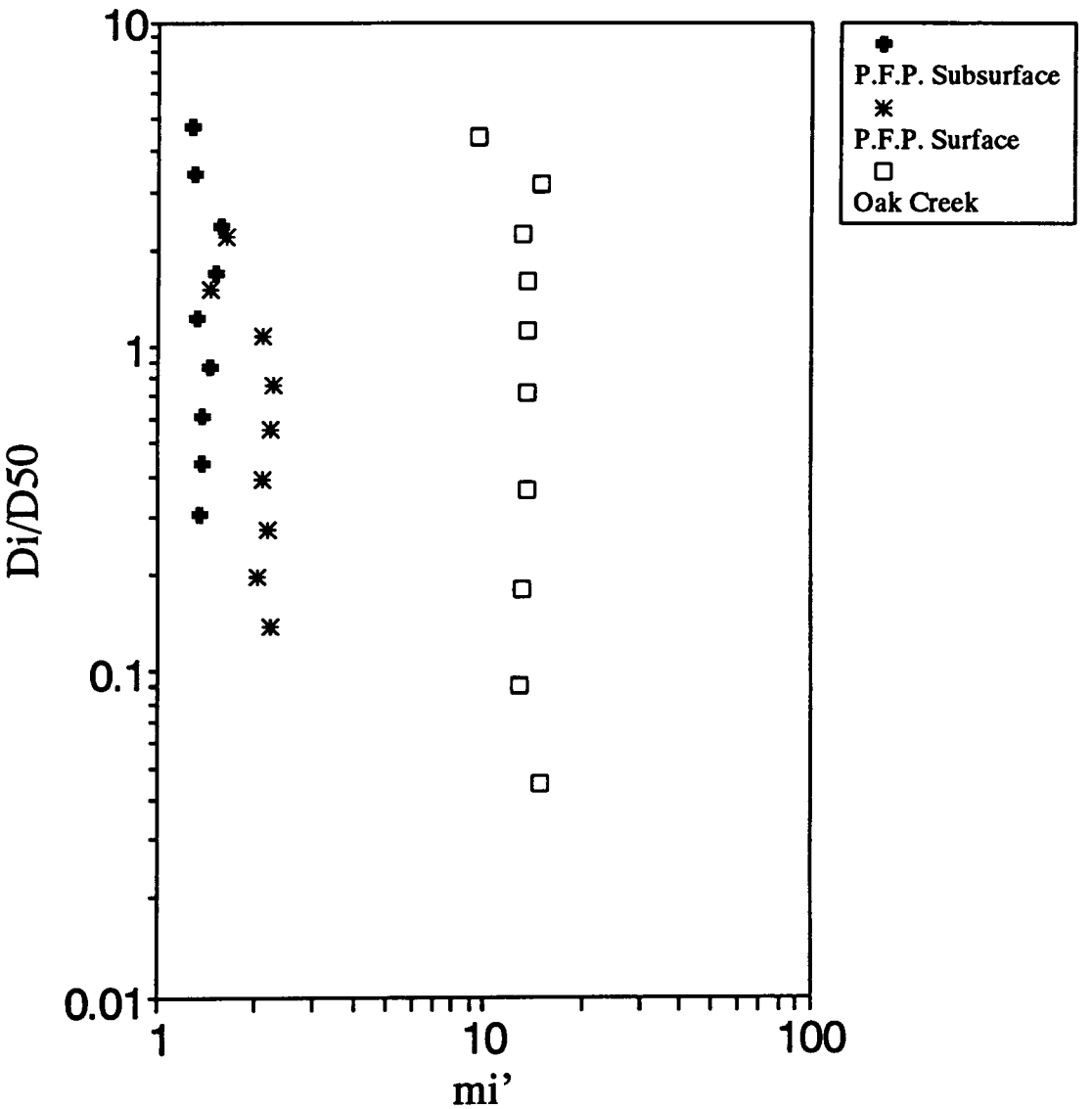

Fig. 16. Plot of m_i' vs. $\bar{D}_i/D_{50}$ for Proffitt Final Phase (P.F.P.) Subsurface and Surface and Oak Creek Data.

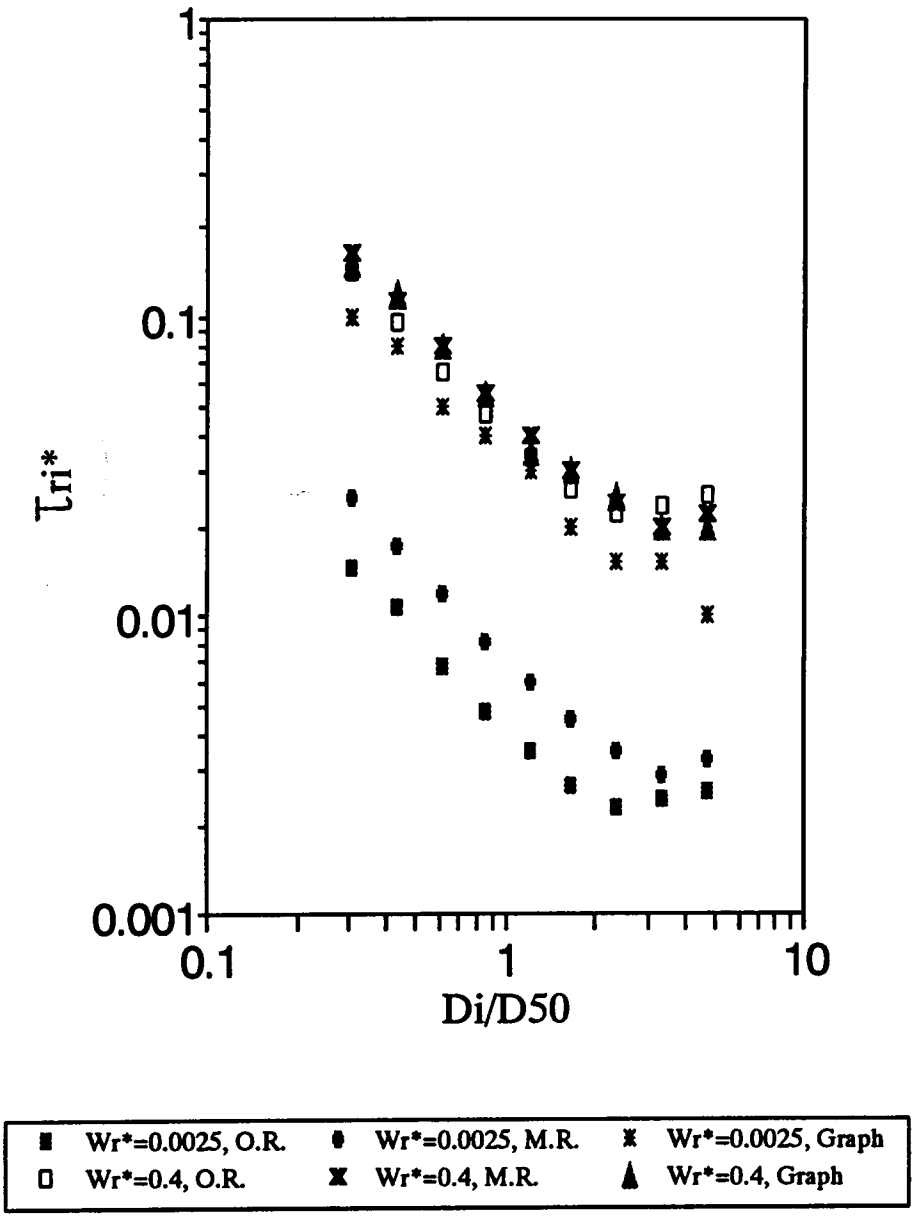

Fig. 17. Plot of τ_{ri}^* vs. $\bar{D}_i/D_{50}$ for W_r^*=0.0025 and W_r^*=0.4. for the Proffitt Initial Phase data where τ_{ri}^* is determined from the original regression (O.R.), modified regression (M.R.), and read from graphs of W_i^*-τ_i^*.

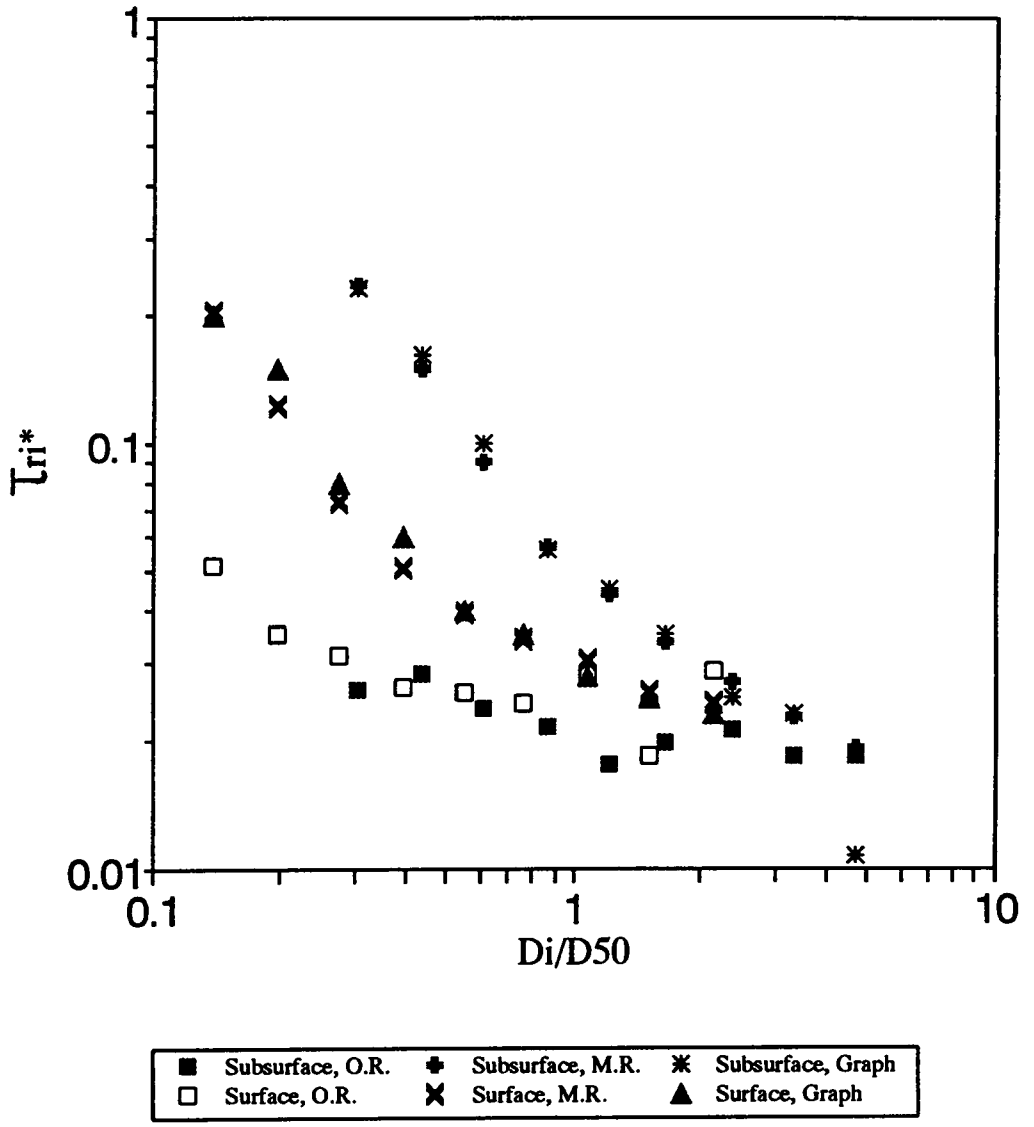

Fig. 18. Plot of τ_{ri}^* vs. $\bar{D}_i/D_{50}$ for $W_r^*=0.0025$ and $W_r^*=0.4$. for the Proffitt Final Subsurface and Surface Approaches where τ_{ri}^* is determined from the original regression (O.R.), modified regression (M.R.), and read from graphs of W_i^*-τ_i^*.

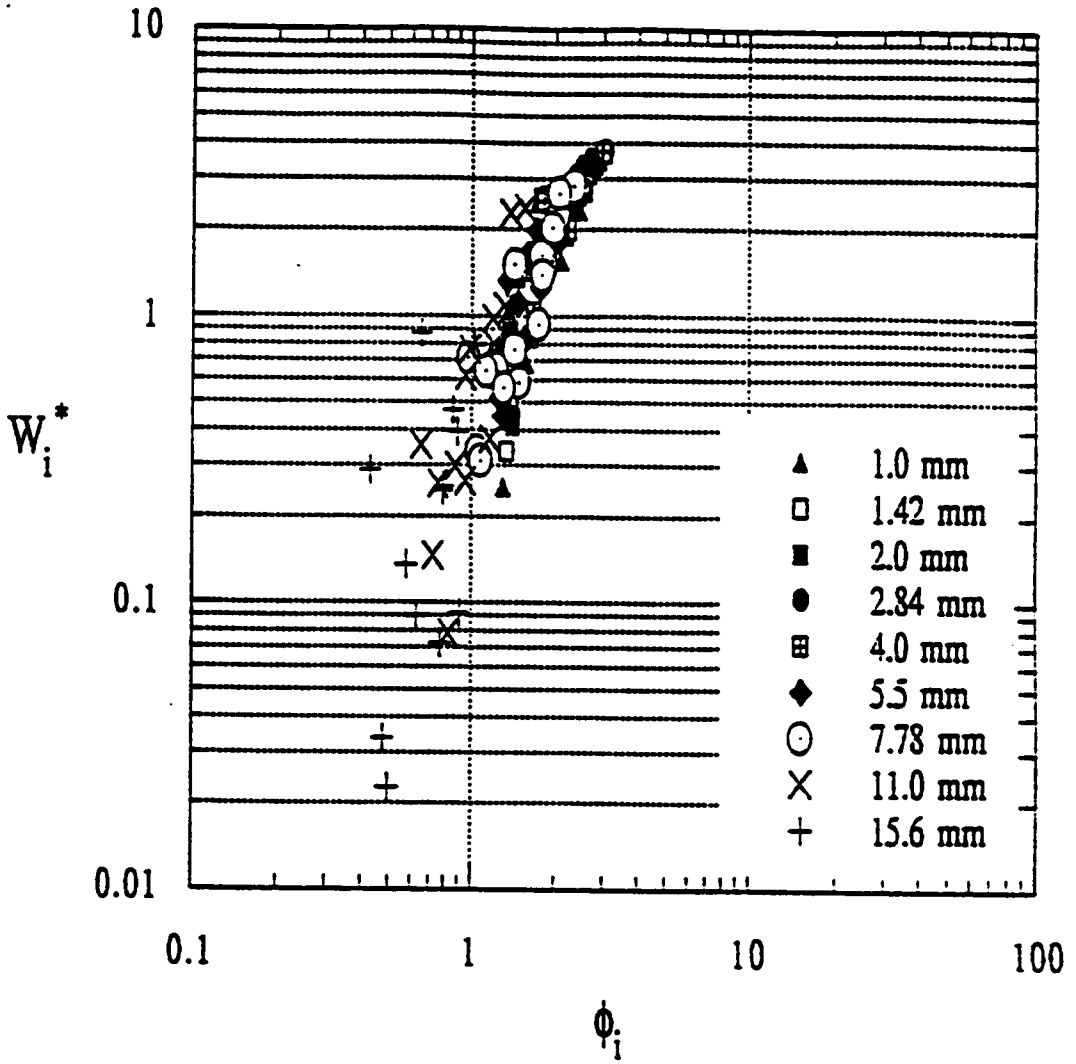

Fig. 19. Similarity Collapse for the Proffitt Initial Phase Data Original Regression Technique, Series 1 through 4.

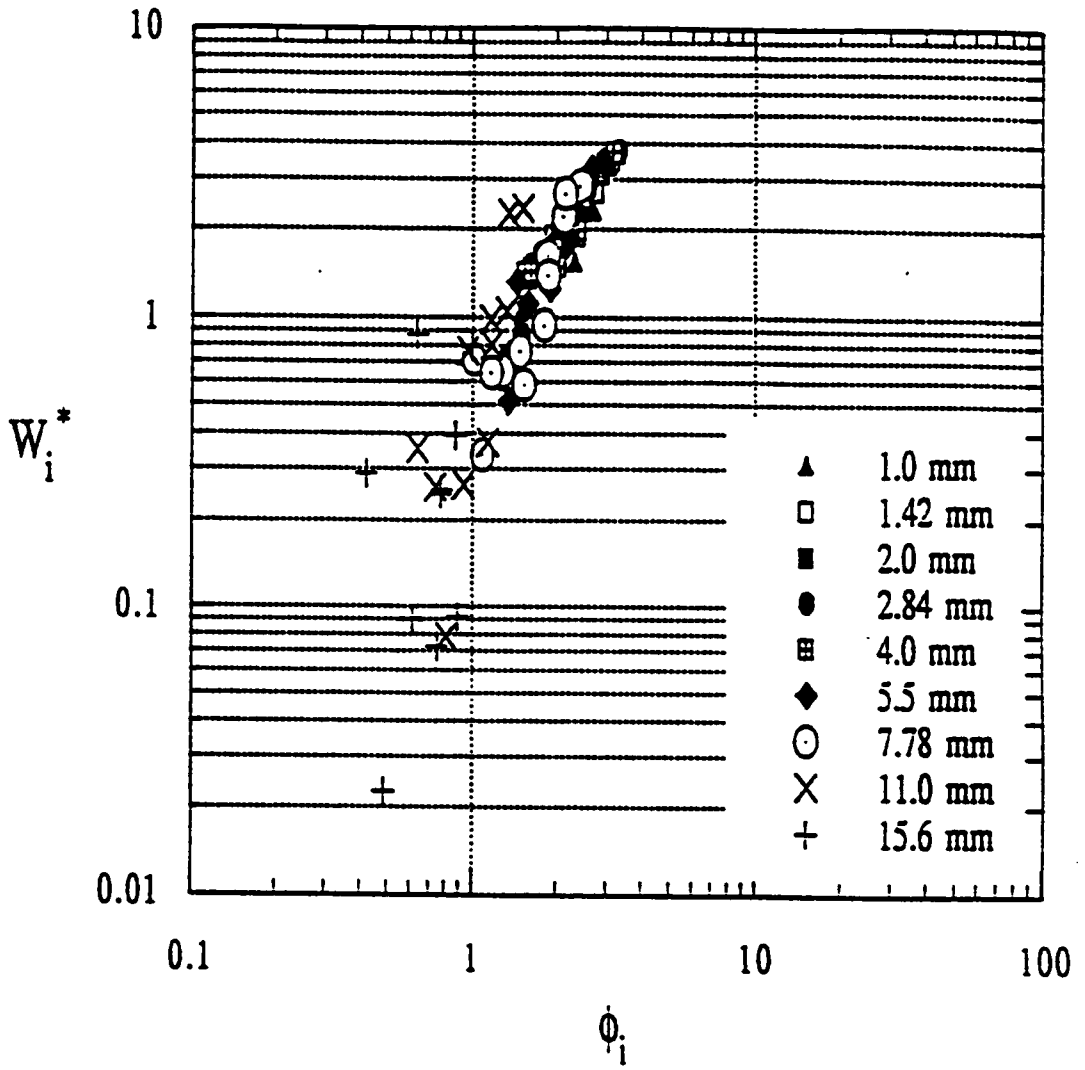

Fig. 20. Similarity Collapse for Proffitt Initial Phase Data Original Regression Technique, Series 1 through 3.

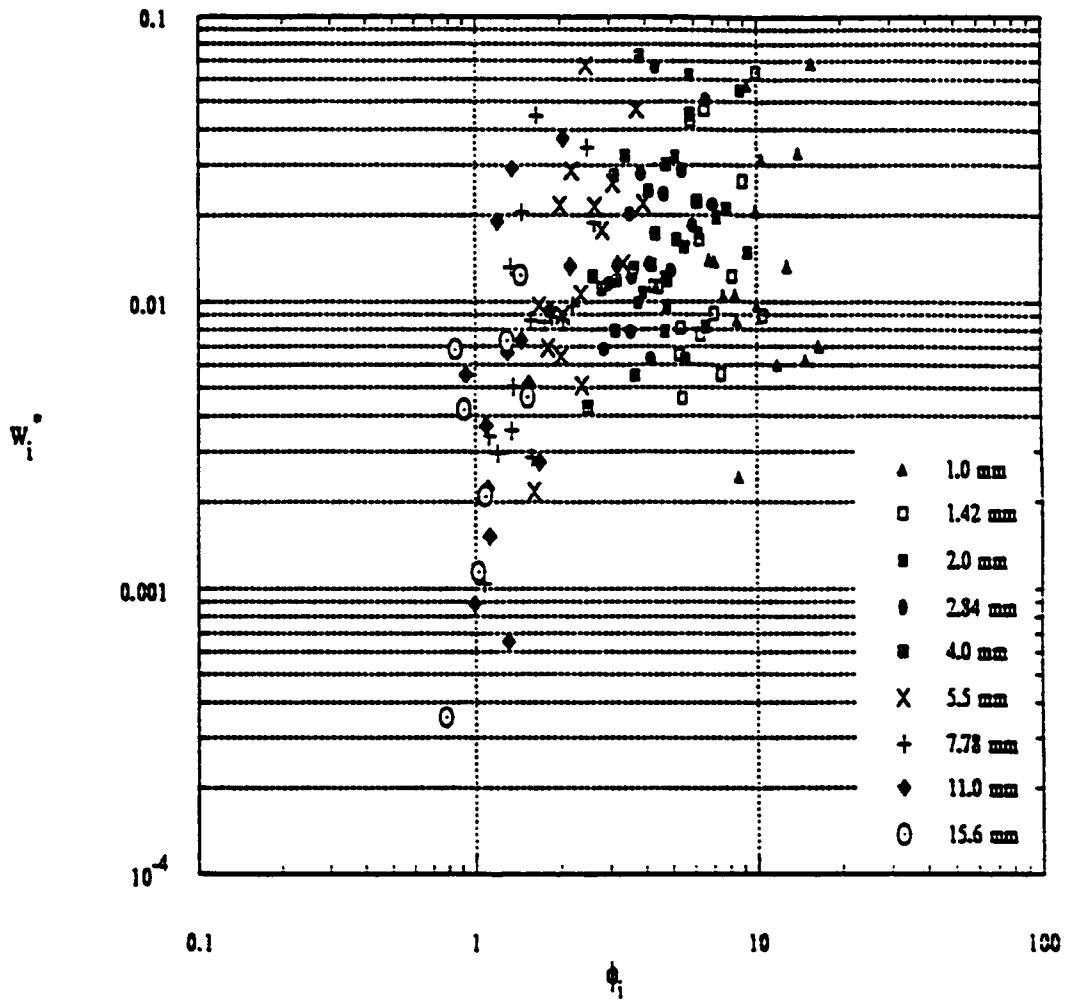

Fig. 21. Similarity Collapse for Proffitt Final Phase Subsurface Original Regression Technique, Series 1 through 4.

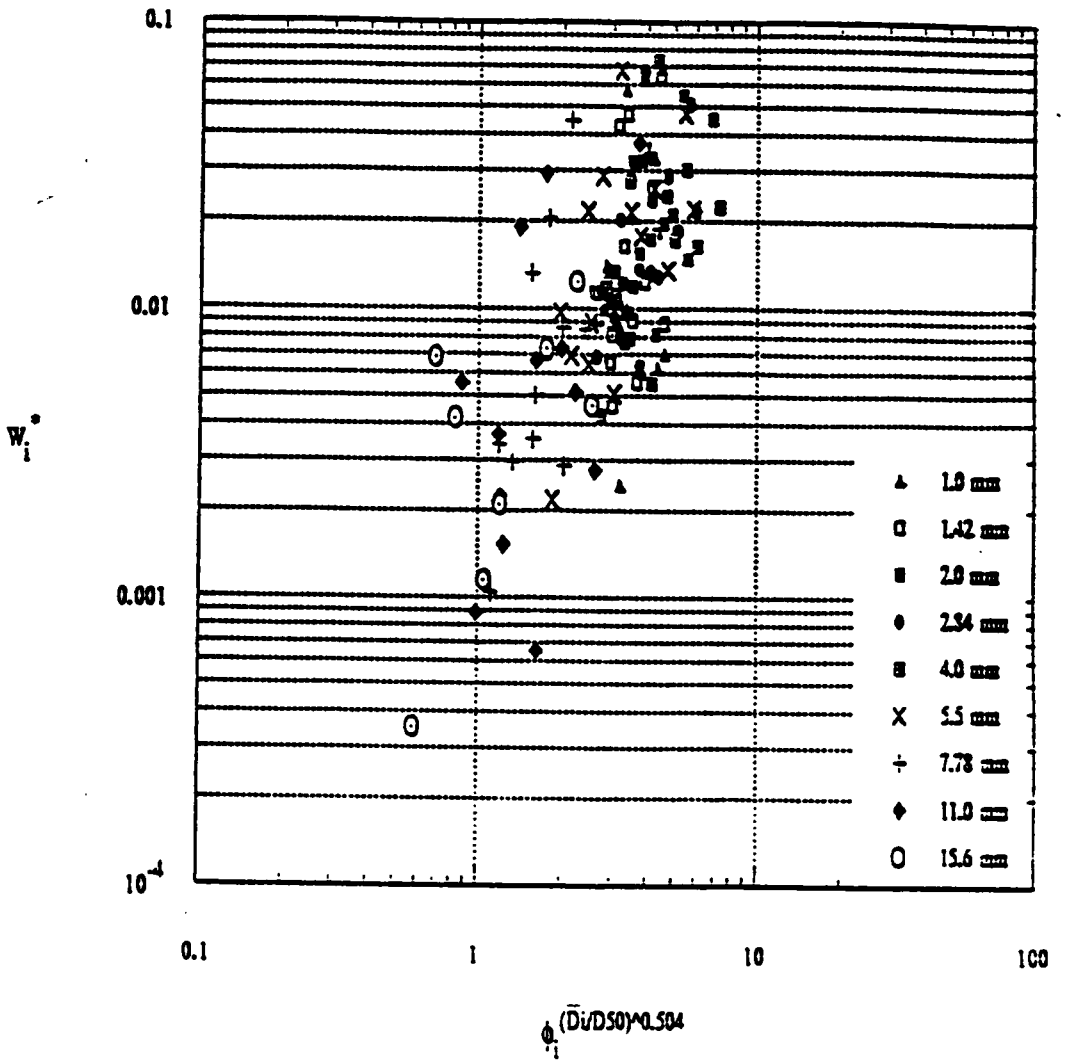

Fig. 22. Modified Similarity Collapse for Proffitt Final Phase Subsurface Original Regression Technique, Series 1 through 4.

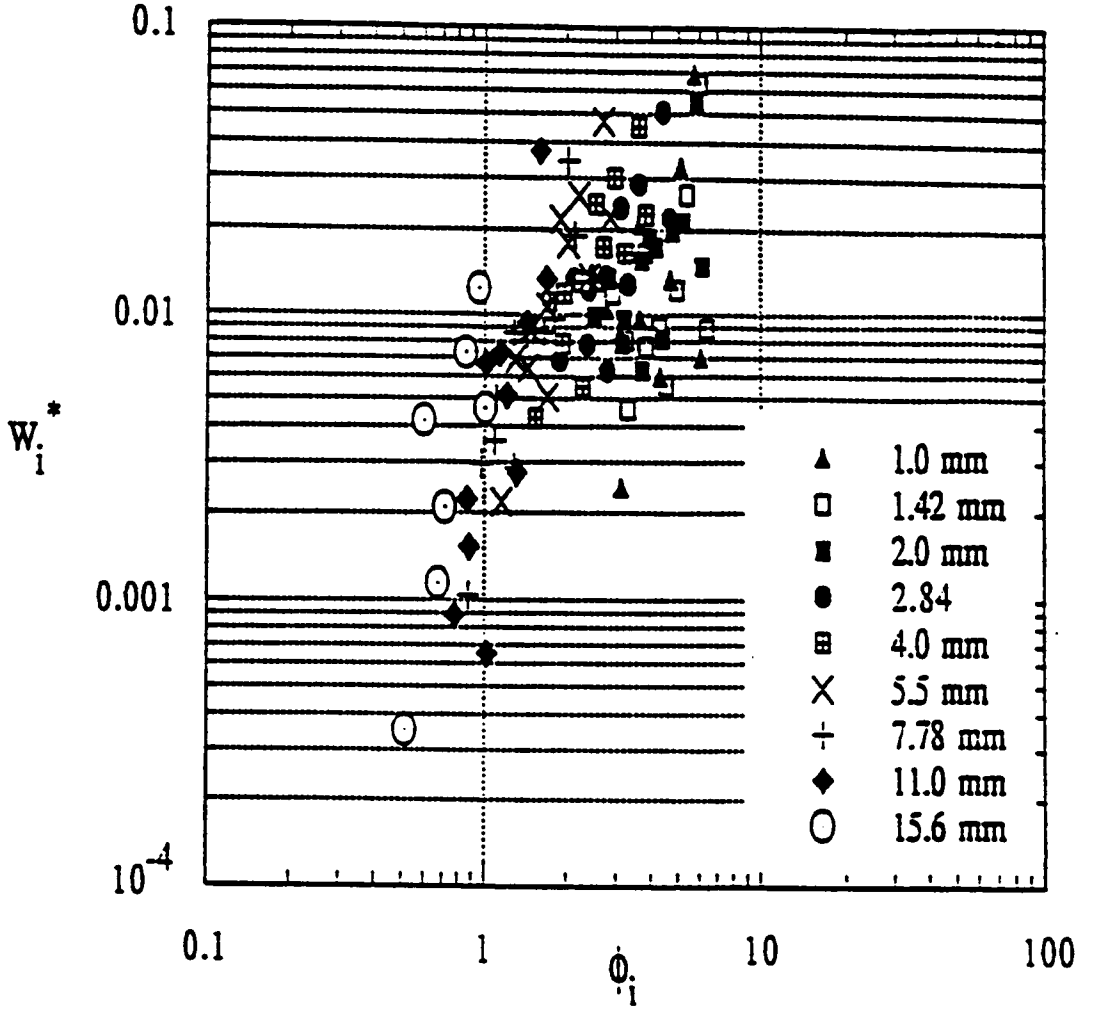

Fig. 23. Similarity Collapse for Proffitt Final Phase Subsurface Original Regression Technique, Series 1 through 3.

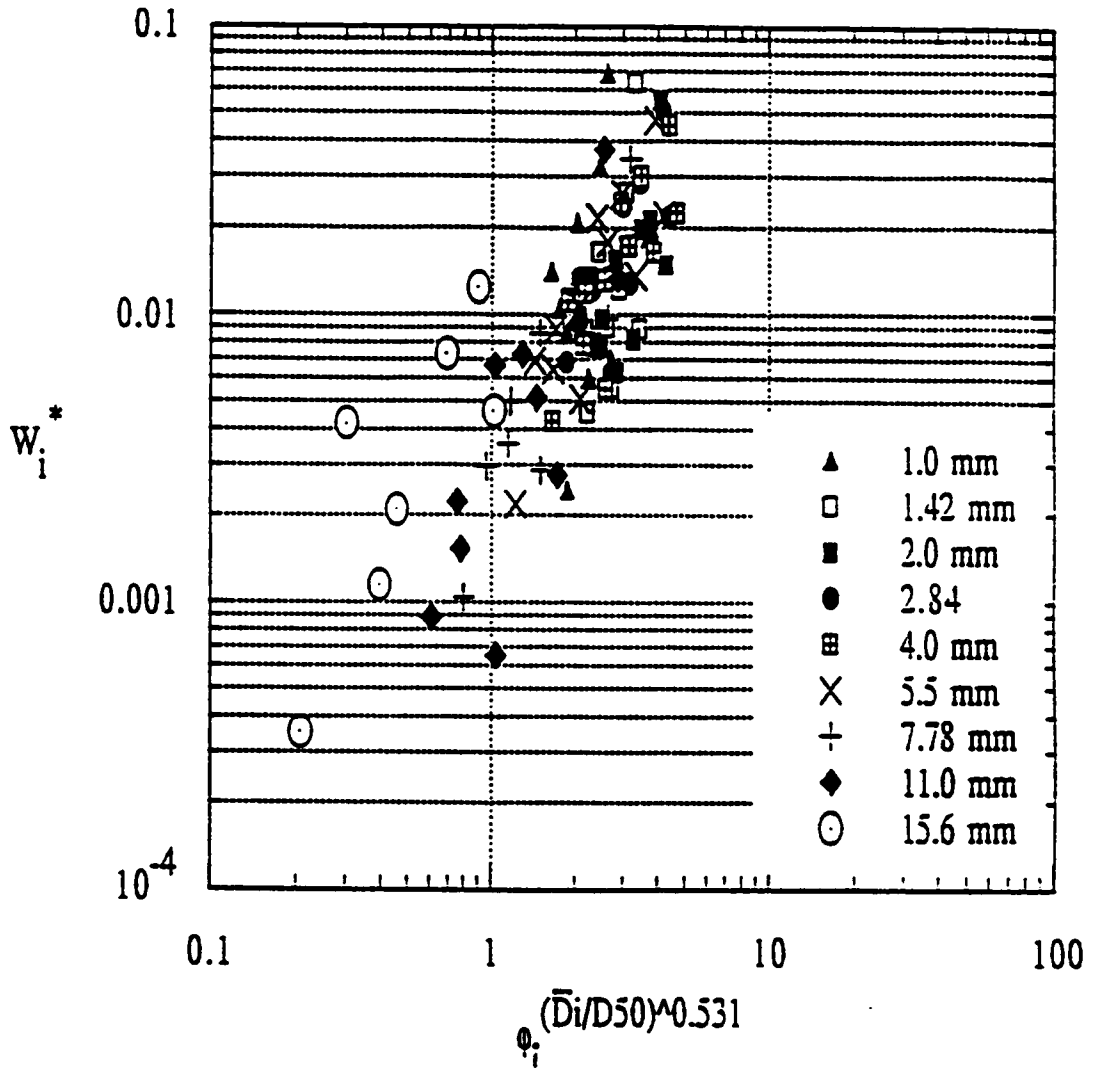

Fig. 24. Modified Similarity Collapse for Proffitt Final Phase Subsurface Original Regression Technique, Series 1 through 3.

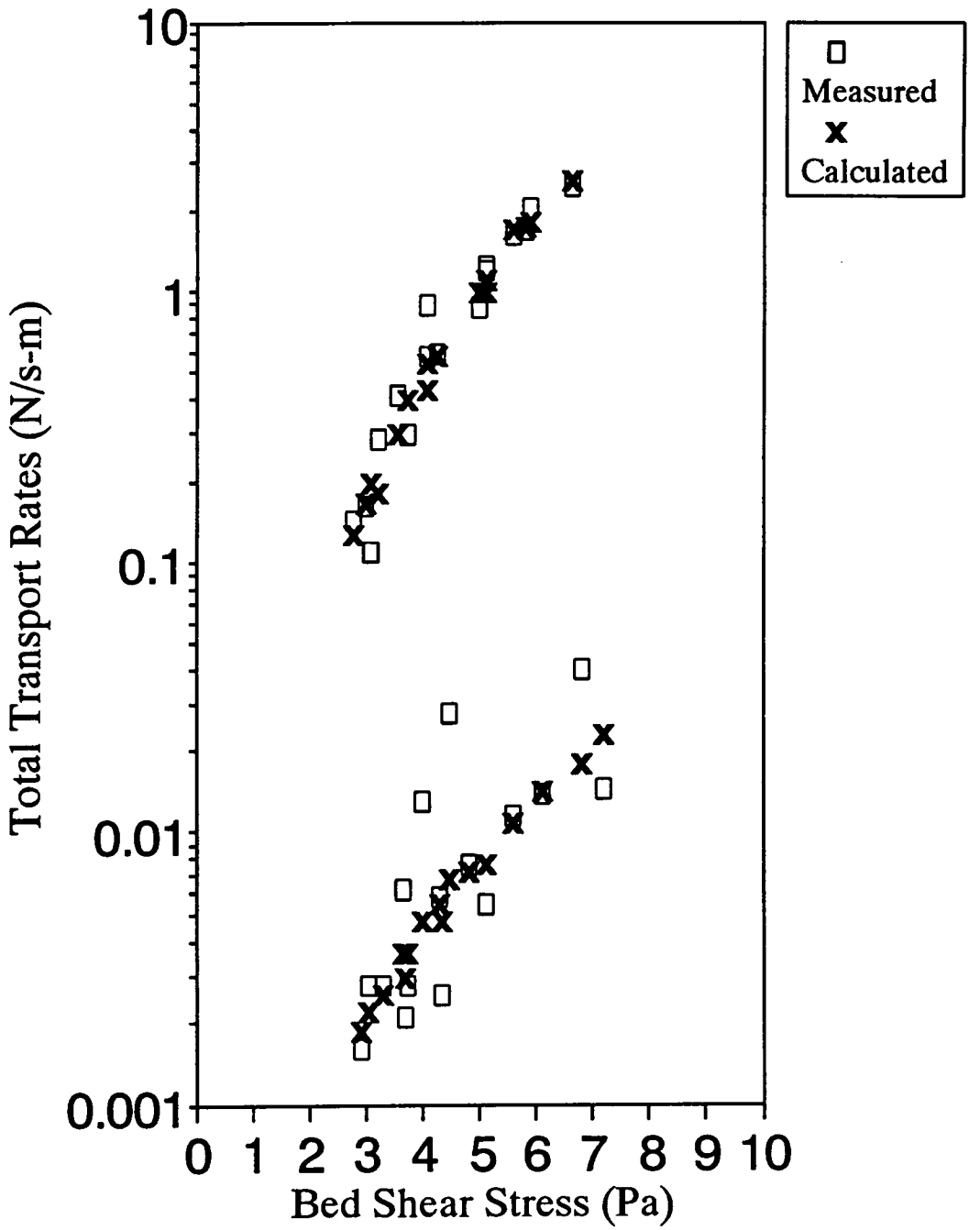

Fig. 25. Plot of calculated and measured total transport rates vs. shear stress for the Proffitt Initial and Final Phases, where the measured values are for all sizes and the calculated values for $\bar{D}_i$ = 1.0 to 15.6 mm are from the W_i^*-τ_i^* regression relations.

Chapter 6. Subsurface - Surface Approach Comparison

The previous analysis and literature review indicated that the total bedload transport rate may be scaled using either the surface or subsurface size distribution to obtain fractional transport rates. The fractional transport rates using the two methods coincide only when a grain size is found in equal amounts in the surface and subsurface, so that $f_i = F_i$, or when there is no coarse surface layer. Therefore, an investigation of these two approaches is required.

6.1 Reasons for a Surface Based Approach

Parker (1990) transforms Parker, et al's (1982) subsurface based relation for Oak Creek into a surface based relation. Parker (1990) asserts that a bedload relation should be based on the surface layer since this is the layer from which grains are entrained. Further, Parker (1990) argues that this surface based relation may be inverted to predict the surface material composition and accounts for nonequilibrium bedload transport conditions.

Parker (1990), Wilcock and McArdell (1993), and Parker and Wilcock (1993) argue that surface scaled fractional transport rates are required to account for the differences between sediment feed and sediment recirculating flumes. Natural streams are often characterized as a combination of sediment feed and sediment recirculation type flumes. It is argued by the above researchers that for

initially identical nonuniform bulk sediment bed mixtures and flow conditions sediment feed and sediment recirculating flumes will develop different surface textures and fractional transport rates. Using the initial subsurface or bulk size distribution to scale transport rates will erroneously yield the same fractional transport rates for each flume. However, it is argued that surface scaled fractional transport rates should be in agreement with the observed fractional transport rates. Therefore, it is suggested by the above authors that the surface approach is more appropriate to predict and compare fractional transport rates for natural streams.

6.2 Reasons for a Subsurface Approach

Ultimately the purpose of fractional bedload transport relations is to determine the bedload transport rate and size distribution for given flow conditions and bed material composition. For surface based bedload transport models, one needs the surface size distribution to determine fractional bedload transport rates. However, the bed surface size distribution changes with flow conditions. Therefore, one must know this relationship prior to calculating the fractional bedload transport rate using a surface material composition relation.

Wilcock and McArdell (1993) made these complicated and tedious coupled observations of bedload, flow, and surface in their laboratory experiments. These coupled observations are even more complicated, if not impossible, if performed

in the field. Typically, for practical reasons, the surface layer is sampled at low flow, which may yield a coarser distribution than would be obtained at higher flows when the coarse surface layer is changing. Sampling the surface layer in the field at higher flows to obtain a relation between the surface layer composition and bed shear is a much more difficult task than sampling at low flow. When obtaining coupled observations of flow, bedload, and surface layer in the laboratory one may interrupt the experiment and sample the surface layer. Since, one cannot do this in the field, one must wait until low flow to sample the surface layer, which may differ significantly from the surface layer at higher flows.

The subsurface size distribution is typically thought to be a stable distribution. That is the subsurface is thought to remain relatively invariant with changing flow conditions. Thus only one subsurface distribution is required, which avoids the problems with the coupled observations needed for the surface approach.

If the relationship between the surface layer and flow conditions is not known, then one must use a single surface layer distribution determined at low flow to calculate the bedload transport, which provides little or no improvement over a subsurface based relation. Further evidence in support of the use of a subsurface based approach comes from the Oak Creek data. Milhous (1973) indicates that the surface layer size distribution varies more widely than the subsurface over the length of the stream.

In the development of the subsurface relation for Oak Creek, Parker, et al (1982) justify the use of the subsurface approach on the observation that the mean annual bedload size distribution is more similar to that of the subsurface than the surface size distribution. This observation may be due more to geomorphilogical constraints than to hydraulic constraints. A stream which is in equilibrium with its basin should transport out of the basin the same sizes and amounts of material with those eroded from the basin and supplied and stored in the stream. If the subsurface layer is considered a good indicator of the type of material supplied to it by the basin, then basin constraints and not hydraulic constraints would produce a mean annual bedload size distribution that corresponds to the subsurface. This argument suggests that the subsurface layer is the source of material for the surface layer from which grains are entrained.

6.3 Proffitt's Data

6.3.1 General Information

In the previous chapter the Proffitt final phase bedload transport rates were scaled both by the subsurface and surface size fractions to obtain corresponding fractional transport rates for each approach. The results of these two approaches are given in the previous chapter, and are compared here. The size ranges used are the same for both the surface and subsurface approaches, however, the subsurface

and surface bed material size fractions in each size range, f_i, and F_i respectively are different.

6.3.2 Transport - Shear Relations

The transport - shear regression results are similar for both approaches. The surface based m_i values are slightly larger than the subsurface values, but both sets of values show the same trends, have similar ranges, and generally increase with grain size. The surface based correlation coefficients, r^2, are higher than the corresponding subsurface r^2 values when series 1 through 4 are analyzed collectively. However, there is little difference in the r^2 values when series 4 is dropped and 1 through 3 are analyzed collectively.

6.3.3 Reference Shear Stresses

The dimensionless reference shear stresses, τ_{ri}^*, were determined for a dimensionless reference transport rate, $W_r^* = 0.0025$, using both a subsurface and surface approach. Values of τ_{ri}^* were determined from the W_i^*-τ_i^* modified regression relations in the previous chapter for this study. These τ_{ri}^* values were then regressed against $\bar{D}_i/D_{50}$ giving relations of the form of Eq. 19 ($\tau_{ri}^* = \tau_{r50}^* (\bar{D}_i/D_{50})^{-\beta}$).

The reference shear stresses for the median grain size were determined in this study for the subsurface and surface approaches, τ_{r50}^*, and τ_{r50s}^*, respectively. The subsurface and surface values determined using the W_i^*-τ_i^* and W_{si}^*-τ_i^* modified regression relations for $W_r^* = 0.0025$ are $\tau_{r50}^* = 0.05827$ and $\tau_{r50s}^* = 0.02613$. When the subsurface value of $\tau_{r50}^* = 0.05827$ is scaled by the surface coarseness (2.24), the surface and subsurface values become equal, and are close to the value of 0.03 proposed by Niell (1968). Further, the subsurface and surface approaches produce similar τ_{ri}^* values for the same size, $\bar{D}_i$. Thus, the two approaches produce similar results in regard to the reference shear stresses.

The final phase β values determined for the subsurface and surface approaches for τ_{ri}^* determined from the W_i^*-τ_i^* modified regression relations are $\beta = 1.0577$ and $\beta = 0.9197$, respectively. While both values indicate selective transport, the subsurface approach predicts that the coarse grains are more mobile, while the surface approach predicts that the fine grains are more mobile. As mentioned earlier, this result occurs because the reference material for the two approaches is different, and this forces the two approaches to produce different selective transport conditions.

6.3.4 Subsurface and Surface Based Transport Trends

The final phase subsurface W_i^* values range from about 0.001 to 0.1 while the surface W_{si}^* values range from about 0.00016 to 0.16. It is convenient to quantify W_i^* and W_{si}^* in terms of their ratio W_i^*/W_{si}^*, or equivalently, F_i/f_i. A value of $W_i^*/W_{si}^* = 1$ indicates that $f_i = F_i$, while $W_i^*/W_{si}^* > 1$ indicates that $F_i > f_i$, and $W_i^*/W_{si}^* < 1$ indicates that $F_i < f_i$.

The ratio W_i^*/W_{si}^* is plotted against grain size in Figures 26 through 29. The figures indicate that the ratio W_i^*/W_{si}^* generally increases with grain size with the ratio $W_i^*/W_{si}^* = 1$ between $\overline{D}_i$ = 4 to 7 mm ($\overline{D}_i/D_{50} > 1.2$ to 2.1). Thus, the subsurface approach predicts smaller dimensionless transport rates than the surface approach for the finer grains, while predicting larger dimensionless transport rates for the coarser grains.

The above result may be obtained intuitively since the surface approach with a coarse surface layer should have higher surface fractions, Fi, for the coarser grains than the subsurface fractions, f_i. Thus, the result that W_i^*/W_{si}^* or equivalently, F_i/f_i, becomes greater than 1 for $\overline{D}_i/D_{50} > 1.2$ to 2.1 indicates that the coarse particles are over represented in the surface layer, so that $F_i > f_i$.

6.4 Surface Relation Applied to Proffitt's Data

6.4.1 Size Ranges

Parker's (1990) surface based bedload transport relation is used in this study to predict fractional bedload transport rates and bedload size distributions for Proffitt's initial and final phase data for $\overline{D}_i$ = 0.25 to 15.6 mm. The previous analysis of the initial and final phase is for $\overline{D}_i$ = 1.0 to 15.6 mm. However, Parker (1990) used Proffitt's data in his analysis and apparently did not exclude sizes smaller than 1.0 mm. Parker and Sutherland (1990) indicate that only a small amount of sand was in suspension during Proffitt's experiments. Previously in this study, it was found that sizes smaller than 0.5 mm were in suspension. However, to facilitate the use of Parker's surface relation all sizes from 0.25 mm to 15.6 mm are used.

6.4.2 Initial Transport Rates

The predictive ability of Parker's surface relation can be observed in plots of predicted and observed transport rates vs. shear stress (Fig. 30). Parker's surface relation predicted the initial high transport rates quite well. The scatter in the plots can be partly attributed to the different initial sediment mixtures (different D_{50}, D_g, and σ_g).

6.4.3 Final Transport Rates

Parker's surface relation consistently over-predicts the final phase transport rates by almost an order of magnitude. Thus, although the constants that appear in Parker's relation may be applicable for Oak Creek and the initial phase as evidenced by the good results with the initial phase, they do not appear suitable for the final phase.

6.4.4 Bedload Size Distributions

Figure 32 provides the variation of the initial and final phase bedload D_{50} with τ_{50}^*. Parker's surface relation consistently predicts a finer than observed bedload size distribution. The observed bedload D_{50} is typically 0.3 mm to 3 mm coarser than the predicted values for the initial and final phases. The coarseness of the predicted bedload size distribution increases as the bed shear stress increases, and the error between the observed and predicted distributions decreases as shear stress increases. The predicted bedload size distributions may be finer than the observed in part due to Parker's hiding function, which always renders finer grains more mobile regardless of the shear stress.

The final phase predicted bedload distributions do not show a consistent increase or decrease in coarseness with shear stress as the initial phase did. Note that the predicted final phase bedload size distribution of Run 3-2 provides the best

agreement with the observed distribution.

6.4.5 Armor Layer Size Distributions

Figure 33 provides the variation of the final phase armor layer median grain size, D_{50s}, with bed shear stress. The bed composition at the end of the initial phase is not provided, and therefore, a comparison with Parker's predicted initial surface layer is not provided. The predicted final phase armor layer D_{50} values were finer than the observed values by 0 - 7 mm, and the difference between the observed and predicted values typically increased with bed shear stress.

6.4.6 Comparison of Bedload Transport Relations

Proffitt (1980) provided a comparison of observed and predicted transport rates using the transport relations of Ackers & White, Engelund & Hansen, Paintal, Schoklitsch, and Einstein. The predicted results of these relations are used for comparison with the predicted results of Parker's surface relation. It is assumed that Proffitt used the subsurface (surface) size distribution values of D_{35} and D_{50} to calculate the initial (final) phase transport rates with the above relations. The observed and predicted transport rates are plotted for the initial and final phases in Figures 30 and 31. The Parker surface based relation does not provide better results than the other relations for the initial phase transport. All methods except

Einstein's relation over-predict the final phase bedload transport rates by as much as an order of magnitude. However, Parker's surface relation does provide slightly better results than the other relations for the final phase.

The predicted and observed bedload size distributions for the various transport relations are plotted in Figures 34 and 35 for Runs 1-2 and 3-3, which Proffitt (1980) indicated were typical eroded distributions. The Parker surface based relation yields distributions finer than observed, but typically better than the other relations with the shape of the Parker distributions similar to the other predicted distributions.

6.4.7 Summary of Application of Surface Relation

Parker's surface based bedload transport relation adequately predicted the high transport rates of Proffitt's initial phase data but over-predicted the low transport final phase data by one order of magnitude, and typically predicted bedload and armor distributions finer than observed. Parker's surface relation did not predict the initial or final transport rates any better than the relations of Ackers & White, Engelund & Hansen, and Paintal, but did provide better results than Einstein's relation for the initial phase. Parker's surface relation provided both bedload and armor size distributions closer to the observed distributions than the predicted distributions of the above relations.

6.5 Surface Based Analysis Applied to Proffitt's Data

6.5.1 Proffitt Final Transport Phase

Although Proffitt's flume data do not provide direct coupled observations of flow, transport, and surface size distributions, an attempt to analyze the data using Wilcock and McArdell's (1993) methods were made. The final phase data are low transport rates with selective transport obtained with no sediment feed or recirculation to illuminate the effects of armoring. Both the surface size fractions, F_i, and the bulk size fractions, f_i, were used in the analysis of the final phase data to provide some comparison between a surface approach and a bulk or subsurface approach.

The values of the dimensional reference shear stresses for each size range, τ_{ri}, obtained for $W_r^* = 0.0025$ for the Proffitt subsurface and surface final phase original and modified regressions do not increase significantly with grain size. However, Wilcock & McArdell's (1993) τ_{ri} values increased with grain size due to their bimodal sediments. The Proffitt data support other data, including Oak Creek, in which the dimensional reference shear stresses, τ_{ri}, do not exhibit a strong size dependence (See Table 22).

Table 22 lists the values of τ_{ri} which were read directly from graphs q_i/F_i (surface) or q_i/f_i (subsurface) vs. shear stress (Figures 36 and 37), and also lists the values of τ_{ri}^* read from graphs of W_i^* (bulk) or W_{si}^* (surface) vs. τ_i^*. Table 22

provides a comparison between the values of the reference shear stress determined using the surface and bulk size approaches. The Proffitt data support Wilcock and McArdell's (1993) finding that the value of the reference shear stress is not strongly dependent on whether the surface or bulk size approach is used. The percent differences between the values are given and reflect the difficulty in estimating τ_{ri} by eye. In addition, the range of the subsurface and surface based τ_{ri} values from the smallest to the largest values (typically 40-60%) is larger than for Oak Creek (25% range) but much smaller than that of Wilcock and McArdell's (1993) values which varied by an order of magnitude. Regression of the τ_{ri}^* values determined from the q_{wi}/f_i and q_{wi}/F_i vs. shear stress graphs for $W_r^* = 0.0025$ gives:

P.F.P. Subsurface Based Relation

$$\tau_{ri}^* \text{ from } q_{wi}/f_i: \qquad \tau_{ri}^* = 0.057619(\bar{D}_i/D_{50})^{-1.0114} \quad r^2 = 0.98830 \qquad \textbf{(61)}$$

P.F.P. Surface Based Relation

$$\tau_{ri}^* \text{ from } q_{wi}/F_i: \qquad \tau_{ri}^* = 0.030115(\bar{D}_i/D_{50s})^{-0.82988} \quad r^2 = 0.93862 \qquad \textbf{(62)}$$

Note that exponents in the above relations depend on whether τ_{ri}^* was read from a surface or subsurface plot. As before, the exponents from the surface plots

are less than unity indicating that the finer grains are more mobile, while the exponents from the subsurface plots are slightly greater than one rendering the coarser grains more mobile.

A plot of τ_{ri} vs. grain size (Fig. 39) for the Proffitt final phase data show a small variation in τ_{ri} with grain size for Proffitt's nonuniform sediments, as opposed to Shield's curve for uniform sediments. In addition, plots of τ_{ri}^* vs. grain size (Fig. 40) and τ_{ri}^* vs. grain Reynold's number (Fig. 41) show a decrease in τ_{ri}^* with grain size and Reynold's number. Wilcock & McArdell's (1993) found an increase in τ_{ri} with grain size and a much smaller decrease in τ_{ri}^* with grain Reynold's number than Proffitt's data.

6.5.2 Proffitt Initial Transport Phase

The initial transport phase data cover the same range of shear stresses as the final phase data, but the transport rates for the initial phase are much higher due to an initially unstable bed with little or no coarse surface layer. Therefore, the size fractions, f_i, for the bulk bed are used for comparison with Wilcock and McArdell's (1993) analysis.

The values of the reference transport rate, τ_{ri}, were read from graphs of q_{wi}/f_i vs. bed shear stress (Fig. 38) as well as graphs of W_i^*-τ_i^* for $W_r^* = 0.0025$. The values of τ_{ri} as well as the percentage difference between the values read from the

two different graphs are given in Table 23. The difference between the values is due to the estimation involved in determining τ_{ri} because there is no data near the reference transport rate, $W_r^* = 0.0025$, for the initial phase.

There is a 25 % range of τ_{ri} values read from graphs of q_{wi}/f_i vs. τ (Fig. 38). This is smaller than the range for the Final Phase data (about 50%). Also note that τ_{ri} is largest for the finest and coarsest grains with a relatively constant value of $\tau_{ri} = 2.0$ for the intermediate sizes. These values are lower than for the Final Phase data due to the initially unstable bed for the Initial Phase.

Plots of τ_{ri} vs. $\bar{D}_i$ (Fig. 42) also demonstrate the small range of τ_{ri} values and near size independence of τ_{ri}. Plots of τ_{ri}^* vs. $\bar{D}_i$ (Fig 43) indicate that, similar to the final phase, τ_{ri}^* decreases significantly with grain size. Regression of τ_{ri}^* for $W_r^*=0.0025$ gives:

P.I.P Relation

τ_{ri}^* from q_{wi}/f_i: $\tau_{ri}^* = 0.03861(\bar{D}_i/D_{50})^{-0.99753}$ $r^2 = 0.9951$ **(63a)**

τ_{ri}^* from W_i^*-τ_i^*: $\tau_{ri}^* = 0.03389(\bar{D}_i/D_{50})^{-0.9395}$ $r^2 = 0.9820$ **(63b).**

The exponents in Eqs. 63a and 63b vary from near 1 to 0.94, but both are from subsurface plots and vary depending on which graphs τ_{ri}^* is read from. This indicates that the τ_{ri}^* relations are not only somewhat sensitive to the surface and

subsurface approaches but also to which graphs the values are read from. The differences between the τ_{ri}^* values might be lowered by fitting curves to the transport - shear relations.

6.5.3. Summary of Surface Analysis

Wilcock and McArdell (1993) observed an increase in τ_{ri} with grain size consistent with previous results for strongly bimodal sediments. The Proffitt subsurface and surface final phase τ_{ri} are typically in the range of 3 to 4 Pa, and exhibit small variation of τ_{ri} with grain size consistent with the Oak Creek data.

The Proffitt final phase data show deviation from Shields curve due to the nonuniformity of Proffitt's sediment, however Proffitt's final phase data show a greater deviation from Shield's curve than does Wilcock and McArdell's (1993) data with bimodal sediments.

Proffitt's initial phase data exhibit a smaller range of τ_{ri} values (25%) than the final phase (50%) for $W_r^* = 0.0025$. In addition the values of τ_{ri} for the initial phase (2.0 - 2.5 Pa) are smaller than the final phase (2 - 4 Pa).

6.6 Summary of Subsurface - Surface Comparison

Theoretically, a surface based fractional transport approach provides consistency between sediment feed and sediment recirculation conditions. However, practical aspects limit the usefulness of surface relations. Surface relations scale the transport rate by the surface size fraction, F_i, which may change with flow conditions. This requires either coupled sampling of bedload, surface layer, and hydraulic conditions, or some specified relation between these parameters. These coupled observations are difficult to obtain, so typically, one surface size distribution is used to scale the transport rates, which limits the usefulness of a surface approach. A subsurface approach is based on the subsurface size distribution which is a relatively stable distribution over varying flow conditions. Therefore, no coupled observations are needed.

Proffitt's final phase data were analyzed using both a subsurface and a surface based similarity approach, and similar results were obtained for each approach. The subsurface and surface transport - shear relation m_i values were similar in magnitude and range, showed similar trends, and increased with grain size. The subsurface and surface based dimensionless reference shear stress values, τ_{ri}^*, were also similar.

Wilcock and McArdell (1993) indicated that the value of the reference shear stress is not strongly dependent on whether a surface or a subsurface approach is

used. The Proffitt final phase data support this finding to some degree. If this is the case, then transport relations using a reference shear stress to determine the transport rates should not be sensitive to whether the subsurface size or surface size distribution is used. However, if a subsurface approach is used one should account for the surface coarseness by scaling the subsurface τ_{r50}^* value by the surface coarseness. However, the subsurface and surface approaches are forced to predict different selective transport conditions because the two approaches are based on different bed grain size distributions. The subsurface approach predicts that the coarser grains are more mobile, while the surface approach predicts that the fine grains are more mobile.

Finally, application of Parker's surface relation indicated that the surface relation adequately predicted the high initial transport rates, but over-predicted the low final phase tranpsort rates. This indicates that a possible modification of the surface relation may be required to more accurately predict the low final phase transport rates.

Table 22. Reference Shear Values for Initial Motion for Proffitt's Final Phase Data read from graphs of q_{wi}/F_i and q_{wi}/f_i vs. τ for $W_r^*=0.0025$. Note that the values in parenthesis are from graphs of W_{si}^* and $W_i^* - \tau_i^*$.

	Surface Based				Subsurface (bulk) Based				
	q_{wi}/F_i		$W_{si}^*-\tau_i^*$		q_{wi}/f_i		$W_i^*-\tau_i^*$		
$\bar{D}_i$ mm	τ_{ri} Pa	τ_{ri}^*	τ_{ri}^*	$q_{wi}/F_i - W_{si}^*$ % Difference	τ_{ri} Pa	τ_{ri}^*	τ_{ri}^*	$q_{wi}/f_i - W_i^*$ % Difference	Surface - Subsurface %Difference
1.0	3.2	0.191	(0.20)	4.7%	3.7	0.221	(0.23)	4.2	16
1.42	3.0	0.126	(0.15)	19%	3.0	0.126	(0.16)	27	0
2.0	2.5	0.0746	(0.08)	7.3%	2.8	0.0426	(0.09)	103	12
2.84	2.8	0.0588	(0.06)	2.0%	2.6	0.0546	(0.055)	0.7	7.7
4.0	2.9	0.0433	(0.04)	8.2%	2.8	0.0418	(0.045)	7.7	3.6
5.5	3.0	0.0325	(0.035)	7.7%	3.0	0.0325	(0.035)	7.7	0
7.78	3.5	0.0268	(0.028)	4.3%	3.0	0.0230	(0.025)	8.6	17
11.0	6.0	0.0326	(0.025)	30%	3.7	0.0201	(0.023)	15	62
15.6	3.8	0.0145	(0.023)	58%	4.2	0.0161	(0.017)	5.8	11

Table 23. Values of reference shear stress for initial motion for Proffitt's Initial Transport Phase Data read from graphs of q_{wi}/f_i vs. τ for $W_r^*=0.0025$. The values in parenthesis are from graphs of $W_i^*-\tau_i^*$.

$\bar{D}_i$ mm	τ_{ri} Pa	τ_{ri}^* $(q_{wi}/f_i-\tau)$	τ_{ri}^* $(W_i^*-\tau_i^*)$	% Difference between qw_i/f_i and W_i^* graph values
1.0	2.0	0.1193	(0.1)	19.3
1.42	2.0	0.0840	(0.08)	5.05
2.0	2.0	0.0660	(0.05)	19.3
2.84	2.0	0.0441	(0.04)	10.3
4.0	2.0	0.0298	(0.03)	5.36
5.5	2.2	0.0239	(0.02)	19.4
7.78	2.0	0.0153	(0.015)	2.27
11.0	2.5	0.0136	(0.015)	10.6
15.6	2.5	0.0096	(0.01)	4.60

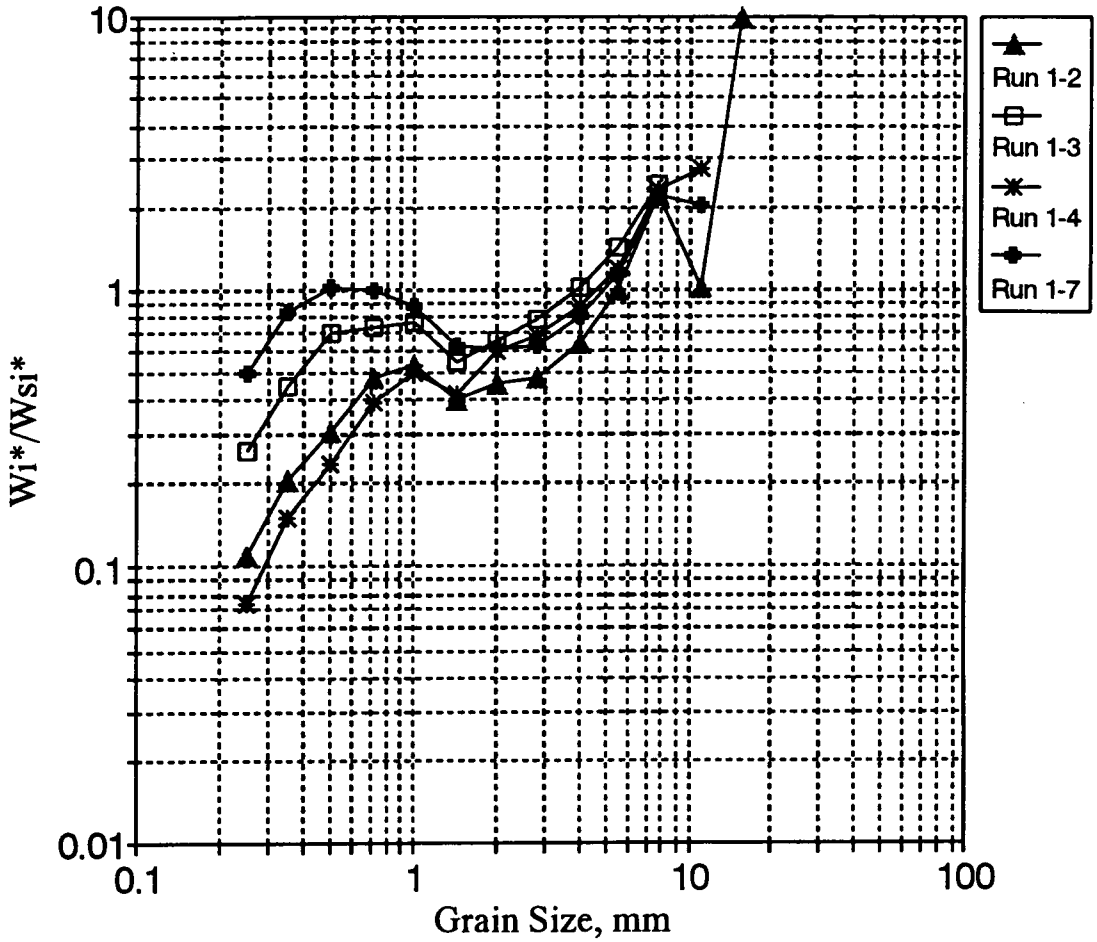

Fig. 26. Plot of W_i^*/W_{si}^* vs. $\bar{D}_i$ for Proffitt Final Phase Series 1.

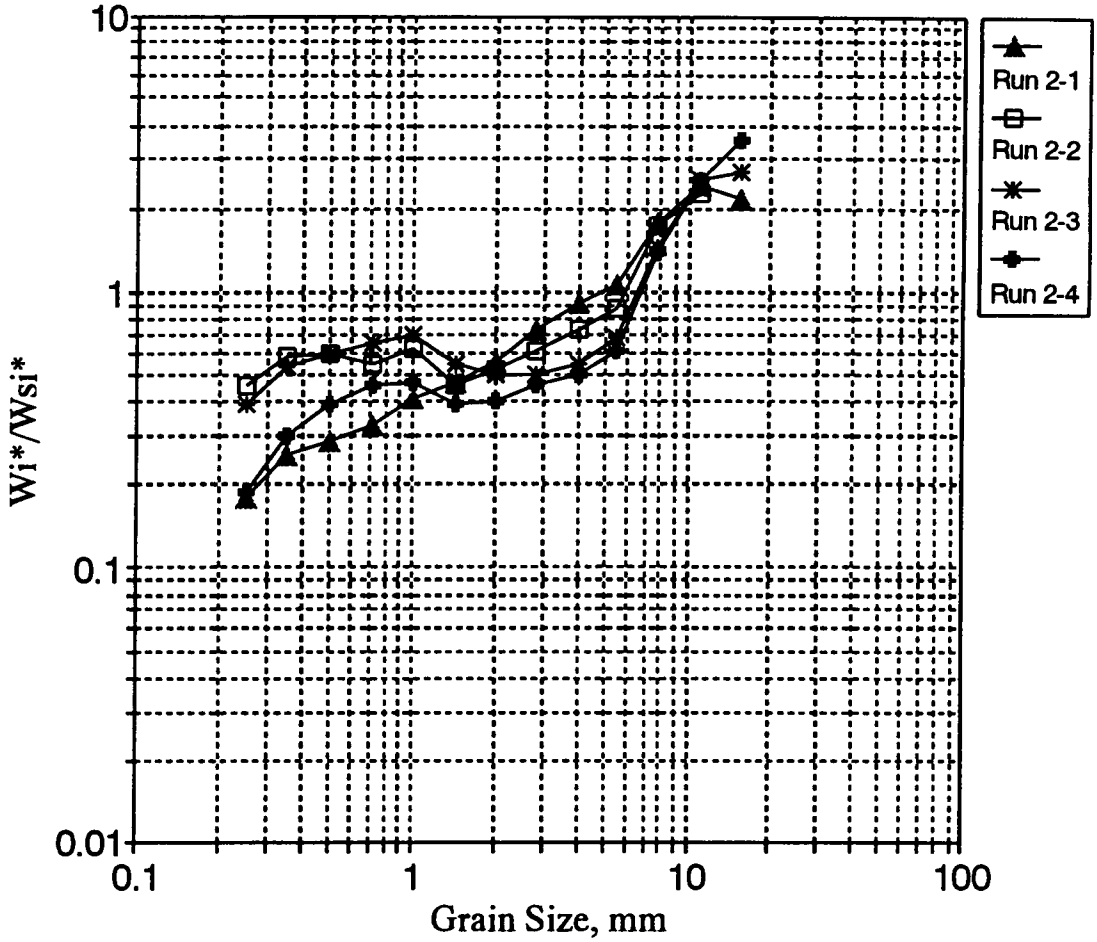

Fig. 27. Plot of W_i^*/W_{si}^* vs. $\bar{D}_i$ for Proffitt Final Phase Series 2.

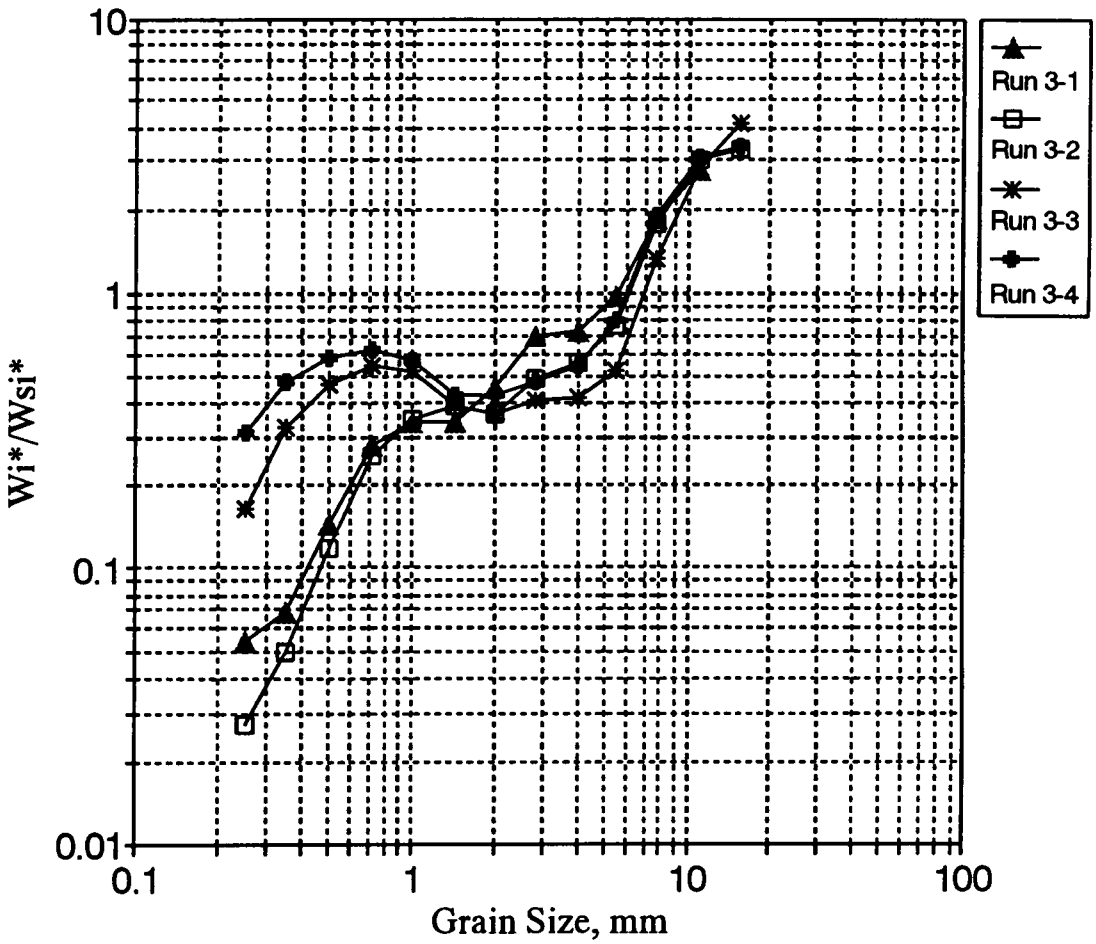

Fig. 28. Plot of W_i^*/W_{si}^* vs. $\bar{D}_i$ for Proffitt Final Phase Series 3.

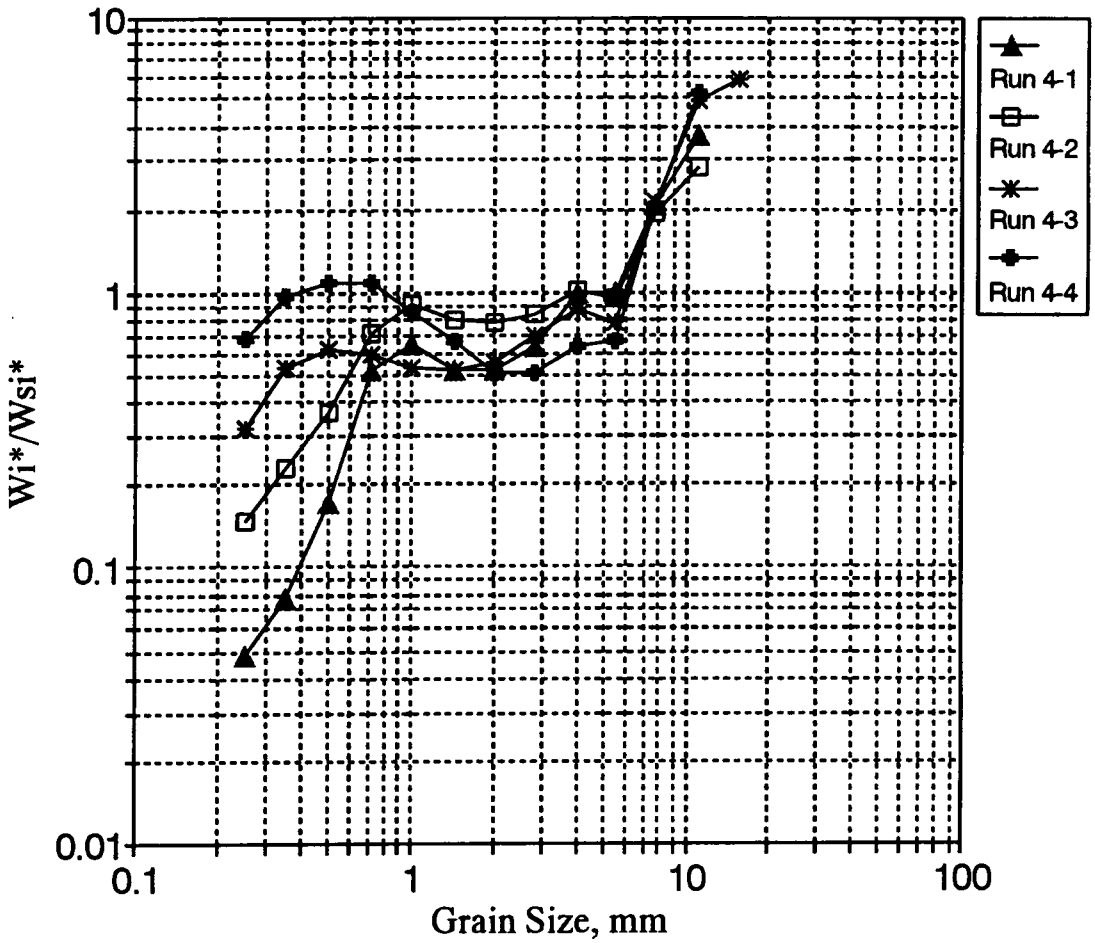

Fig. 29. Plot of W_i^*/W_{si}^* vs. $\bar{D}_i$ for Proffitt Final Phase Series 4.

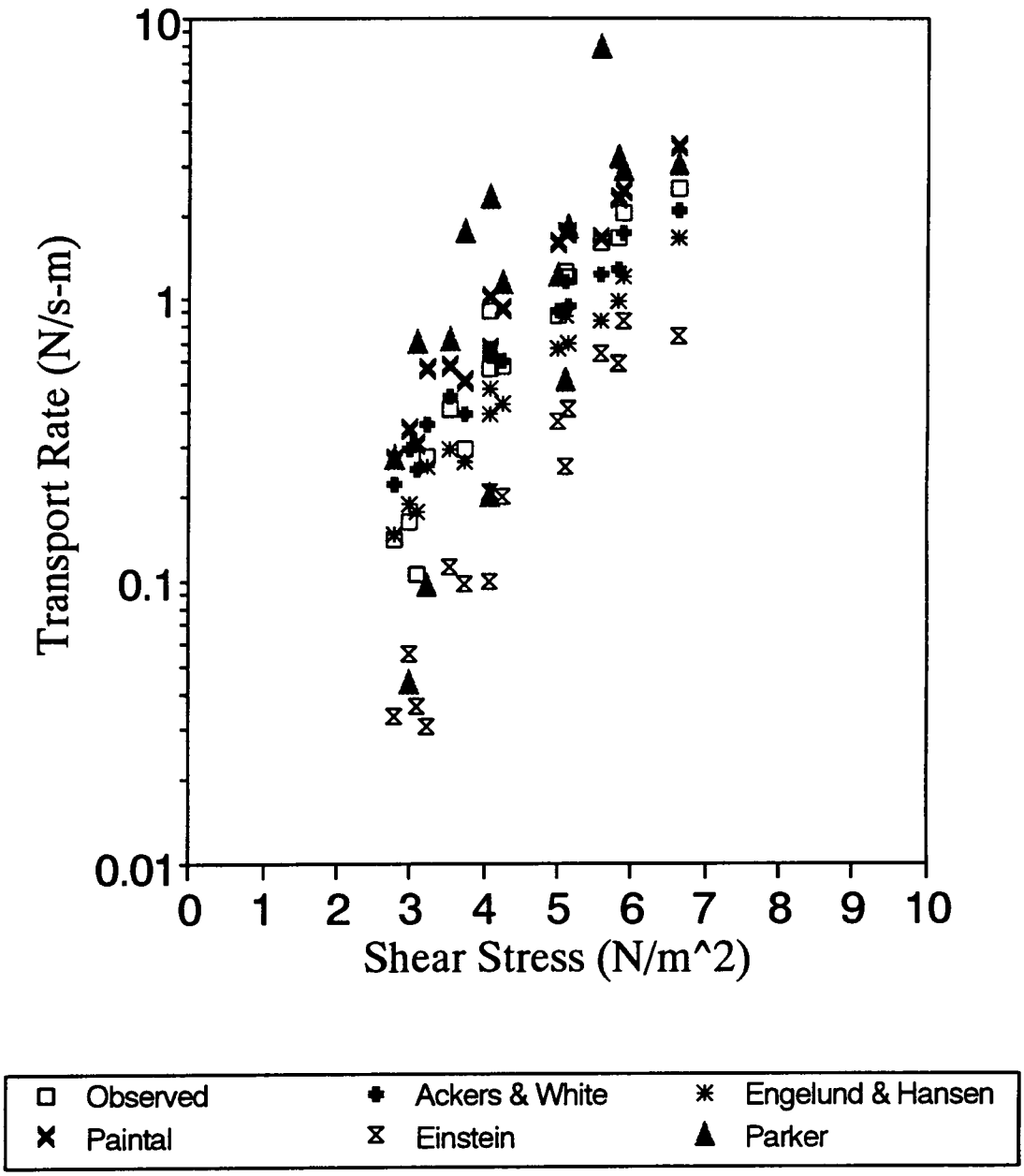

Fig. 30. Plot of calculated and measured total transport rates vs. shear stress for the Proffitt Initial Phase Data using various bedload transport relations.

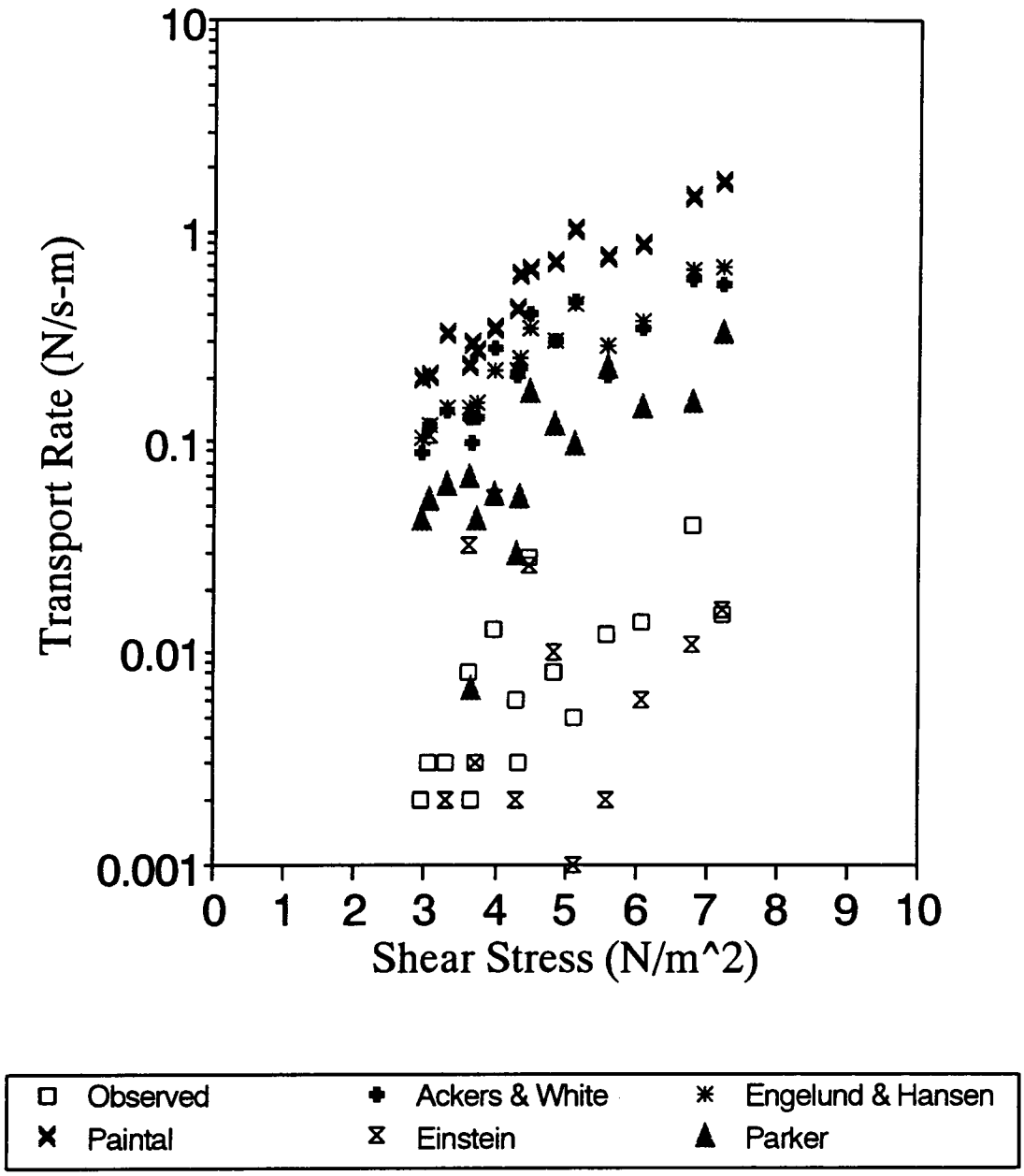

Fig. 31. Plot of calculated and measured total transport rates vs. shear stress for the Proffitt Final Phase Data using various bedload transport relations.

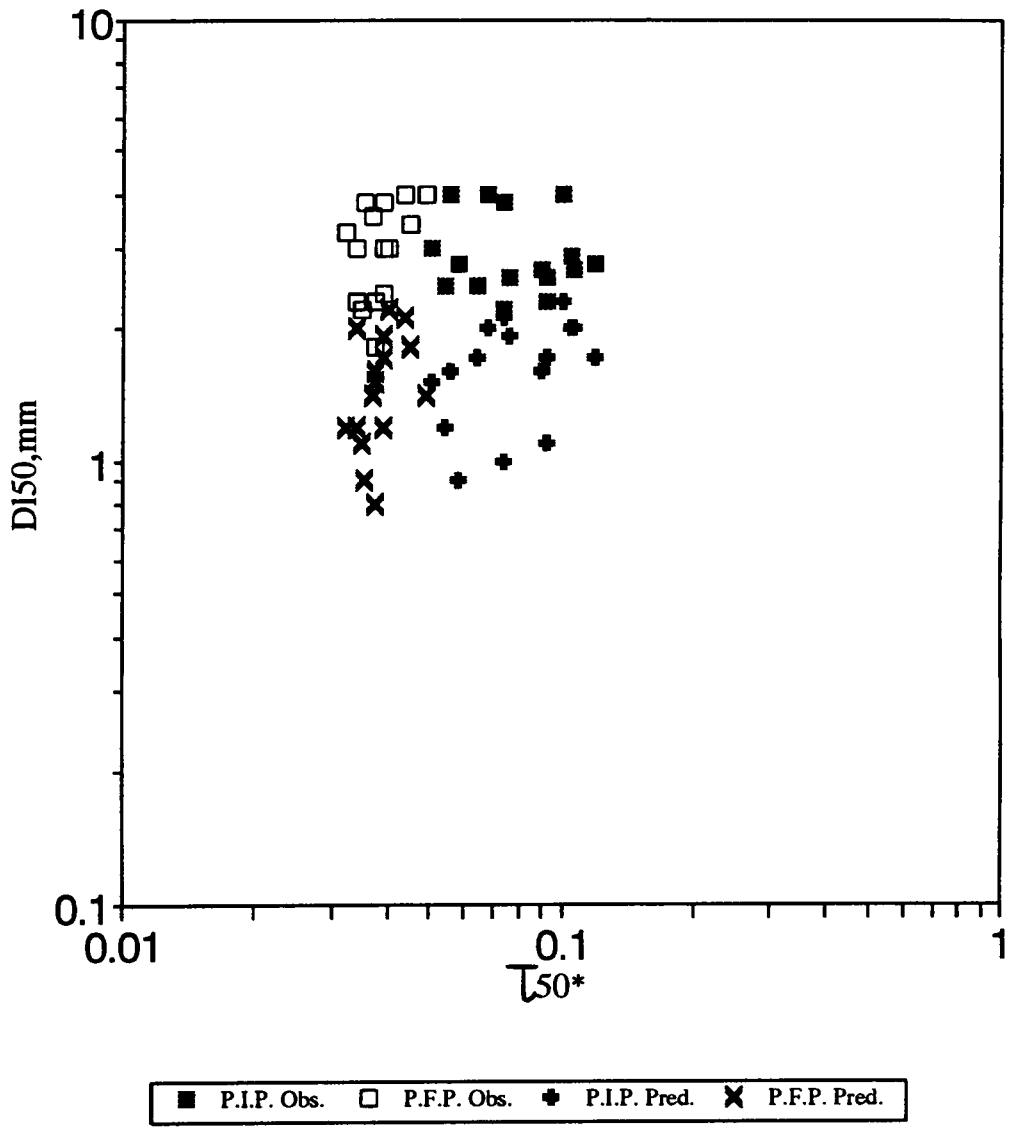

Fig. 32. Plot of bedload D_{150} vs. τ_{50}* for the Proffitt intial and final phases including the predicted bedload D_{150} from Parker's (1990) surface based relation.

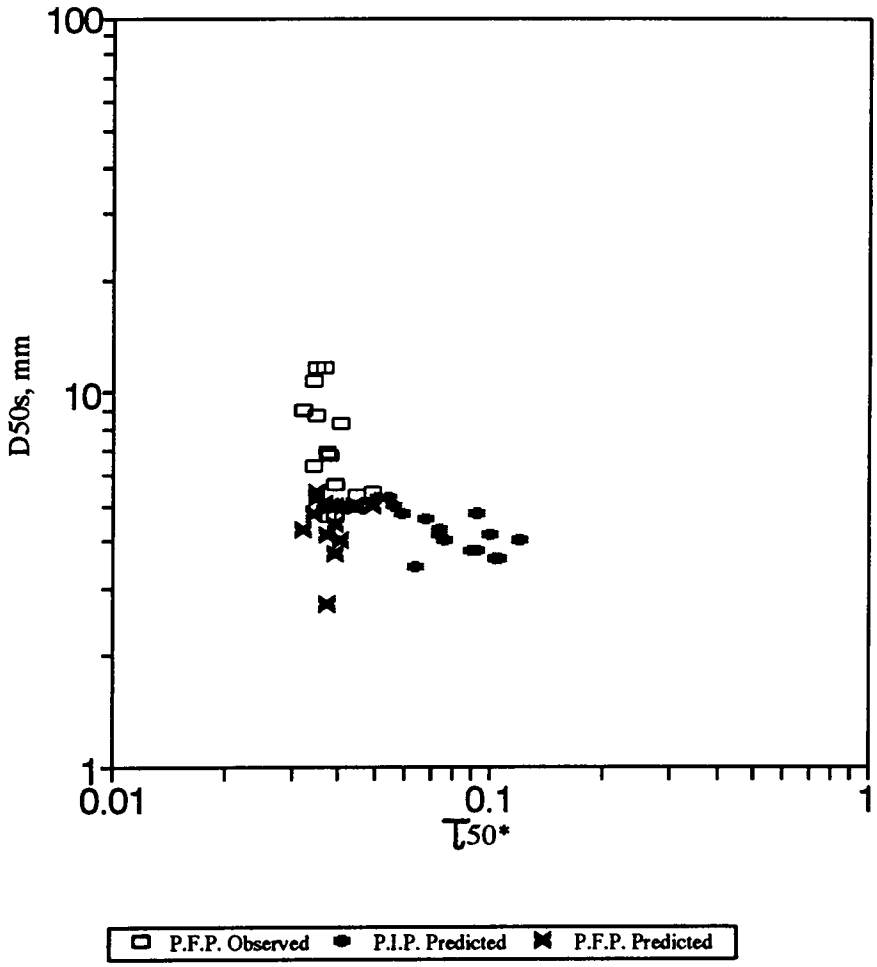

Fig. 33. Plot of armor D_{50s} vs. τ_{50}* for the Proffitt intial and final phases including the predicted armor D_{50s} from Parker's (1990) surface based relation.

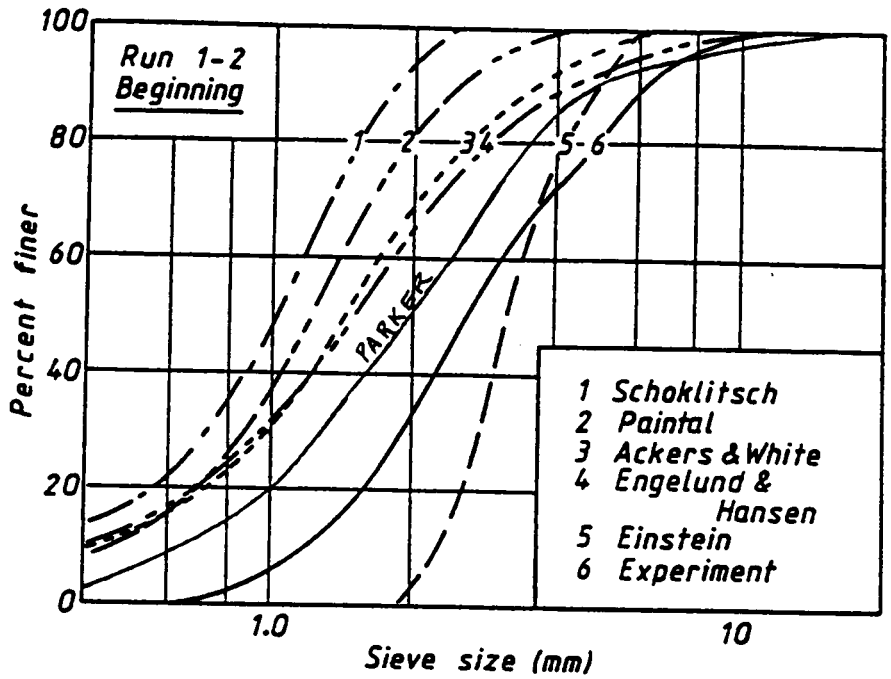

Fig 34a. Plot of predicted and observed bedload size distributions for the beginning of Run 1-2 for various bedload transport relations

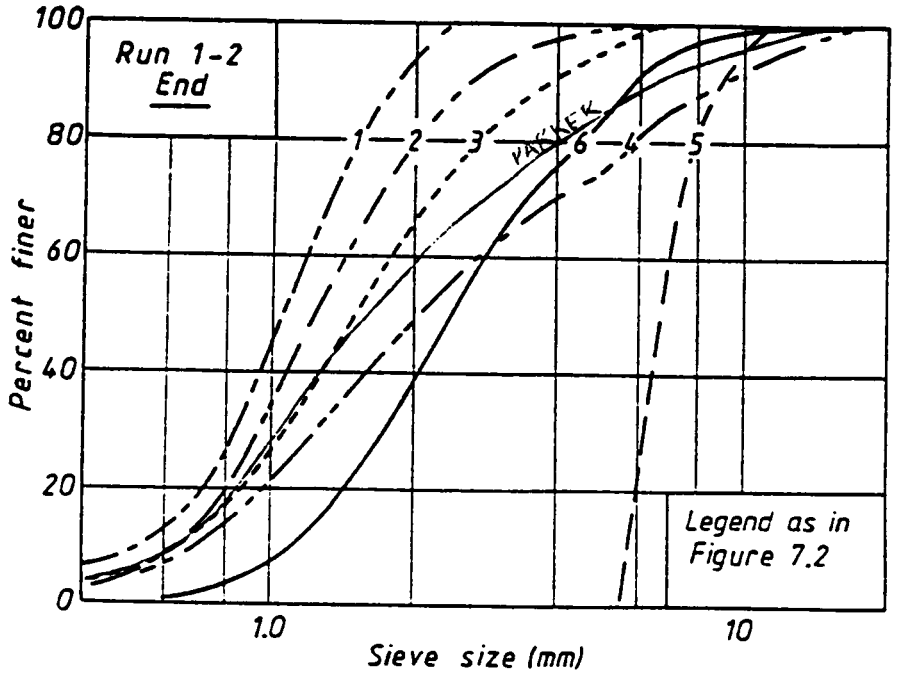

Fig 34b. Predicted and observed bedload size distributions for the end of Run 1-2.

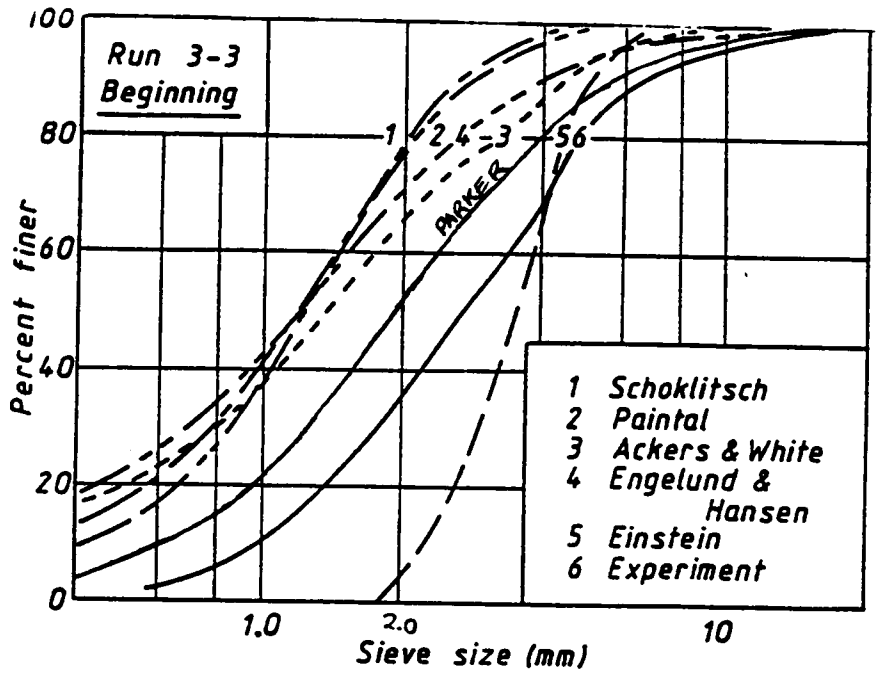

Fig. 35a. Plot of predicted and observed bedload size distributions for the beginning of Run 3-3 for various bedload transport relations.

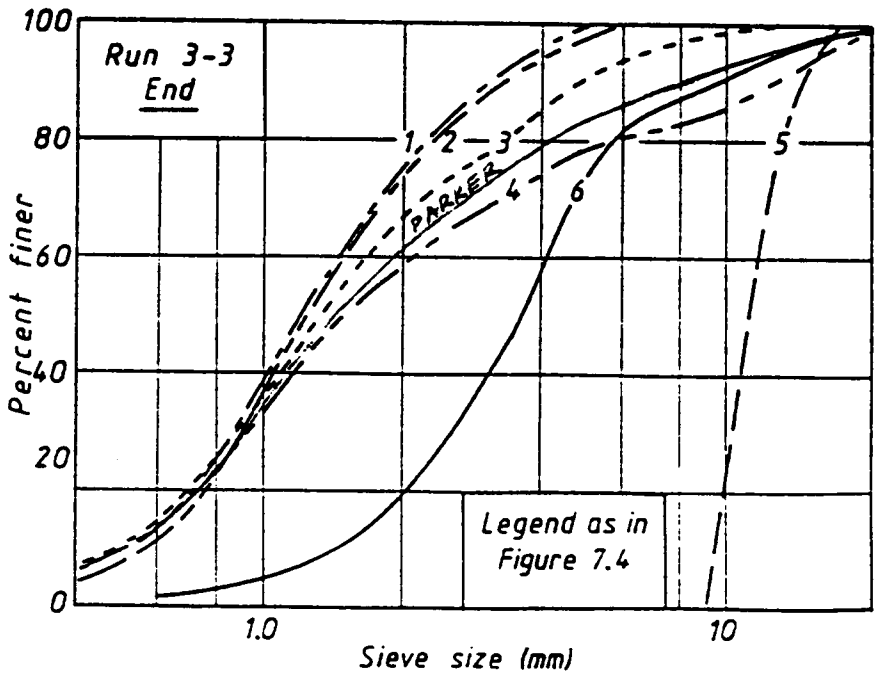

Fig 35b. Predicted and observed bedload size distributions for the end of Run 3-3.

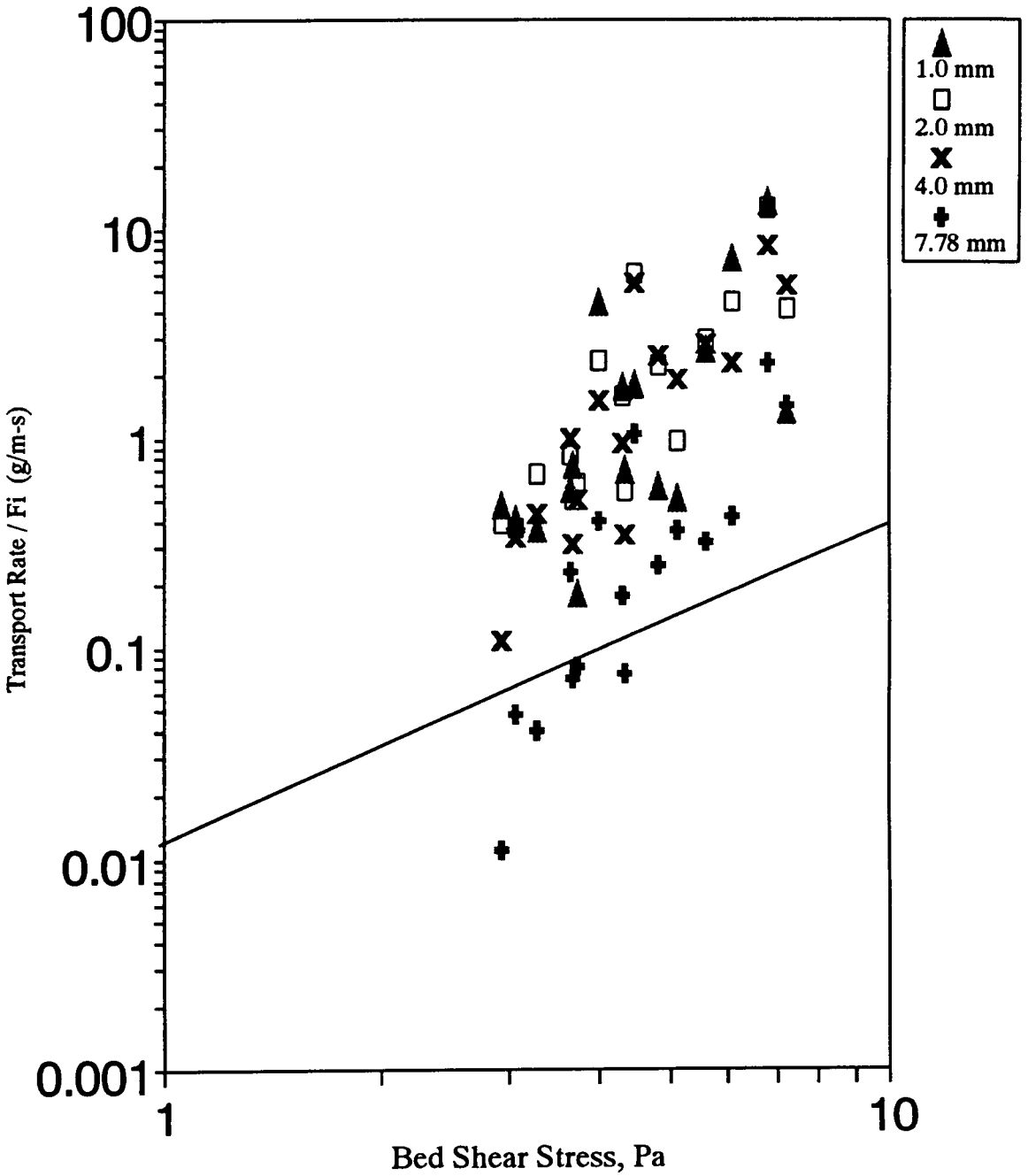

Fig. 36. A plot of Transport Rate $(q_{wi})/F_i$ vs. shear stress for Proffitt Final Phase Surface Approach.

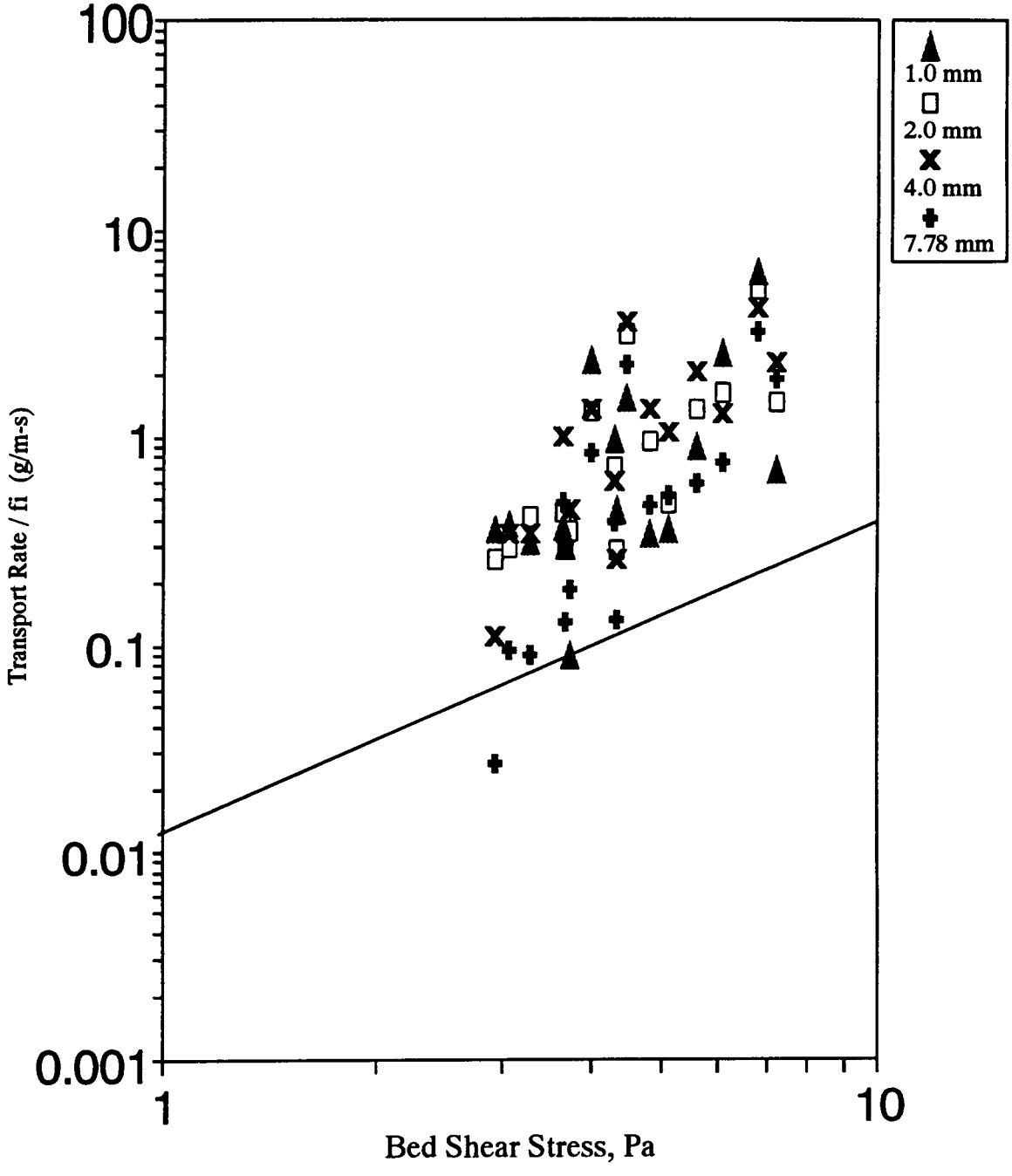

Fig. 37. Plot of Transport Rate $(q_{wi})/f_i$ vs. shear stress for Proffitt Final Phase Subsurface Approach.

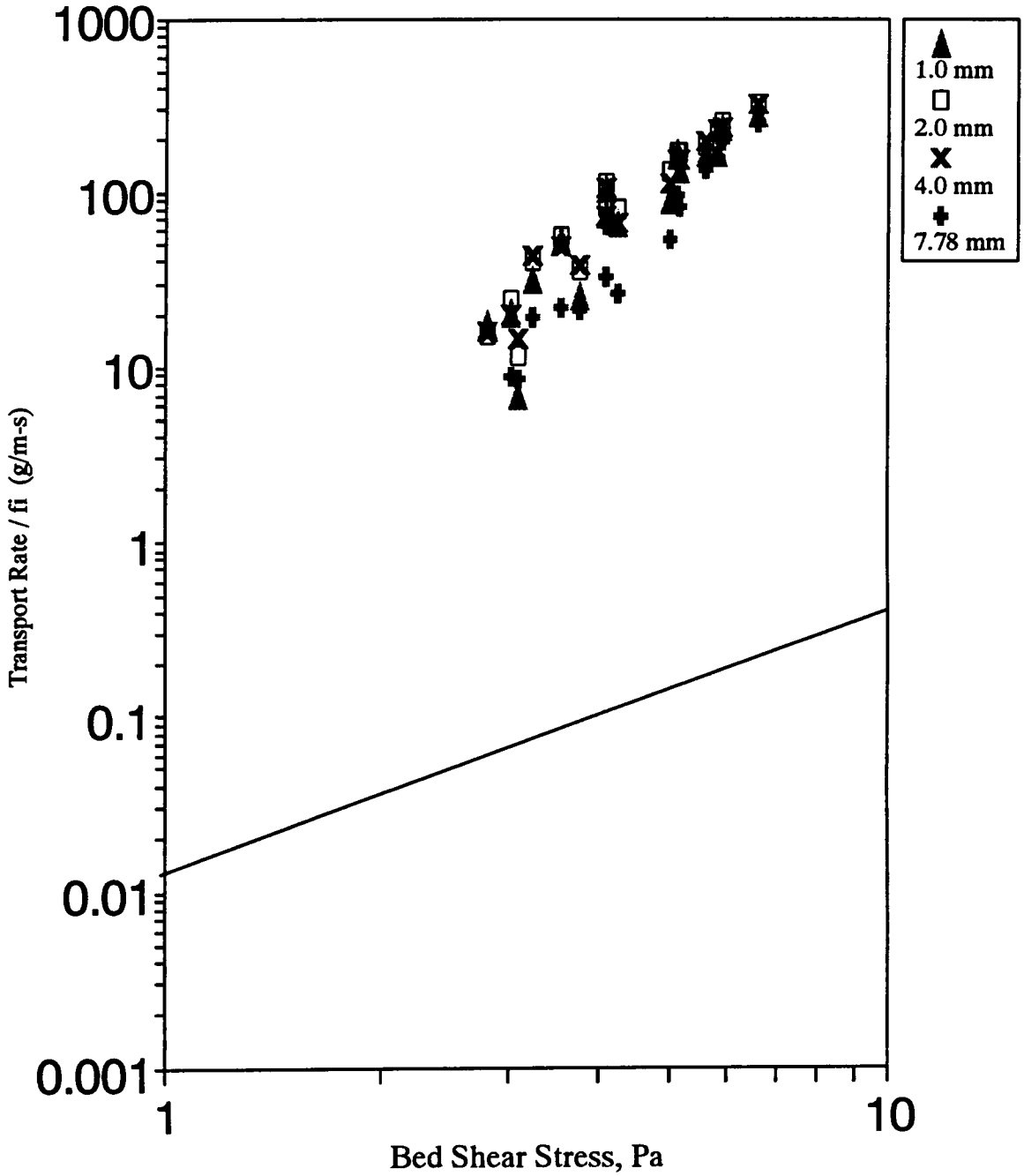

Fig. 38. Plot of Transport Rate $(q_{wi})/f_i$ vs. shear stress for the Proffitt Initial Phase.

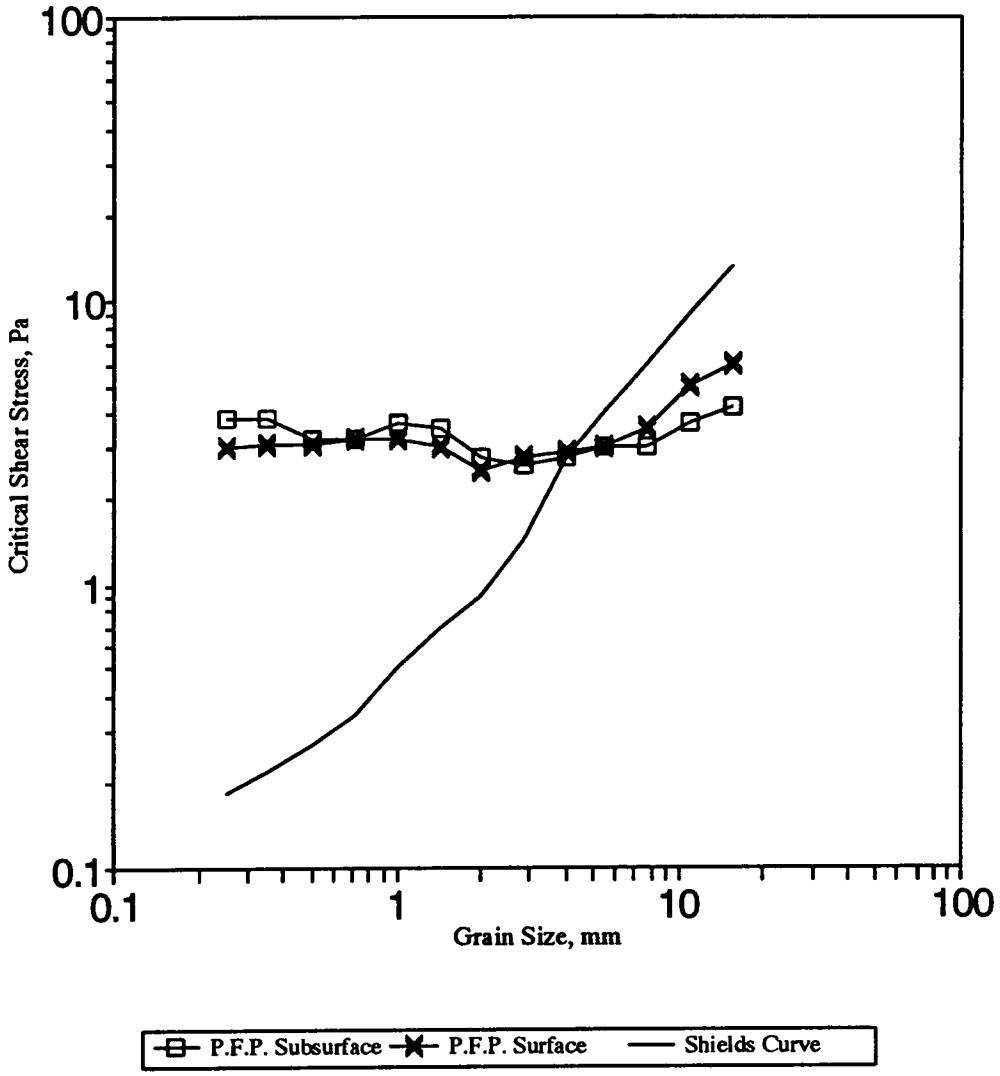

Fig. 39. Plot of τ_{ri} vs. $\bar{D}_i$ for Proffitt Final Phase (P.F.P.) Subsurface and Surface Data with Shields Curve included.

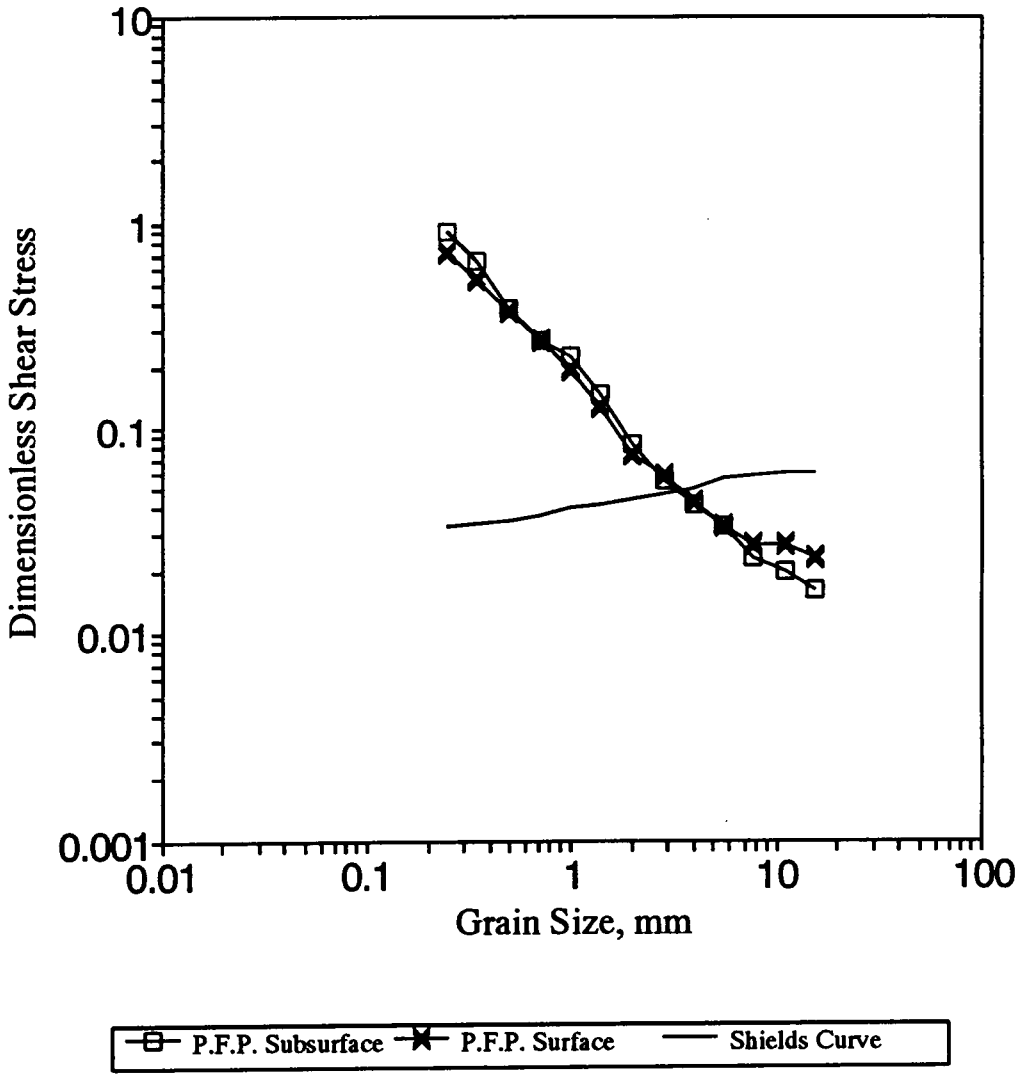

Fig. 40. Plot of dimensionless reference shear stress, τ_{ri}^*, vs. grain size, $\bar{D}_i$, for Proffitt Final Phase (P.F.P.) Surface and Subsurface Data with the Shields Curve included.

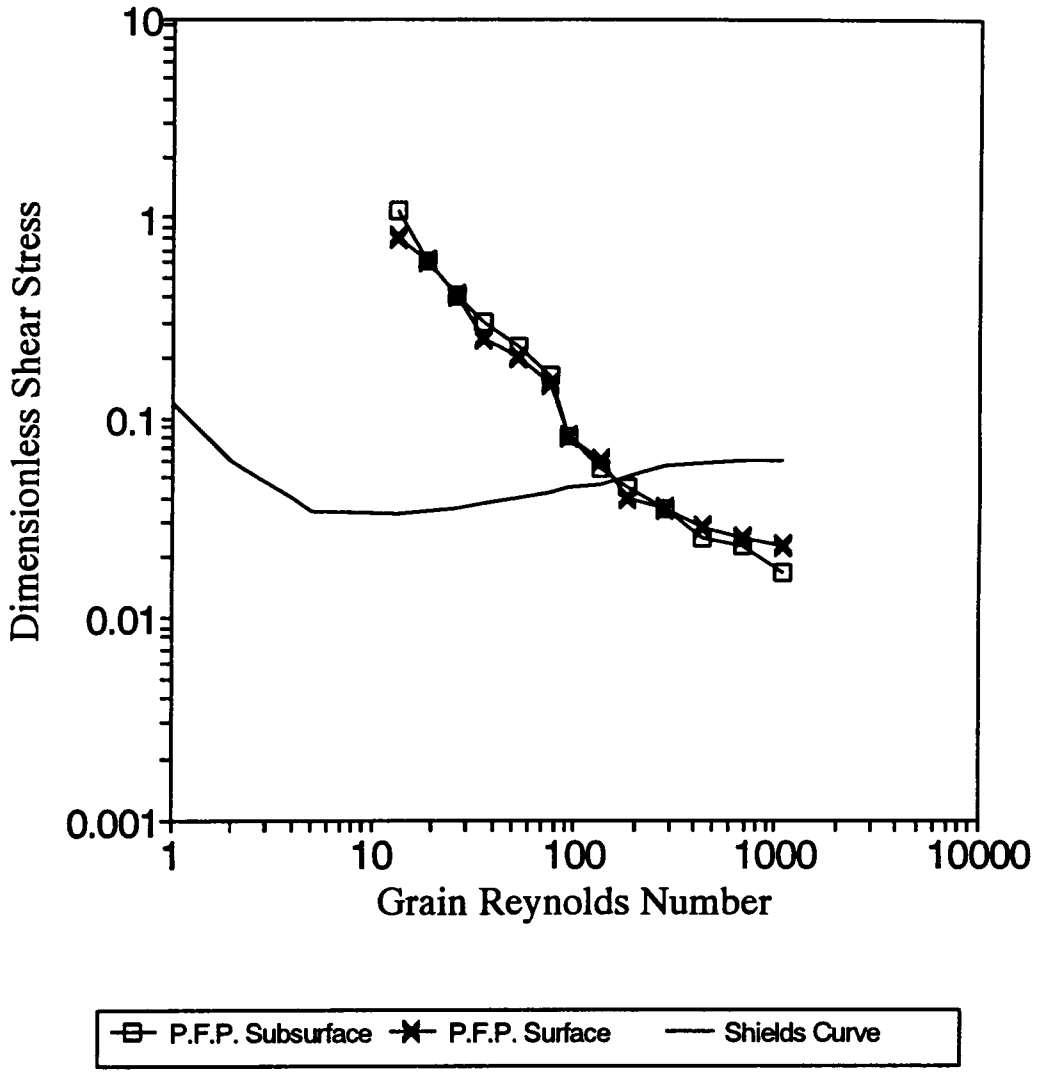

Fig. 41. Plot of dimensionless reference shear stress, τ_{ri}^*, vs. grain Reynolds number, R_*, for Proffitt Final Phase (P.F.P.) Subsurface and Surface Data with the Shields Curve included.

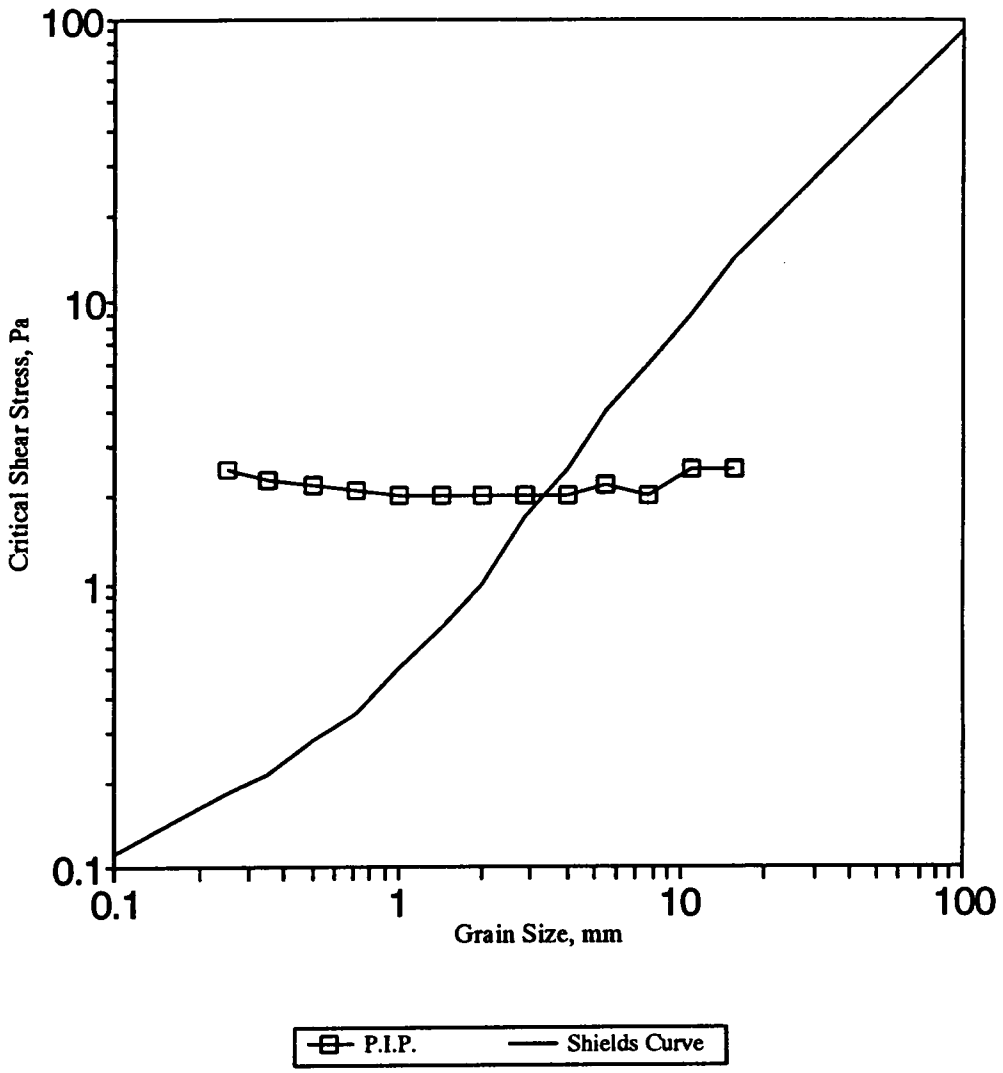

Fig. 42. Plot of reference shear stress, τ_{ri}, vs. grain size, $\bar{D}_i$, for Proffitt Initial Phase (P.I.P.) Data with the Shields Curve included.

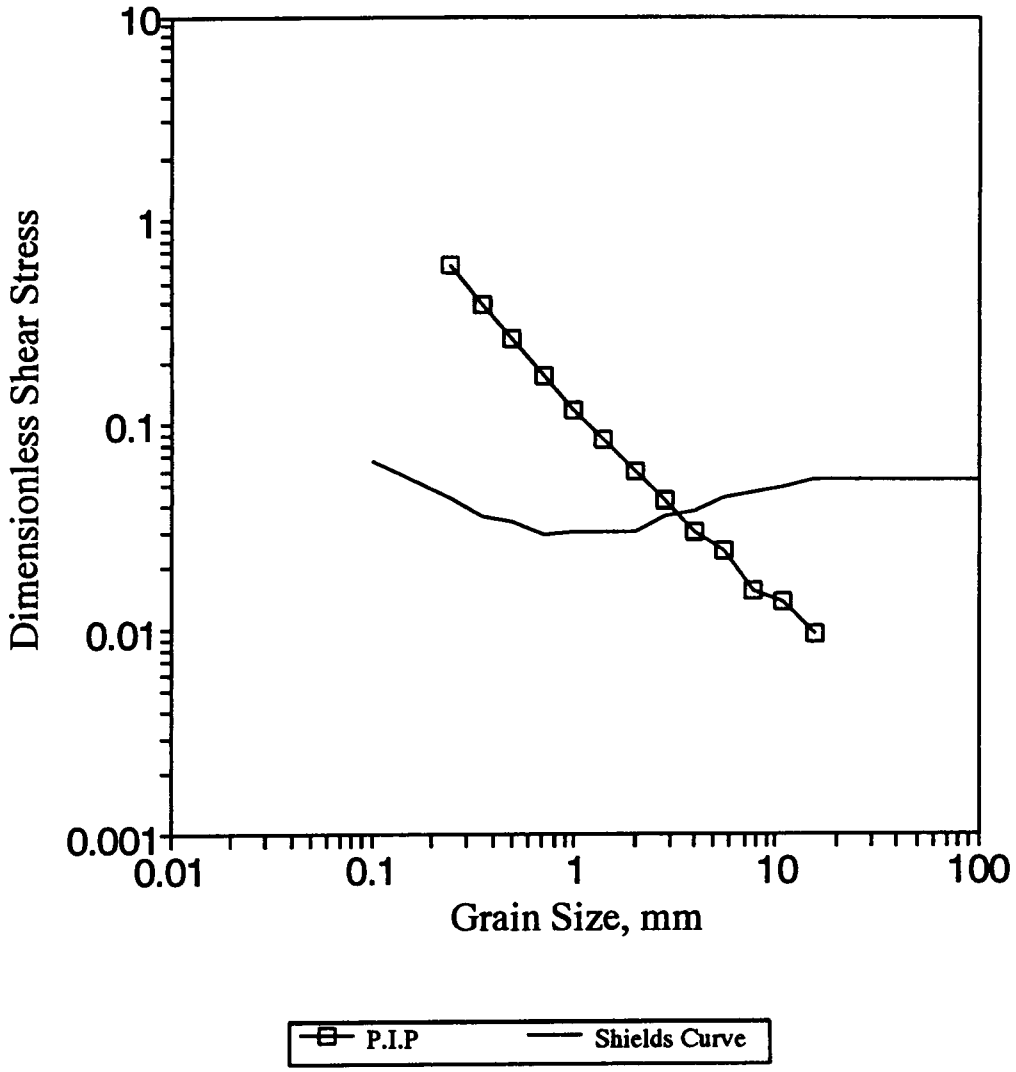

Fig. 43. Plot of dimensionless reference shears stress, τ_{ri}^*, vs. grain size, $\bar{D}_i$, for Proffitt Initial Phase (P.I.P.) Data with the Shields Curve included.

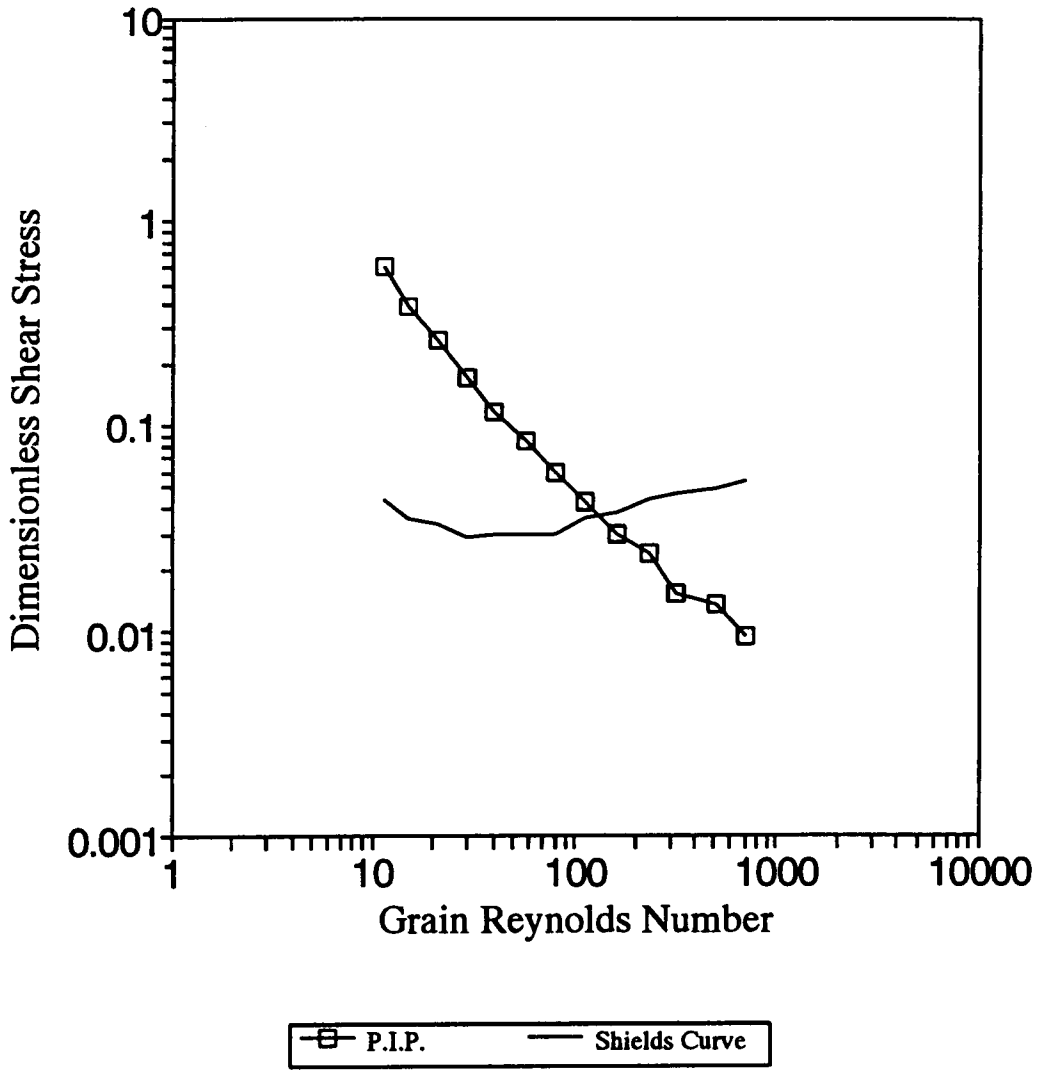

Fig. 44. Plot of dimensionless reference shear stress, τ_{ri}^*, vs. grain Reynlods number, R_*, for Proffitt Initial Phase (P.I.P.) Data with the Shields curve included.

Chapter 7. Conclusion

7.1 The Effects of Particle Shape

The flat shale particles of Piceance Creek have dimensionless reference shear stresses for the median size, τ_{ri}^*, equal to 0.0971 - 0.1024 for W_r^*=0.04 and equal to 0.0804 - 0.0906 for W_r^*=0.0025. The critical shear stress for typical coarse material is often taken to be 0.03. These values indicate that the disc-like particles of Piceance Creek have a critical shear stress 2 to 3 times higher than that of more bulky particles. This implies that disc-like particles in Piceance Creek are relatively less mobile than more spherical particles.

The above finding is in agreement with previous studies on imbricated discs. The results of Mantz (1980) suggest that imbricated discs have critical shear stresses 3.33 times higher than other non-imbricated grains. Further, Lane and Carlson (1954) found that imbricated discs had the same mobility as spheres weighing 2.5 times as much. These results imply that imbricated discs are relatively less mobile than spheres.

These results may be used to develop or modify bedload transport relations to account for the effects of particle shape. This may be done by introducing a shape factor or possibly using a fractional analysis based not only on size and density, but also on shape.

7.2 Wide Range of Transport Rates

Analysis of a wide range of transport rates verifies that the slope of the log-log bedload transport rate - bed shear stress relation, m_i, decreases with increasing transport rate. Proffitt's initial phase data, which correspond to very high transport rates, have m_i values that are lower than both the final phase and Oak Creek data, which correspond to lower transport rates than the initial phase.

Further, this investigation verifies that the dependence of transport rate on grain size diminishes with increasing transport rate. The dependence of the transport rate on grain size is demonstrated by an increase in the slope of the transport -shear relation, m_i, with grain size. The initial phase data have m_i values that do not vary significantly with grain size. However, both the final phase and Oak Creek data have m_i values that increase with grain size.

A standard regression technique produced m_i values for the final phase that were typically lower than the initial phase, a result that was not anticipated. This outcome occurred because the final phase data are quite scattered. However, a modified regression technique that accounts for the error in both variables produced m_i values for the final phase that were higher than the initial phase values. Further, the modified regression technique produced similar reference shear stresses as a graphical procedure. It is argued that the modified regression relations describe the

final phase data more accurately, and it is suggested that the modified regression technique be used to determine the reference shear stresses when their is considerable scatter in the transport - shear data.

7.3 Surface - Subsurface Approach Comparison

The Proffitt Final Phase data were analyzed using both a subsurface and surface layer based approach. The two approaches produce similar transport - shear relations with similar slope values, m_i, which increase with grain size. The two approaches also produce similar dimensionless reference shear stress values. This finding is in agreement with Wilcock and McArdell's (1993) findings. The fact that the reference shear stresses are similar for both surface and subsurface approaches implies that bedload transport relations using reference shear stresses should not be sensitive to the approach taken, at least in regard to the reference shear stress.

REFERENCES

Andrews, E.D. (1983). "Entrainment of Gravel from Naturally Sorted Riverbed Material." *Geological Survey of America Bulletin*, Vol 94, October, pp 1225 - 1231.

Ashida, K., and Michuiue, M. (1972). "Study on Hydraulic Resistance and Bedload Transport in Alluvial Streams." *Transactions*, Japan Society of Civil Engineering, 206, 59-69.

Ashworth, P.J., and Ferguson, R.L. (1989). "Size-Selective Entrainment of Bed Load in Gravel Bed Streams." *Water Resources Research*, Vol 25, No 4, pp 627-634.

Baker, V.R., and Ritter, D.F. (1975). "Competence of Rivers to Transport Coarse Bedload Material," *Geol. Soc. Am. Bull.*, Vol 86, pp 975-978.

Bagnold, R.A. (1941). The Physics of Blown Sand and Desert Dunes. Methuen, London.

Bridge, J.S., and Bennett, S.J. (1992). "A Model for the Entrainment and Transport of Sediment Grains of Mixed Sizes, Shapes, and Densities." *Water Resources Research*, Vol 28, No 2, pp 337-363.

Carling, P.A. (1983). "Threshold of Coarse Sediment Transport in Broad and Narrow Natural Streams." *Earth Surface Processes and Landforms,* Vol 8, pp 1-18.

Carling, et. al. (1992). "Effect of Bed Roughness, Particle Shape and Orientation on Initial Motion Criteria." Dynamics of Gravel-bed Rivers, Chapter 2, Edited by Billi, P. et al, John Wiley & Sons Ltd.

Chepil, W.S. (1958). "The Use of Evenly Spaced Hemispheres to Evaluate Aerodynamic Forces on a Soil Surface." *Transactions*, American Geophysical Union, Vol 39, No 3, pp 397-404.

Chin, C.O. (1985). "Stream Bed Armoring." *Report No 403*, Department of Civil Engineering, University of Auckland, Auckland, New Zealand.

Coleman, N.L. (1967). "A Theoretical and Experimental Study of Drag and Lift Forces Acting on a Sphere Resting on a Hypothetical Stream Bed." *Proceedings of the Twelfth Congress*, International Association for Hydraulic Research, Fort Collins, CO, Vol 3, pp 185-192.

Corey, A.T. (1949). "Influence of Shape on the Fall Velocity of Sand Grains." MS thesis, Colorado A&M College, Fort Collins, Colorado.

Davies, T.R.H., Samad, M.F.A. (1978). "Fluid Dynamic Lift on a Bed Particle." *Journal of the Hydraulics Division*, ASCE, Vol 104, No HY8, pp 1171-1181.

Dietrich, W.E., (1982). "Settling Velocities of Natural Particles." *Water Resources Research*, 18, 1615-1626.

Diplas, P. (1987). "Bedload Transport in Gravel-Bed Streams." *Journal of the Hyraulics Division*, ASCE, Vol 108, No HY3, pp 277-291.

Diplas, P. (1992). "Equal Mobility Versus Changing Bedload Grain Sizes in Grave-bed Streams, Discussion." Dynamics of Gravel-Bed Rivers, Ch. 5, John-Wiley and Sons.

Emmett, W.W. (1980). "A Field Calibration of the Sediment-Trapping Characteristics of the Helley-Smith Beldoad Sampler." *Geological Survey Professional Paper 1139*, United States Government Printing Office, Washington, D.C..

Fenton, J.D., and Abbott, J.E. (1977). "Initial Movement of grains on a stream bed: the effect of relative protrusion." *Proc. R. Soc. Lond. A.* 352, pp 523-537.

Fripp, J.B., and Diplas, P. (1993). "Surface Sampling in Gravel Streams." *Journal of Hydraulic Engineeing*, ASCE, Vol 119, No 4.

Ikeda, S. (1982). "Incipient Motion of Sand Particles on Side Slopes." *Journal of the Hydraulics Division*, ASCE, Vol 108, No HY1, pp 95-113.

Jain, S. (1990). "Armor or Pavement." *Journal of Hydraulic Engineering*, ASCE, Vol 116, No 3, pp 436-440.

Johansson, C.E. (1976). "Structural Studies of Frictional Sediments." *Geografiska Annaler*, Vol 58 A, No 4, pp 201 - 301.

Komar, P.D., and Li, Z. (1986). "Pivoting analyses of the selective entrainment of sediments by shape and size with application to gravel threshold." *Sedimentology*, Vol 33, pp 425-436.

Lane, E.W. (1947). "Report to the Subcommittee on Sediment Terminology." *Transactions*, American Geophysical Union, Vol 28, No 6, pp 936-938.

Lane, E.W., and Carlson, E.J. (1954). "Some observations on the effect of particle shape on the movement of coarse sediments." *Transactions, American Geophysical Union*, Vol 35, No 3, June 1954, pp 453-462.

Li, Z., and Komar, P.D. (1986). "Laboratory measurements of pivoting angles for applications to selective entrainment of gravel in a current." *Sedimentology*, Vol 33, pp 413-423.

Magalhaes, L., and Chau, T.S. (1983). "Initiation of motion conditions for shale sediments." *Canadian Journal of Civil Engineering*, Vol 10, pp 549-554.

Mantz, P.A. (1977). "Incipient Transport of Fine Grains and Flakes by Fluids - Extended Shields Diagram." *Journal of the Hyrdraulics Division*, ASCE, Vol 103, No HY6, pp 601-615.

Mantz, P.A. (1980). "Low Sediment Transport Rates over Flat Beds." *Journal of the Hydraulics Division*, ASCE, Vol 106, No HY7, pp 1173-1190.

Meyer-Peter, E., and Muller, R. (1948). "Formulas for Bed-Load Transport." *Proceedings*, Third Conference, International Association of Hydraulic Research, Stockholm, Sweden, pp 39-64.

Milhous, R.T. (1973). "Sediment Transport in a Gravel-Bottomed Stream." Ph.D. Thesis, Oregon State University, Corvallis, Oregon.

Mosconi, C.E. (1988). "River-Bed Variations and Evolution of Armor Layers." Ph.D. Thesis, University of Iowa, Iowa City, Iowa.

Neill, C.R. (1968). "A Re-examination of the Beginning of Movement for Coarse Granular Bed Materials." *Report No. INT68*, Hydraulics Research Station, Wallingford, United Kingdom.

Paintal, A.S. (1971). "Concept of critical shear stress in loose boundary open channels." *Journal of the Hydraulics Division*, ASCE, Vol 9, pp 91-114.

Paintal, A.S. (1971). "A Stocahastic model of bedload transport." *Journal of Hydraulic Research*, IAHR, Vol 9, No 4, pp. 527-554.

Parker, G. (1990). "Surface-based bedload transport relation for gravel rivers." *Journal of Hydrualic Research*, Vol 28, No 4, pp 417-436.

Parker, G., Klingeman, P.C., and McLean D.G. (1982). "Bedload and Size Distribution in Paved Gravel Bed Streams." *Journal of the Hydraulics Division,* ASCE, Vol 108, No HY4, pp 544-569.

Parker, G., and Klingeman, P.C. (1982). "On Why Gravel Bed Streams are Paved." *Water Resources Research,* Vol 18, No 5, pp 1409-1423.

Parker, G., and Sutherland, A.J. (1990). "Fluvial armor." *Journal of Hydraulic Research,* Vol 28, No 5, pp 529-544.

Parker, G., and Wilcock, P.R. (1993). "Sediment Feed and Recirculating Flumes: Fundamental Difference." *Journal of Hydraulic Engineering,* ASCE, Vol 119, No 11, pp 1192-1204.

Proffitt, G.T. (1980). "Selective transport and armouring of non-uniform alluvial sediments." Report no. 80/22, Department of Civil Engineering, Univerisity of Canterbury, New Zealand, 203p.

Proffitt, G.T., and Sutherland, A.J. (1983). "Transport of non-uniform sediment." *Journal of Hydraulic Research,* IAHR, Vol 21, No 1, pp 33-43.

Shih, S.M., and Komar, P.D. (1990). "Differential Bedload Transport Rates in a Gravel Bed Stream: A Grain-size Distribution Approach." *Earth Surface Processes and Landforms,* Vol 15, pp 539-552.

Shields, A. (1936). "Anwendung der Aenlichkeitsmechanik und der Turbulenzforshug auf die Geschiebewegung." Mitteilungen der Preussischen Versuchsanstaff fur Wasserbau und Schiffbau, Berlin, Germany, translated to English by W.P. Ott and J.C. Van Uchelen, California Institute of Technology, Pasadena, California.

Taylor, B.D., and Vanoni, V.A. (1972). "Temperature effects in low transport, flat bed flow." *Journal of the Hydraulics Division,* ASCE, Vol 28, pp 1427-1445.

Vanoni, V.A. (1975). Sedimentation Engineering, ASCE, p 96.

White, C.M. (1940). "The Equilibrium of Grains on the Bed of an Alluvial Channel." *Proceedings of the Royal Society, London, England, Series A,* Vol 174, pp 332-338.

Wiberg, P.L., and Smith, D.J. (1987). "Calculations of the critical shear stress for motion of uniform and heterogeneous sediments." *Water Resources Research,* Vol 23, No 8, pp 1471-1480.

Wilcock, P.R. (1988). "Methods for Estimating the Critical Shear Stress of Individual Fractions in Mixed-Size Sediment." Water Resources Research, Vol 24, No 7, pp 1127-1135.

Wilcock, P.R. (1992). "Experimental Investigation of the effect of Mixture Properties on Transport Dynamics." Dynamics of Gravel-Bed Rivers, Ch. 6, John-Wiley and Sons.

Wilcock, P.R. (1993). "Critical Shear Stress of Natural Sediments." *Journal of Hydraulic Engineering*, ASCE, Vol 119, No 4.

Wilcock, P.R., and Southard, J.B. (1988). "Experimental Study of Incipient Motion in Mixed-Size Sediment." *Water Resources Research*, Vol 24, No 7, pp 1137-1151.

Wilcock, P.R., and McArdell, B.W. (1993). "Surface-Based Fractional Transport Rates: Mobilization Thresholds and Partial Transport of a Sand-Gravel Sediment." *Water Resources Research*, Vol 29, No 4, pp 1297-1312.

Yalin, S.M., and Karahan, E. (1979). "Inception of Sediment Transport." *Journal of the Hydraulics Division*, ASCE, Vol 105, No HY11, pp 1433-1443.

Yang, T.C. (1973). "Incipient Motion and Sediment Transport." *Journal of the Hydraulics Division*, ASCE, Vol 99, No HY10, pp 1679-1703.

Zingg, (1935). Beitrag Zur Schotteranalyse, Schweiz Min. Pet. M.H., v 15, pp 39-40.

Appendix I. Proffitt Data

Included in this appendix are the measured transport rates and size distriubutions, corresponding hydraulic data, and bed material size distributions for Runs 1-1 through 4-4.

Initial Transport Phase

RUN No.	Unit Discharge m^2/s	Kinem. Visc. m^2/s x10^6	Hyd Radius m	Frict Slope %	Shear Veloc m/s	Mean Veloc m/s	Frict Factor	Water Density kg/m^3	Shear Stress N/m^2	Transport Rate N/s-m	Transport Rate m^2/s
1-2	0.152	1.08	0.149	0.29	0.065	0.822	0.05	999	4.235	0.578	2.18E-05
1-3	0.07	1.11	0.092	0.31	0.053	0.657	0.052	999	2.795	0.141	5.31E-06
1-4	0.121	1.09	0.129	0.28	0.06	0.769	0.049	999	3.540	0.408	1.54E-05
1-7	0.089	1.1	0.106	0.29	0.055	0.7	0.049	999	3.013	0.162	6.10E-06
2-1	0.093	1.1	0.11	0.3	0.057	0.709	0.052	999	3.234	0.281	1.06E-05
2-2	0.143	1.1	0.144	0.29	0.064	0.812	0.05	999	4.093	0.568	2.14E-05
2-3	0.22	1.1	0.18	0.29	0.071	0.928	0.047	999	5.116	1.243	4.68E-05
2-4	0.248	1.09	0.183	0.37	0.082	1.042	0.05	999	6.636	2.486	9.36E-05
3-1	0.122	1.1	0.122	0.43	0.072	0.856	0.057	999	5.141	1.189	4.48E-05
3-2	0.179	1.11	0.156	0.38	0.076	0.936	0.053	999	5.810	1.676	6.31E-05
3-3	0.225	1.09	0.172	0.35	0.077	1.016	0.046	999	5.900	2.027	7.63E-05
3-4	0.139	1.1	0.134	0.38	0.071	0.86	0.055	999	4.990	0.865	3.26E-05
4-1	0.104	1.13	0.116	0.33	0.061	0.756	0.052	999	3.752	0.297	1.12E-05
4-2	0.083	1.12	0.102	0.31	0.056	0.697	0.052	999	3.099	0.108	4.07E-06
4-3	0.152	1.11	0.144	0.29	0.064	0.841	0.046	999	4.093	0.892	3.36E-05
4-4	0.217	1.13	0.173	0.33	0.075	0.967	0.048	999	5.595	1.621	6.10E-05

Final Transport Phase

RUN NO.	Unit Discharge m^2/s	Kinem Visc m^2/s x10^6	Hyd. Radius m	Frict Slope %	Shear Vel m/s	Mean Vel m/s	Frict Factor	Water Density kg/m^3	Shear Stress N/m^2	Transport Rate N/s-m	Transport Rate m^2/s
1-2	0.152	1.08	0.157	0.28	0.066	0.785	0.056	999	4.308	0.0057	2.15E-07
1-3	0.07	1.11	0.1	0.3	0.054	0.612	0.063	999	2.940	0.0016	6.02E-08
1-4	0.121	1.09	0.141	0.27	0.061	0.712	0.058	999	3.731	0.0027	1.02E-07
1-7	0.089	1.1	0.116	0.29	0.057	0.652	0.061	999	3.297	0.0027	1.02E-07
2-1	0.093	1.1	0.121	0.31	0.061	0.663	0.067	999	3.676	0.0021	7.91E-08
2-2	0.143	1.1	0.158	0.28	0.065	0.744	0.062	999	4.336	0.0025	9.41E-08
2-3	0.22	1.1	0.194	0.27	0.071	0.873	0.053	999	5.133	0.0054	2.03E-07
2-4	0.248	1.09	0.199	0.35	0.082	0.973	0.057	999	6.826	0.0403	1.52E-06
3-1	0.122	1.1	0.136	0.42	0.075	0.781	0.073	999	5.598	0.0116	4.37E-07
3-2	0.179	1.11	0.164	0.38	0.078	0.897	0.06	999	6.107	0.0138	5.20E-07
3-3	0.225	1.09	0.189	0.39	0.085	0.961	0.063	999	7.224	0.0146	5.50E-07
3-4	0.139	1.1	0.145	0.34	0.069	0.803	0.06	999	4.831	0.0076	2.86E-07
4-1	0.104	1.13	0.124	0.3	0.06	0.708	0.058	999	3.646	0.0062	2.33E-07
4-2	0.083	1.12	0.108	0.29	0.056	0.658	0.058	999	3.069	0.0027	1.02E-07
4-3	0.152	1.11	0.151	0.27	0.063	0.805	0.049	999	3.996	0.013	4.89E-07
4-4	0.217	1.13	0.191	0.24	0.067	0.857	0.049	999	4.492	0.0276	1.04E-06

PROFFITT FLUME DATA--BED SEDIMENT GRADINGS

Grain Size mm	Di mm	Percent Finer Series 1	fi, %	Series 2	fi, %	Series 3	fi, %	Series 4	fi, %
38.1		100.00		100.00		100.00		100.00	
	32.01		1.55		3.00		1.80		0.00
26.9		98.45		97.00		98.20		100.00	
	22.64		0.94		3.39		1.13		0.00
19.05		97.51		93.61		97.07		100.00	
	15.55		2.43		6.42		7.10		2.48
12.7		95.08		87.19		89.97		97.52	
	11.00		5.01		5.00		5.47		2.66
9.52		90.07		82.19		84.50		94.86	
	7.78		7.38		5.76		5.28		3.22
6.35		82.69		76.43		79.22		91.64	
	5.50		13.65		12.25		8.15		31.96
4.76		69.04		64.18		71.07		59.68	
	3.99		12.10		13.26		17.87		20.75
3.35		56.94		50.92		53.20		38.93	
	2.84		16.04		9.31		11.80		7.04
2.41		40.90		41.61		41.40		31.89	
	2.01		15.68		12.55		14.48		11.95
1.68		25.22		29.06		26.92		19.94	
	1.42		11.68		9.29		10.46		8.60
1.2		13.54		19.77		16.46		11.34	
	1.01		6.65		7.67		7.86		6.33
0.853		6.89		12.10		8.60		5.01	
	0.72		3.48		5.43		4.13		2.59
0.6		3.41		6.67		4.47		2.42	
	0.50		1.36		3.12		1.94		0.98
0.42		2.05		3.55		2.53		1.44	
	0.35		0.73		1.60		1.01		0.52
0.3		1.32		1.95		1.52		0.92	
	0.25		0.54		1.06		0.74		0.41
0.21		0.78		0.89		0.78		0.51	
	0.18		0.30		0.47		0.36		0.20
0.15		0.48		0.42		0.42		0.31	
	0.11		0.27		0.25		0.25		0.19
0.075		0.21		0.17		0.17		0.12	
D50, mm		2.9		3.25		3.07		4.2	
Dg, mm		2.95		3.3		3.28		2.83	
Geom Std Dev		2.26		3.24		2.78		1.95	

INITIAL ERODED DISTRIBUTIONS - % FINER

Size mm	1-2	1-3	1-4	1-7	2-1	2-2	2-3	2-4	3-1	3-2	3-3	3-4	4-1	4-2	4-3	4-4
38.1	100.00	100.00	100.00	100.00	100.00	100.00	100.00	100.00	100.00	100.00	100.00	100.00	100.00	100.00	100.00	100.00
26.9	100.00	100.00	100.00	100.00	100.00	100.00	100.00	100.00	100.00	100.00	100.00	100.00	100.00	100.00	100.00	100.00
19.05	100.00	99.45	100.00	100.00	100.00	100.00	100.00	100.00	99.76	100.00	99.71	100.00	100.00	100.00	100.00	100.00
12.7	98.42	98.29	100.00	100.00	99.85	99.58	99.27	98.26	98.88	98.84	99.48	99.67	99.59	99.79	100.00	99.53
9.52	95.54	95.38	99.68	99.94	98.51	98.62	97.00	94.20	96.74	96.46	95.09	98.36	98.62	98.81	99.24	98.36
6.35	92.29	86.64	95.77	95.95	94.68	95.42	92.67	88.60	93.15	91.57	90.12	95.18	96.41	96.28	96.99	95.70
4.76	79.41	72.29	83.46	84.70	78.01	82.48	79.10	74.55	83.92	81.68	80.73	85.49	63.88	60.33	67.82	63.87
3.35	65.77	59.13	69.30	70.01	58.34	65.80	63.30	57.58	61.32	58.10	60.06	62.62	37.69	32.90	43.69	39.51
2.41	44.84	41.44	47.54	47.53	43.79	52.60	50.80	45.59	45.47	42.09	45.37	44.99	29.60	24.87	35.55	31.70
1.68	23.55	24.69	26.86	25.14	26.19	34.55	33.83	29.80	25.82	23.41	27.88	23.49	15.57	12.47	20.93	18.59
1.2	10.24	13.01	12.86	10.74	14.04	21.67	21.50	18.76	12.69	11.60	15.91	10.68	6.70	5.18	10.71	9.39
0.85	2.78	4.79	4.41	2.48	5.73	11.59	11.59	10.00	4.02	3.97	6.93	2.81	1.42	1.15	3.44	2.96
0.6	0.80	1.06	1.49	0.28	1.50	5.59	5.59	4.57	1.18	1.32	2.83	0.64	0.28	0.21	0.94	0.86
0.42	0.31	0.33	0.68	0.04	0.57	1.95	2.59	1.99	0.52	0.58	1.31	0.24	0.11	0.06	0.34	0.36
0.3	0.13	0.16	0.36	0.01	0.24	0.87	1.14	0.81	0.27	0.26	0.62	0.11	0.06	0.02	0.16	0.18
0.21	0.05	0.09	0.16	0.00	0.07	0.28	0.32	0.21	0.10	0.08	0.21	0.04	0.03	0.00	0.06	0.07

PROFFITT FLUME DATA
INITIAL ERODED DISTRIBUTIONS - pi values

Size Range mm	1-2	1-3	1-4	1-7	2-1	2-2	2-3	2-4	3-1	3-2	3-3	3-4	4-1	4-2	4-3	4-4
26.9-38.1	0.00	0.00	0.00	0.00	0.00	0.00	0.00	0.00	0.00	0.00	0.00	0.00	0.00	0.00	0.00	0.00
19.05-26.9	0.00	0.55	0.00	0.00	0.00	0.00	0.00	0.00	0.24	0.00	0.29	0.00	0.00	0.00	0.00	0.00
12.7-19.05	1.58	1.16	0.00	0.00	0.15	0.42	0.73	1.74	0.88	1.16	0.23	0.33	0.41	0.21	0.00	0.47
9.52-12.7	2.88	2.91	0.32	0.06	1.34	0.96	2.27	4.06	2.14	2.38	4.39	1.31	0.97	0.98	0.76	1.17
6.35-9.52	3.25	8.74	3.91	3.99	3.83	3.20	4.33	5.60	3.59	4.89	4.97	3.18	2.21	2.53	2.25	2.66
4.76-6.35	12.88	14.35	12.31	11.25	16.67	12.94	13.57	14.05	9.23	9.89	9.39	9.69	32.53	35.95	29.17	31.83
3.35-4.76	13.64	13.16	14.16	14.69	19.67	16.68	15.80	16.97	22.60	23.58	20.67	22.87	26.19	27.43	24.13	24.36
2.41-3.35	20.93	17.69	21.76	22.48	14.55	13.20	12.50	11.99	15.85	16.01	14.69	17.63	8.09	8.03	8.14	7.81
1.68-2.41	21.29	16.75	20.68	22.39	17.60	18.05	16.97	15.79	19.65	18.68	17.49	21.50	14.03	12.40	14.62	13.11
1.2-1.68	13.31	11.68	14.00	14.40	12.15	12.88	12.33	11.04	13.13	11.81	11.97	12.81	8.87	7.29	10.22	9.20
0.85-1.2	7.46	8.22	8.45	8.26	8.31	10.08	9.91	8.76	8.67	7.63	8.98	7.87	5.28	4.03	7.27	6.43
0.60-0.85	1.98	3.73	2.92	2.20	4.23	6.00	6.00	5.43	2.84	2.65	4.10	2.17	1.14	0.94	2.50	2.10
0.42-0.60	0.49	0.73	0.81	0.24	0.93	3.64	3.00	2.58	0.66	0.74	1.52	0.40	0.17	0.15	0.60	0.50
0.30-0.42	0.18	0.17	0.32	0.03	0.33	1.08	1.45	1.18	0.25	0.32	0.69	0.13	0.05	0.04	0.18	0.18
0.21-0.30	0.08	0.07	0.20	0.01	0.17	0.59	0.82	0.60	0.17	0.18	0.41	0.07	0.03	0.02	0.10	0.11

PROFFITT FLUME DATA
FINAL ERODED DISTRIBUTIONS - % FINER

Size mm	1-2	1-3	1-4	1-7	2-1	2-2	2-3	2-4	3-1	3-2	3-3	3-4	4-1	4-2	4-3	4-4
38.1	100.00	100.00	100.00	100.00	100.00	100.00	100.00	100.00	100.00	100.00	100.00	100.00	100.00	100.00	100.00	100.00
26.9	100.00	100.00	100.00	100.00	100.00	100.00	100.00	100.00	100.00	100.00	100.00	100.00	100.00	100.00	100.00	100.00
19.05	100.00	100.00	100.00	100.00	100.00	100.00	100.00	100.00	100.00	100.00	97.17	100.00	100.00	100.00	100.00	100.00
12.7	99.20	100.00	100.00	100.00	99.62	100.00	98.55	98.24	100.00	97.16	94.98	99.43	100.00	100.00	99.48	100.00
9.52	96.59	100.00	98.98	99.51	97.75	99.41	95.78	94.12	99.14	94.37	90.13	96.64	99.45	98.53	97.92	98.66
6.35	91.61	98.79	94.02	97.09	94.32	96.43	90.31	89.71	96.52	91.58	83.48	93.49	97.05	97.44	95.89	96.17
4.76	80.23	94.10	77.75	86.65	81.08	85.18	66.83	76.91	84.40	85.52	71.53	81.19	58.23	66.63	67.80	59.02
3.35	67.77	85.93	58.51	71.72	63.48	71.92	42.10	63.59	53.63	69.35	44.76	50.57	26.02	41.12	47.08	32.91
2.41	50.60	68.62	32.29	48.01	51.27	61.31	29.25	53.08	34.30	57.40	27.70	30.95	18.00	32.99	41.00	24.80
1.68	31.43	44.10	12.10	24.62	34.66	46.95	18.16	37.74	17.98	40.57	13.36	13.37	9.79	20.19	29.17	11.88
1.2	16.27	23.14	4.92	9.18	21.99	34.05	12.56	24.59	10.63	25.43	7.14	6.72	6.63	10.55	17.81	4.90
0.85	5.40	8.40	2.74	1.42	10.89	20.66	7.59	12.92	4.63	11.23	3.47	3.27	2.87	1.83	6.62	1.47
0.6	1.28	2.58	1.40	0.30	3.66	9.28	3.50	5.12	1.59	3.78	1.75	1.37	0.53	0.23	1.97	0.55
0.42	0.36	0.61	0.66	0.05	0.96	2.84	1.46	1.65	0.44	1.04	0.86	0.34	0.09	0.06	0.51	0.25
0.3	0.13	0.16	0.35	0.01	0.27	0.88	0.69	0.57	0.21	0.30	0.45	0.10	0.03	0.02	0.14	0.13
0.21	0.05	0.08	0.15	0.00	0.07	0.26	0.21	0.51	0.08	0.08	0.19	0.04	0.01	0.00	0.05	0.05

15.55 0.3
11 2.61
7.78 4.93
5.5 11.38
3.99 12.46
2.84 17.17
2.01 19.17
1.42 15.16
1.01 10.87

final

PROFFITT FLUME DATA
FINAL ERODED DISTRIBUTIONS - pi values

Size Range mm	1-2	1-3	1-4	1-7	2-1	2-2	2-3	2-4	3-1	3-2	3-3	3-4	4-1	4-2	4-3	4-4
26.9-38.1	0.00	0.00	0.00	0.00	0.00	0.00	0.00	0.00	0.00	0.00	0.00	0.00	0.00	0.00	0.00	0.00
19.05-26.9	0.00	0.00	0.00	0.00	0.00	0.00	0.00	0.00	0.00	0.00	2.83	0.00	0.00	0.00	0.00	0.00
12.7-19.05	0.80	0.00	0.00	0.00	0.38	0.00	1.45	1.76	0.00	2.84	2.19	0.57	0.00	0.00	0.52	0.00
9.52-12.7	2.61	0.00	1.02	0.49	1.87	0.59	2.77	4.12	0.86	2.79	4.85	2.79	0.55	1.47	1.56	1.34
6.35-9.52	4.98	1.21	4.96	2.42	3.43	2.98	5.47	4.41	2.62	2.79	6.65	3.15	2.40	1.09	2.03	2.49
4.76-6.35	11.38	4.69	16.27	10.44	13.24	11.25	23.48	12.80	12.12	6.06	11.95	12.30	38.82	30.81	28.09	37.15
3.35-4.76	12.46	8.17	19.24	14.93	17.60	13.26	24.73	13.32	30.77	16.17	26.77	30.62	32.21	25.51	20.72	26.11
2.41-3.35	17.17	17.31	26.22	23.71	12.21	10.61	12.85	10.51	19.33	11.95	17.06	19.62	8.02	8.13	6.08	8.11
1.68-2.41	19.17	24.52	20.19	23.39	16.61	14.36	11.09	15.34	16.32	16.83	14.34	17.58	8.21	12.80	11.83	12.92
1.2-1.68	15.16	20.96	7.18	15.44	12.67	12.90	5.60	13.15	7.35	15.14	6.22	6.65	3.16	9.64	11.36	6.98
0.85-1.2	10.87	14.74	2.18	7.76	11.10	13.39	4.97	11.67	6.00	14.20	3.67	3.45	3.76	8.72	11.19	3.43
0.60-0.85	4.12	5.82	1.34	1.12	7.23	11.38	4.09	7.80	3.04	7.45	1.72	1.90	2.34	1.60	4.65	0.92
0.42-0.60	0.92	1.97	0.74	0.25	2.70	6.44	2.04	3.47	1.15	2.74	0.89	1.03	0.44	0.17	1.46	0.30
0.30-0.42	0.23	0.45	0.31	0.04	0.69	1.96	0.77	1.08	0.23	0.74	0.41	0.24	0.06	0.04	0.37	0.12
0.21-0.30	0.08	0.08	0.20	0.01	0.20	0.62	0.48	0.06	0.13	0.22	0.26	0.06	0.02	0.02	0.09	0.08

PROFFITT FLUME DATA
ARMOUR DISTRIBUTIONS - % FINER

Size mm	1-2	1-3	1-4	1-7	2-1	2-2	2-3	2-4	3-1	3-2	3-3	3-4	4-1	4-2	4-3	4-4
38.1	100	100	100	100	100	100	100	100	100	100	100	100	100	100	100	100
26.9	96.21	99.17	98.37	98.90	92.86	91.94	90.93	88.60	96.78	95.49	95.34	98.34	100	100	100	100
19.05	92.38	98.18	97.34	96.63	86.55	82.62	82.33	78.52	90.41	85.31	85.88	92.85	100	100	100	100
12.7	68.30	94.77	88.34	90.25	72.70	69.74	64.75	55.65	69.16	61.57	56.36	68.58	90.16	95.75	85.21	81.72
9.52	63.22	88.16	74.33	80.06	60.45	58.45	52.23	43.15	53.85	44.83	40.80	51.72	80.38	88.16	71.92	67.44
6.35	46.80	70.18	57.02	63.78	50.04	48.27	43.88	35.14	44.02	35.47	33.81	41.78	73.69	81.90	65.10	60.66
4.76	33.17	50.73	40.90	48.09	36.99	37.48	35.54	27.65	36.01	29.26	29.55	35.27	41.53	51.78	40.29	39.00
3.35	25.48	38.41	30.35	38.47	24.71	27.77	28.30	21.07	22.86	19.35	22.04	25.47	21.00	30.46	22.11	25.63
2.41	17.73	25.79	19.37	28.43	17.99	22.08	23.67	16.85	14.57	13.56	17.15	19.77	16.51	24.54	17.21	22.07
1.68	10.63	15.48	10.06	18.91	10.95	15.54	17.40	11.81	7.90	8.25	11.91	13.53	10.21	15.15	10.48	15.99
1.2	5.92	9.10	5.19	11.56	6.61	11.26	12.26	8.13	4.32	4.13	7.78	9.10	5.74	8.28	5.95	10.15
0.85	2.32	4.06	1.88	5.82	3.42	6.47	6.91	4.51	1.62	1.37	3.69	4.56	1.57	2.42	2.60	4.75
0.6	0.66	1.50	0.51	2.39	1.62	3.46	3.31	2.01	0.45	0.31	1.40	1.95	0.23	0.56	1.06	1.94
0.42	0.25	0.55	0.19	1.00	0.72	1.62	1.43	0.79	0.17	0.08	0.49	0.81	0.06	0.20	0.45	0.87
0.3	0.10	0.22	0.08	0.39	0.31	0.68	0.57	0.31	0.10	0.03	0.16	0.32	0.02	0.08	0.17	0.36
0.21	0.04	0.08	0.04	0.12	0.12	0.20	0.15	0.11	0.06	0.01	0.04	0.09	0.00	0.02	0.04	0.08
0.15	0.02	0.03	0.02	0.07	0.05	0.06	0.04	0.03	0.03	0.00	0.01	0.03	0.00	0.00	0.01	0.02

PROFFITT FLUME DATA
ARMOUR DISTRIBUTIONS - Fi values

Size Range mm	Di, m	1-2	1-3	1-4	1-7	2-1	2-2	2-3	2-4	3-1	3-2	3-3	3-4	4-1	4-2	4-3	4-4
26.9-38.1	32	3.79	0.83	1.63	1.1	7.14	8.06	9.07	11.4	3.22	4.51	4.66	1.66	0	0	0	0
19.05-26.9	22.64	3.83	0.99	1.03	2.27	6.31	9.32	8.6	10.08	6.37	10.18	9.46	5.49	0	0	0	0
12.7-19.05	15.55	24.08	3.41	9	6.38	13.85	12.88	17.58	22.87	21.25	23.74	29.52	24.27	9.84	4.25	14.79	18.28
9.52-12.7	11	5.08	6.61	14.01	10.19	12.25	11.29	12.52	12.5	15.31	16.74	15.56	16.86	9.78	7.59	13.29	14.28
6.35-9.52	7.78	16.42	17.98	17.31	16.28	10.41	10.18	8.35	8.01	9.83	9.36	6.99	9.94	6.69	6.26	6.82	6.78
4.76-6.35	5.5	13.63	19.45	16.12	15.69	13.05	10.79	8.34	7.49	8.01	6.21	4.26	6.51	32.16	30.12	24.81	21.66
3.35-4.76	4	7.69	12.32	10.55	9.62	12.28	9.71	7.24	6.58	13.15	9.91	7.51	9.8	20.53	21.32	18.18	13.37
2.41-3.35	2.84	7.75	12.62	10.98	10.04	6.72	5.69	4.63	4.22	8.29	5.79	4.89	5.7	4.49	5.92	4.9	3.56
1.68-2.41	2	7.1	10.31	9.31	9.52	7.04	6.54	6.27	5.04	6.67	5.31	5.24	6.24	6.3	9.39	6.73	6.08
1.2-1.68	1.42	4.71	6.38	4.87	7.35	4.34	4.28	5.14	3.68	3.58	4.12	4.13	4.43	4.47	6.87	4.53	5.84
0.85-1.2	1	3.6	5.04	3.31	5.74	3.19	4.79	5.35	3.62	2.7	2.76	4.09	4.54	4.17	5.86	3.35	5.4
0.60-0.85	0.72	1.66	2.56	1.37	3.43	1.8	3.01	3.6	2.5	1.17	1.06	2.29	2.61	1.34	1.86	1.54	2.81
0.42-0.60	0.5	0.41	0.95	0.32	1.39	0.9	1.84	1.88	1.22	0.28	0.23	0.91	1.14	0.17	0.36	0.61	1.07
0.30-0.42	0.35	0.15	0.33	0.11	0.61	0.41	0.94	0.86	0.48	0.07	0.05	0.33	0.49	0.04	0.12	0.28	0.51
0.21-0.30	0.25	0.06	0.14	0.04	0.27	0.19	0.48	0.42	0.2	0.04	0.02	0.12	0.23	0.02	0.06	0.13	0.28
0.15-0.21	0.18	0.02	0.05	0.02	0.05	0.07	0.14	0.11	0.08	0.03	0.01	0.03	0.06	0	0.02	0.03	0.06

Surface

The vita has been removed from the scanned document